Polymer composites incorporating engineered electrospun fibres: flexible design and novel properties for biomedical applications

Xi Zhang

2017

Submitted in partial fulfilment of the requirements of the Degree of Doctor of Philosophy at Queen Mary University of London

Statement of Originality

I, Xi Zhang, confirm that the research included within this thesis is my own work or that where it has been carried out in collaboration with, or supported by others, that this is duly acknowledged below and my contribution indicated. Previously published material is also acknowledged below.

I attest that I have exercised reasonable care to ensure that the work is original, and does not to the best of my knowledge break any UK law, infringe any third party's copyright or other Intellectual Property Right, or contain any confidential material.

I accept that the College has the right to use plagiarism detection software to check the electronic version of the thesis.

I confirm that this thesis has not been previously submitted for the award of a degree by this or any other university.

The copyright of this thesis rests with the author and no quotation from it or information derived from it may be published without the prior written consent of the author.

Signature: 

Date: 19/07/2017

List of Publications

1. Zhang X, Geven MA, Grijpma DW, Gautrot JE, Peijs T. Polymer-polymer composites for the design of strong and tough degradable biomaterials. *Materials Today Communications* **2016**, 8, 53-63.
2. Luo D, Zhang X, Shahid S, Cattell MJ, Gould D, Sukhorukov GB. Electrospun poly(lactic acid) fibers containing novel chlorhexidine particles with sustained antibacterial activity. *Biomaterials Science* **2017**, 5, 111-119.
3. Zhang X, Geven MA, Grijpma DW, Peijs T, Gautrot JE. Tunable and processable shape memory composites based on degradable polymers. *Polymer* **2017**, 122, 323-331.
4. Zhang X, Guillaume O, Eglin D, Geven MA, Grijpma DW, Peijs T, Gautrot JE. Advanced drug delivery system based on drug-loaded electrospun PLA fibres in photo-crosslinkable PTMC matrix. *Biomaterials Science* **2017**, to be submitted
5. Zhang X, Peijs T, Gautrot JE. Functionalization of electrospun PLA fibres using amphiphilic block copolymers for use in carboxy-methyl-cellulose hydrogel composites. In preparation

In addition, I confirm that the *in vitro* cell experiments and related data/images in Chapter 5 are conducted and provided by Dr. Olivier Guillaume from AO Research Institute Davos, Switzerland.

Acknowledgements

First of all, I would like to express my sincerest gratitude to my supervisors Prof. Ton Peijs and Dr. Julien Gautrot, who helped me all the way through my four-year PhD degree. Thanks to their fantastic ideas, knowledge, research experience and guidance, I was able to start working on this interesting project, make progress and finally finish my work. By no means could I complete my PhD study without their assistance. I would also like to thank those lab technicians in Queen Mary University of London, especially Dr. Alice Williams, Mr. Chris Mole, Mr. Maurizio Leo, Mr. Shafir Iqbal, Mr. Russell Bailey, Dr. Ben Milsom for their supports during my work in the various labs.

I would like to thank all the partners from the EU funded Rapidos project. Thanks are given to Prof. Dirk Grijpma and Mr. Mike Geven from University of Twente, Netherlands for collaborating with me in developing polymeric composites biomaterials. I also greatly appreciate the in-vitro cell tests done by Dr. Olivier Guillaume and Dr. David Eglin from AO Research Institute Davos, Switzerland. Prof. Lin Qing, Dr. Xinluan Wang and Dr. Yuxiao Lai from Shenzhen Institute of Advanced Technology, China as well as Prof. Tingting Tang from Shanghai Jiaotong University, China are also thanked for their valuable discussions and generous supports.

My appreciation also goes to my friends and group members in SEMS. I want to thank Dr. Olivier Picot, Dr. Han Zhang, Dr. Guangchang Wu, Dr. Maria Crespo-Ribadeneyra, Dr. Burcu Colak, Dexu Kong, Pei Tang, Khai Duong Quang Nguyen, Stefania Di Cio, Danyang Li, Fan Wu, Oliver Brooks, William Megone, Dong Luo, Yaqi You, Yi Liu, Dr. Rui Mao, Dr. Fengfeng Zhang, Wenjun Sun. Yet there are so many others who are not mentioned here. Their company and support are most important during my PhD life in SEMS.

Finally I want to thank my wife Zhang Li and parents for their understanding and encouragements. It is their absolute trust and selfless support that held me strong in hard times.

Abstract

Due to their unique structure and flexible choice of materials, electrospun degradable and biocompatible polymer fibres are considered to be extremely suitable for biomedical applications such as tissue engineering and drug delivery, either on their own or integrated within composites. Conventional electrospun fibre composites are typically based on non-woven mats and therefore limited to simple-curved geometries (films, membranes, etc.). For aqueous composites such as hydrogels, the hydrophobicity of the materials sometimes prohibits fibres to be easily integrated or distributed in these composites.

In this thesis, a review on the topic is firstly presented in Chapter 2, introducing and discussing engineering of electrospun fibre as well as their biomedical applications. In Chapter 3, electrospun polylactide (PLA) fibres reinforced poly(trimethylene carbonate) (PTMC) composites are prepared. The composites are loaded with both continuous and short PLA fibres, achieving significant mechanical enhancement and offering opportunities to produce composites conveniently using liquid formulations. Chapter 4 presents the development of shape memory polymer composites based on a combination of PLA fibres and a PTMC matrix. By loading different amounts of short fibres with different aspect ratios or by using plasticisers, the shape memory behaviour is modulated; and composites of more complex geometries are produced. In Chapter 5, PTMC-PLA fibre composites are made into drug release system. Dexamethasone-loaded PLA fibres are integrated into a PTMC matrix, showing sustained drug release and stimulating stem cell osteogenic differentiation. This concept gives promise to loading various drugs into photo-crosslinked structures without denaturation. In Chapter 6, electrospun PLA fibres are functionalized by amphiphilic block copolymer polylactide-block-poly[2-(dimethylamino)ethyl methacrylate] (PLA-b-PDMAEMA) for the development of carboxymethylcellulose composites hydrogels. Functionalization of PLA fibres not only allows for easy integration and dispersion into the hydrogel, but also enhances the interfacial bonding between fibre and hydrogel. In the last chapter (Chapter 7), some conclusions are drawn and future works are discussed.

Table of Contents

List of Abbreviations

AFM	Atomic force microscope
AIN	Aluminum nitride
ALP	Alkaline phosphatas
ARS	Alizarin red staining
BCP	Block-co-polymer
BN	Boron nitride
CMC	Carboxy-methyl-cellulose
DCM	Dichloromethane
DMA	Dynamic mechanical analysis
DMAP	4-(Dimethylamino) pyridine
DMF	Dimethylformamide
DMSO	Dimethyl sulfoxide
DSA	Drop shape analysis
DSC	Differential scanning calorimetry
GPC	Gel permeation chromatography
HA	Hyaluronic acid
hBMSCs	Human bone marrow mesenchymal stem cells
^{1}H-NMR	Proton nuclear magnetic resonance
HPLC	High performance liquid chromatography
$\overline{M_w}$	Weight average molecular weight
MWNTs	Multi-wall carbon nanotubes
OM	Osteogenic media
PAN	Polyacrylonitrile
PBS	Phosphate buffered saline
PCL	Polycaprolactone
PDEAEMA	Poly(*N,N*-diethylaminoethyl methacrylate)
PDMAEMA	Poly[2-(dimethylamino)ethyl methacrylate]
PE	Polyethylene
PEG	Poly(ethylene glycol)

PEO	Poly(ethylene oxide)
PI	Polyimide
PLA	Polylactide
PLGA	Poly(lactic-co-glycolic acid)
PLLA	Poly(L-lactic acid)
PMDETA	N,N,N’,N’’,N’’-pentamethyldiethylenetriamine
PMMA	Poly(methyl methacrylate)
pOEGMA	Poly(ethylene glycol) methyl ether methacrylate
PPDO	Poly(p-dioxanone)
PS	Polystyrene
PTMC	Poly(trimethylene carbonate)
PVA	Poly(vinyl alcohol)
PVDF	Poly(vinylidene fluoride)
PVP	Polyvinylpyrrolidone
SEM	Scanning electron microscope
SLA	Stereolithography
SMPCs	Shape memory polymer composites
TCP	Tissue culturing polystyrene
TEM	Transmission electron microscope
TFE	2,2,2-Trifluoroethanol
THF	Tetrahydrofuran

List of Figures

List of Tables

Chapter 1 - General introduction

1.1 Background and Motivation

Facile and cost-effective electrospinning has become a most popular technique for continuously fabricating one-dimensional materials on the micro or even nano-scale. Due to their large surface areas, high porosity and aspect ratio as well as flexible choice of materials, electrospun fibres have been extensively studied for biomedical applications, filtration, composites, etc. [1] Among all the areas of interests, electrospun degradable and biocompatible polymer fibres are considered to be extremely suitable for biomedical applications such as tissue engineering and drug delivery, either on their own or integrated within composites. Electrospun fibres in composite biomaterials not only perform as structural reinforcements but also introduce novel properties such as electrical, thermal, biological, environment responsive, etc. [2-6] However, due to the fabrication process and fibre entanglement, conventional electrospun fibre based composites are typically limited to simple-curved geometries (films, membranes or multilayer structure). Moreover, the fibre entanglements present in electrospun fibre mats can severely hamper composites fabrication. For aqueous composites such as hydrogels, the hydrophobicity of the materials sometimes prohibits fibres to be easily integrated or well distributed in the resulting composites.

Poly(trimethylene carbonate) (PTMC) is a biocompatible and degradable polymer material that can be synthesized via a ring-opening reaction of 1,3-trimethylene carbonate [7]. Its degradation, mediated by a surface-erosion mechanism, is characterized by an extremely low level of non-enzymatic hydrolysis and non-acidic degradation by-products, which makes PTMC an attractive material for biological applications [8]. *In vitro* degradation of PTMC in the absence of enzymes showed only less than 2 wt% mass loss after 8 weeks tests and was independent of pH [9]. In contrast, lipases from *Candida antarctica* and *Thermomyces lanuginosus* have been reported to effectively degrade PTMC in surface-erosion mode, producing by-products including TMC monomer, oligomers and 1,3-propane diol [9, 10]. It was also reported that macrophages, which could secret hydrolytic enzymes (e.g., cholesterol esterase)

and oxidative species, were able to erode PTMC rapidly [11]. In addition, the hydrophilicity of PTMC is also affecting degradation rate with hydrobobic PTMC having faster degradation rate. Moreover, stereolithography (SLA) is a common additive manufacturing technique employed to build PTMC-based structures with unprecedented degree of precision in the control of three-dimensional architectures [12], making PTMC a very attractive material for tissue engineering and drug delivery applications. However, PTMC is usually considered to have poor mechanical performance, which limits it from certain usages that require good dimensional stability. The UV-curing fabrication process intrinsically restricts the potential of the SLA-fabricated PTMC scaffolds to be used as drug delivery carriers, due to many bioactive compounds' light sensitivity, chemical UV cross-reaction and incompatibility between the therapeutics and PTMC.

Therefore, it is proposed in this work to combine electrospun poly(lactic acid) (PLA) fibres and UV-crosslinkable PTMC macromers to produce PLA fibre reinforced PTMC composites. PLA is a well-established biodegradable polymer used for food packaging as well as for the design of implants [13]. It can be derived from renewable resources, is fully degradable, and much stiffer and stronger than PTMC. The incorporation of PLA fibres is thus considered to be able to enhance the mechanical performance of PTMC. To tackle some of the electrospun fibre reinforced composite fabrication issues (fibre entanglements, reinforcement geometry limitation, etc.), we developed short fibre reinforced PTMC/PLA composites by cutting as-spun PLA fibres, allowing for the composites to be processed using flow moulding techniques. The use of short nanofibres is particularly important to enable 3D processing technologies such as injection moulding or SLA to generate polymer-polymer composites with precise, tailored and complex shapes.

To enable bioactive compounds (e.g., drugs) to be loaded into UV-crosslinkable PTMC without denaturation, we propose to use PLA fibres as a protection medium to isolate drugs from direct contact with PTMC. A model drug (dexamethasone) is electrospun with PLA to produce bioactive fibres and these fibres are incorporated into PTMC. By doing this, not only the mechanical performance of PTMC is improved, but also the drug is prevented from cross-reactions with PTMC macromers during UV curing.

Finally, to enable hydrophobic PLA fibres to be integrated into aqueous phases like hydrogels, an amphiphilic block copolymer (BCP) polylactide-block-poly[2-(dimethylamino)ethyl methacrylate] (PLA-b-PDMAEMA) is employed to functionalize PLA fibres. By introducing PLA based amphiphilic block copolymers, the hydrophilicity of PLA fibres is increased, which allows for an easy incorporation into the hydrogel. The functionalization is believed to improve the wetting and interaction between fibres and hydrogels. Furthermore, the use of functionalized short PLA fibres allowed the mechanical properties of the composites being modulated. Moreover, such liquid composite formulations (chopped PLA fibres together with hydrogel precursor solution) also offer the opportunity for the design of injectable systems.

1.2 Thesis Outline

In this thesis, a review on the topic is firstly presented in Chapter 2, introducing and discussing morphological engineering and functionalization of electrospun fibre as well as their biomedical applications. In Chapter 3, electrospun PLA fibre reinforced PTMC composites were prepared. Two different techniques for cutting electrospun PLA fibres were developed and compared. The interaction between fibres and PTMC was characterized and the thermo-mechanical properties of composites (containing both continuous and short fibres) were investigated. In addition, the experimental data was evaluated using a modified rule of mixture.

Chapter 4 presents the development of shape memory polymer composites (SMPCs) based on a combination of PLA fibres and a PTMC matrix (from Chapter 3). The shape memory properties were modulated by varying fibre aspect ratios, fibre loading, molecular weight of PTMC, and the use of plasticiser. The properties of different samples were investigated and their shape fixing and recovery efficiency for each condition were evaluated. Finally, some shape memory composites with more complex geometries were produced using short fibres.

In Chapter 5, PTMC/PLA fibre composites are designed for drug release systems. A model drug (dexamethasone, Dexa) was co-electrospun with PLA to produce bioactive fibres. These fibres were integrated into PTMC macromer followed by UV-curing to generate dexamethasone-loaded PTMC/PLA composite structure. The composites'

physiochemical properties and Dexa release profile were characterized. The bioactivity of Dexa was further confirmed by *in-vitro* cell experiment.

In Chapter 6, electrospun PLA fibres were functionalized by PLA-b-PDMAEMA for carboxymethylcellulose (CMC) composites hydrogel. PLA-b-PDMAEMA with different PDMAEMA content was synthesized. The impact of PDMAEMA content on PLA hydrophilicity was evaluated. Both continuous and discontinuous functionalized fibres were employed for CMC composite hydrogels and their influences on hydrogel's mechanical properties were investigated. In the final chapter (Chapter 7), some conclusions are drawn and potential future works are discussed.

Chapter 2 - Nanoengineered electrospun fibres and their biomedical applications

2.1 Introduction

Nanoengineering refers to the engineering at the nano-scale. Materials engineered at the nano scale possess fundamental difference compared to macro-scale materials due to their size effect. Their extraordinary properties have been investigated and applied to chemical, physical and biological areas [14-16]. For example, Ma et al. designed non-metal flexible oxygen electrodes of excellent performance by growing phosphorous-doped graphitic carbon nitride on carbon-fibre paper [17]. Berthelot et al. fabricated nano-tweezers (metal-coated optical fibre with bowtie nano-aperture) that were able to trap and manipulate 50 nm sized nanoparticles [18]. Gujrati et al. reported preparation of bacterial outer membrane vesicles with low immunogenicity and cancer cell targeting properties [19]. When searching literatures, many cutting-edge nanostructures are achieved by either spontaneous or directed assembly [20, 21]. Among different nanostructures, 1D nanomaterials like nanotubes, nanorods and nanowires (to name a few) have been extensively reported and applied to mechanics, electronics and energy realm [22-25]. Synthesis of these 1D nanostructures usually requires bottom-up techniques, which provide people with fascinating ways to exploit nanotechnology. On the other hand, most bottom-up manufacturing processes are nevertheless considered to induce high costs. Facile and cost-effective top-down methods like electrospinning are therefore becoming an attractive alternative in producing 1D nanomaterials. In addition, electrospinning is able to produce continuous fibres, which is difficult to realise via other bottom-up method. Electrospun fibres have been widely reported as wound dressing or tissue engineering scaffolds in literature [6, 26-28]. Since first being developed in 1934, electrospinning has become a convenient and easy way to produce micro or nano scale fibres, with over two thousand papers on electrospinning-related topics published every year since 2014 (see Figure 2.1). During a typical electrospinning process, polymer solution or melt is supplied to a spinning tip or spinneret at constant rate. A droplet is formed at the spinning tip and a high voltage

is applied to the spinneret which accumulates charges on the droplet to form a Taylor cone when the electrostatic force is sufficient to overcome the droplet surface tension. A fluid jet is ejected from the Taylor cone tip towards a grounded collector, during which the fluid jet solidifies and forms fibres. Randomly distributed fibre mats are obtained on a static collector while oriented fibres are achieved on specific rotating collectors [29-31] or by using auxiliary setups and post-processing [32, 33]. Electrospinning is optimised by controlling parameters like solution/melt viscosity, feeding rate and electric field. High viscosity and slow feeding rate will result in spinneret blockage while low viscosity and high feeding rate will lead to discontinuity of fibres or droplets. The electric field has to be properly set as a high field strength will decrease the time for fluid jets to solidify while low field strength is unable to form a Taylor cone. Ambient conditions like temperature and humidity are also to some degree influencing electrospinning [34].

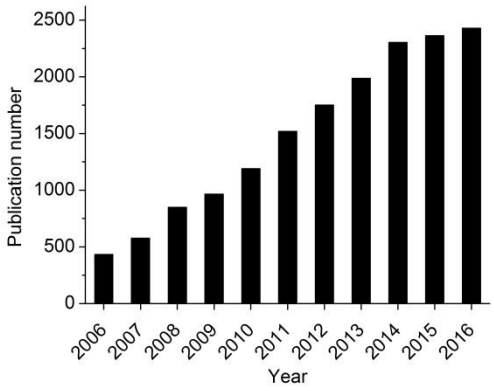

Figure 2.1 *Number of publications on electrospinning topic since 2006 to 2016 (source: Web of Science, key word: electrospinning).*

The electrospinning technique has been extensively studied. Many reviews that comprehensively summarize electrospinning processing technique and applications have been published previously [35-38]. However, reviews on the nanoengineering and application of nanostructured electrospun fibres are relatively difficult to find. Zhang and Yu reviewed the fabrication of nanoparticle-electrospun fibre composites, in which they summarized different techniques to obtain anisotropic fibres with nano-features using nanoparticles as well as their applications for energy, mechanics and sensors [39].

The incorporation of nanoparticles has introduced significantly interesting nanostructures and novel properties into conventional electrospun fibres. In addition to using nanoparticles, nanoengineered electrospun fibres can be obtained by developing new electrospinning techniques or functionalization. In this chapter, we first discuss different nanoengineering techniques for electrospun fibres; then we introduce the application of these fibres and finally conclude with some perspective on future work.

2.2 Nanoengineering of Electrospun Fibres

2.2.1 Modification on electrospinning set-up and experimental conditions

Traditional electrospinning is optimised by appropriately selecting experimental parameters, including spinning solution/melt viscosity, electrical field, feeding rate, ambient condition as well as the intrinsic properties of the polymer/solvent. Changes in parameters can result in fibre defects or even failure to spin fibres. However, it was found that through tuning these parameters, fibres with nanostructures were obtained. Over a decade ago, people have successfully electrospun fibres with nano-size pores by using highly volatility solvents [40, 41]. Formation of porous structure was explained by rapid phase separation during electrospinning, which generated solvent rich areas that later transformed into pores. It was also believed to be concerned with water in the air that formed water droplet on rapidly-cooled spinning jets due to solvent evaporation. In addition to porous structures, by using specific solvent combinations, hierarchical nanostructured fibres were fabricated [42]. Nanoporous electrospun fibres were also achieved by using lower molecular weights. Lin and colleagues electrospun different molecular weight polystyrene (PS) and they found that decreasing molecular weight led to porous nanostructures [43]. They believed that lower molecular weight accelerated solvent evaporation and diffusion and further caused rapid phase separation on the fluid jet surface. Using selective solvents, they were also able to generate other secondary surface textures in addition to pores. Liu et al. electrospun PS fibres with grooved surface textures by using a series of solvent system [44]. The grooved textures were considered to be attributed to surface void-stretching, wrinkle stretching, or collapse jet stretching. Ambient conditions (temperature and humidity) are also known to affect electrospun fibre's nanostructured surfaces [45]. Temperature is influencing

solvent evaporation rate while humidity is determining the imprints left by water droplets on the fluid jet surface. Some nanostructured electrospun fibres are presented in Figure 2.2. Although manipulating electrospinning parameters seems an easy way of obtaining nanostructured electrospun fibres, the nanostructures it offers are relatively limited and less reproducible. More precise control and quantification of the nanostructures are still yet to be achieved.

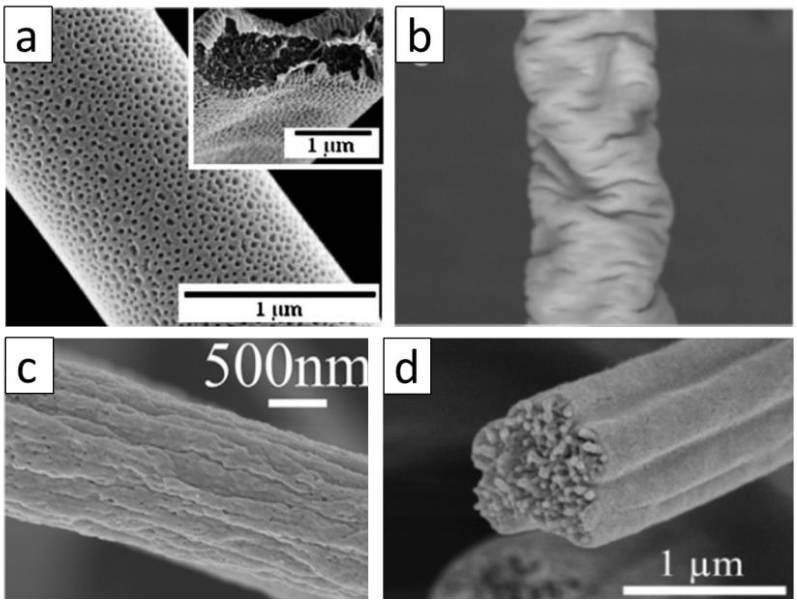

Figure 2.2 (*a) SEM image of electrospun PS fibres from 20% PS solution in THF, spinning at 4 ml/h, 20 kV and 15 cm distance (adapted from ref [43]); (b) SEM image of electrospun PS fibres from 15% PS solution in BuOH/DCM 1/3, spinning at 1.5 ml/h, 12 kV and 15 cm distance (adapted from ref [44]); (c) SEM image of electrospun PMMA fibres from 12 wt% PMMA solution in N,N-dimethylacetamide/acetone 6/4, spinning at 0.8 ml/h, 15 kV and 15 cm distance (adapted from ref [42]); (d) SEM image of electrospun PS fibres from 15% PS solution in THF/DMF 1/1, spinning at 1.5 ml/h, 12 kV and 15 cm distance (adapted from ref [44]).*

In addition to manipulating electrospinning parameters, using specific electrospinning setups also renders nanostructured fibres. Schematics showing specific electrospinning setups and their produced fibres are shown in Figure 2.3. Co-axial electrospinning is the electrospinning technique in which two immiscible liquids are supplied through a coaxial, two capillary spinneret respectively. Both the core and shell fluid are

undergoing the bending instability and elongated at the same magnitude and finally form continuous core-shell structured fibres [46]. Core-shell electrospun fibres were also obtained by free surface electrospinning where wired electrodes are placed in a liquid bath consisting of two immiscible liquid layers [47]. Multichannel tubular structures can be produced by feeding two immiscible fluids separately through an inner and outer capillary [48]. McCann and colleagues reported the fabrication of highly porous fibres by immersing the collector in a cryogenic liquid. Electrospun fibres were directly deposited in liquid nitrogen. The porous fibre is a result of phase separation between solvent-rich and solvent-poor areas followed by removing solvent after spinning [49]. Electrospun fibres with nanorods deposited on their surface were reported by Chen et al; they electrospun PMMA fibres on anodic aluminium oxide template and thermal-annealed PMMA fibres. PMMA was drawn into the nanopores by capillary force and nanorods formed on the fibre surface after removing the template [50]. The use of specific spinning setups allowed for the production of fibres with nanostructures which are difficult to achieve by tuning polymer solution properties or humidity/temperature. These nano-tubular structures inspired great interests and application as template, carrier, etc. Moreover, the nanostructures they built became more quantifiable and controllable. However as a result, the spinning requires a specific spinning set-up, which is not as lab-accessible as traditional electrospinning. Moreover, the spinning becomes more sensitive and difficult as more electrospinning factors emerge. Further disadvantages also include the low output that restricts their scaled-up production.

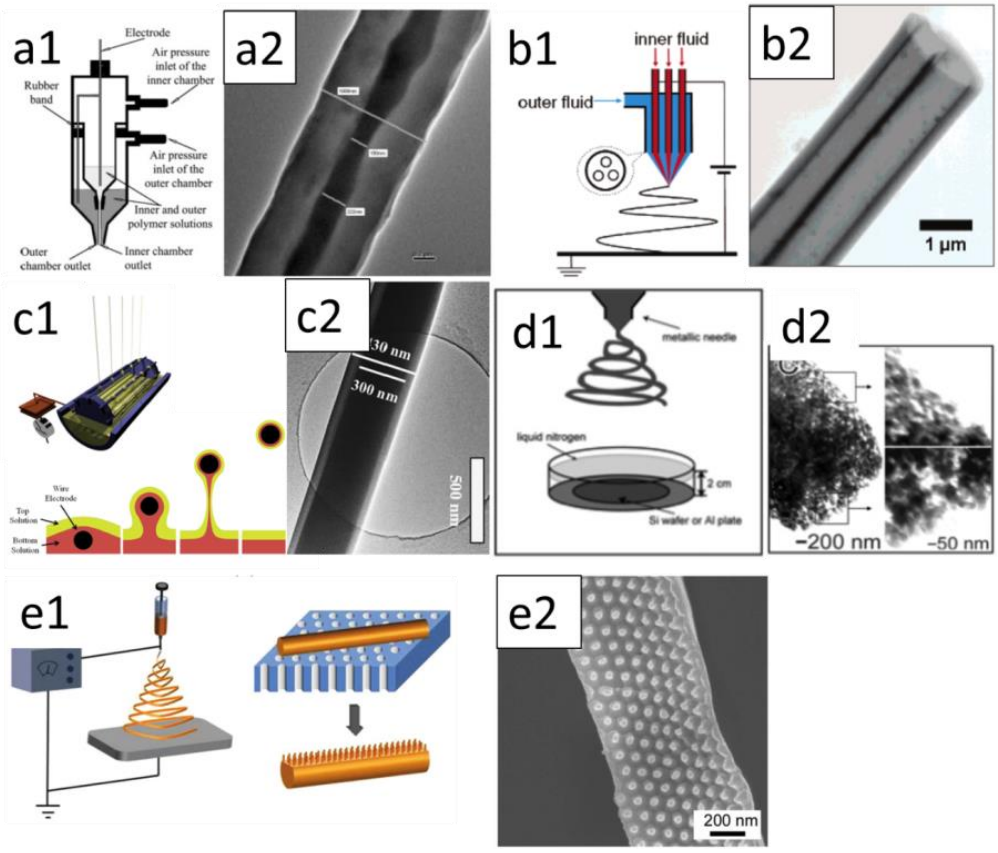

Figure 2.3 (*a1) Co-axial electrospinning and (a2) TEM image of core-shell electrospun fibre (adapted from ref [46]); (b1) multichannel electrospinning and (b2) TEM image of multichannel tubular electrospun fibre (adapted from ref [48]); (c1) free surface electrospinning and (c2) TEM image of core-shell electrospun fibre (adapted from ref [47]); (d1) electrospinning in cryogenic liquid and (d2) TEM image of electrospun porous fibre (adapted from ref [49]); (e1) electrospun fibre with nanorods structure and (e2) SEM image of fibre (adapted from ref [50]).*

2.2.2 Post-processing on electrospun fibre

Instead of directly electrospun nanostructured fibre, post-processing has also proven to be a powerful tool of creating secondary structures on normal electrospun fibres. Some previously reported techniques that introducing nanostructure are shown in Figure 2.4. It was found that by drawing electrospun fibres, ripple-like features can occur on fibre surfaces. The features are considered to occur due to the mismatch of Poisson's ratio between the fibre's dense glassy core and flexible rubbery shell [51, 52]. Non-spherical cross-section fibres were obtained by pressing at elevated temperature using flat or

nano-patterned substrates [53]. Hollow fibres are produced by removing core material from core-shell electrospun fibres. Müller et al. prepared hollow PE fibres by removing the PVA core from core-shell electrospun PVA/PE fibres. It is worth noting that the core-shell structured PVA/PE fibres they used were fabricated by electrospinning PVA fibres followed by PE polymerization on the PVA fibre surface [54]. This not only produces hollow fibres, but also provides a new route of building core-shell structures. Rather than polymerization on fibre surfaces, Haider et al. performed atomic layer deposition and successfully fabricated AIN/BN bi-shell hollow nanofibres. The bi-shell hollow structure was achieved by first electrospinning nylon 6,6 fibres followed by atomic layer deposition before calcination to remove polymeric core [55]. Saetia et al. deposited multi-wall carbon nanotubes (MWNTs) on electrospun fibres using a layer-by-layer assembly of opposite-charged MWNTs, building multi-layer MWNT coatings on fibre surfaces [56]. A shish-kebab structure was formed by electrospinning and subsequent crystallization. Jing et al. reported the fabrication of shish-kebab structured PCL fibres decorated with chitosan-PCL copolymers. The introduction of biomolecules and topography showed enhanced cell attachment and viability [57]. Chemical modification is also considered to be a facile way of achieving nanostructured fibres. Che et al. reported electrospun fibres of PMMA-co-PDEAEMA whose surface roughness was modified by exposure to CO_2 [58]. Devarayan et al. produced fibres with nanospicules structure by treating electrospun cellulose fibres with NaOH and aluminium foil. The nanospicules were believed to be caused by the elemental hydrogen that generated from NaOH-aluminium corrosion, destructing the glycoside bonds in the cellulose backbone [59]. In addition, electrospun fibre surface textures can also be developed by plasma treatment, chemical etching or photo-embossing [60-62]. Hughes-Brittain et al. introduced relief texture onto electrospun fibres by electrospinning of photopolymer blends followed by photoembossing using interference of two coherent UV laser beam and thermal development [62]. Post-processing provides alternative ways to add nanofeatures to electrospun fibres. Using post-processing, it becomes possible to improve nanostructured fibres' output by using conventional electrospinning combined with additional treatments. Novel surface topography can be engineered on electrospun fibres in a relatively easy manner. However, limitations still exist. For most hollow fibres, they still depend strongly on the co-axial electrospinning technique. Polymerization or coating can be used to achieve core-shell structure, but it there is a concern that the process (and also other treatment)

are likely to damage the electrospun fibre's initial properties or integrity (such as continuity), while their efficiency is also considered to be relatively low.

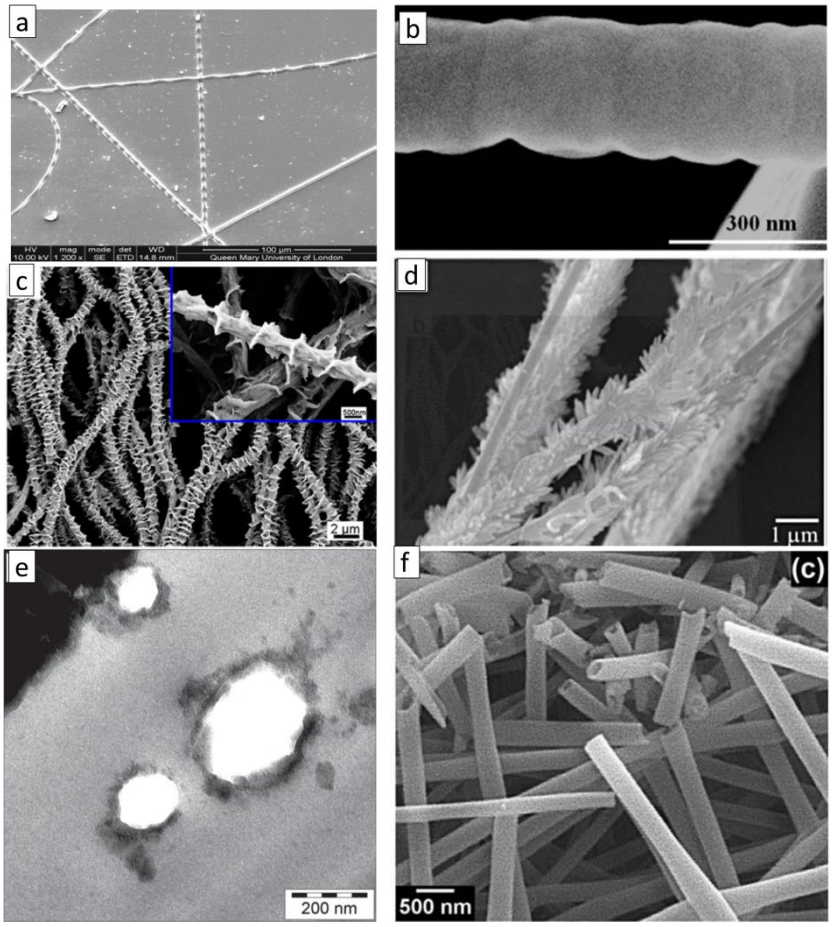

Figure 2.4 *(a) SEM image of fibres with relief texture, produced by photoembossing (adapted from [62]); (b) surface morphology of fast drawn PAN nanofibre (adapted from [51]); (c) SEM image of PCL fibre decorated with shish-kebab nanostructure (adapted from ref [57]); (d) SEM image of electrospun cellulose nanofibre using 0.1 M NaOH solution (adapted from ref [59]);* ***(****e) TEM image of hollow ultra-high molecular weight PE nanofibres (adapted from ref [54]); (f) SEM image of aluminium nitride hollow nanofibres synthesized by depositing aluminium nitride followed by calcination (adapted from ref [55]).*

2.2.3 Emulsion electrospinning

Most of the core-shell or multichannel electrospun nanofibres described above depend on either specifically-designed spinnerets or coating techniques, whose fabrication

process is complicated compared to conventional electrospinning. Thus emulsion electrospinning was developed, during which the dispersion droplets are spun from polymer solutions into fibres. The dispersion droplets also undergo stretch and elongation similar to the main spinning fluid jet. Chen's group produced porous electrospun TiO_2 fibres by electrospinning an emulsion of metal alkoxide (continuous phase) and paraffin oil (dispersed phase) followed by calcination (see Figure 2.5 a) [63]. The pore sizes varied from nano to macro-scale, which was a result of demulsification and merging of small dispersion droplets. Due to stretching during electrospinning, the pores are also oriented along the fibre direction with lengths up to hundreds of nanometres. Wang et al. electrospun core-shell fibres by using emulsions consisting of PS/limonene (continuous phase) and bovine serum (dispersed phase). The relationship between fibre morphologies and polymer molecular weight were investigated [64]. They found by using higher molecular weight PS, that the viscosity of the organic phase increased and emulsion droplet movement became retarded. Therefore droplets were likely to be located close to or even absorbed onto the fibre surface (see Figure 2.5 b). Emulsion electrospinning enables fabrication of core-shell or multi-channel nanostructures in fibres without using any auxiliary equipment or complex spinnerets. Fibres with hierarchical structures can be achieved after removing one or more components. Emulsion electrospinning is also considered to be a safe method for biomedical applications, especially when encapsulating biomolecules in emulsion droplets. By separating biomolecules from harmful electrospinning solvent, it significantly decreases the potential of contamination to biomolecules or even further danger in bio-related applications. The main issue of emulsion electrospinning is concerned with the stability of the emulsion. They are kinetically stable although after a certain time destabilization occurs via various mechanism and finally separate into different phases [65]. Moreover, challenges still exist in the control over emulsion size, especially to obtain nano-emulsions and their size distribution. Highly stable and size-controlled nano-emulsions are desired in order to optimise emulsion electrospinning for nanostructured fibres.

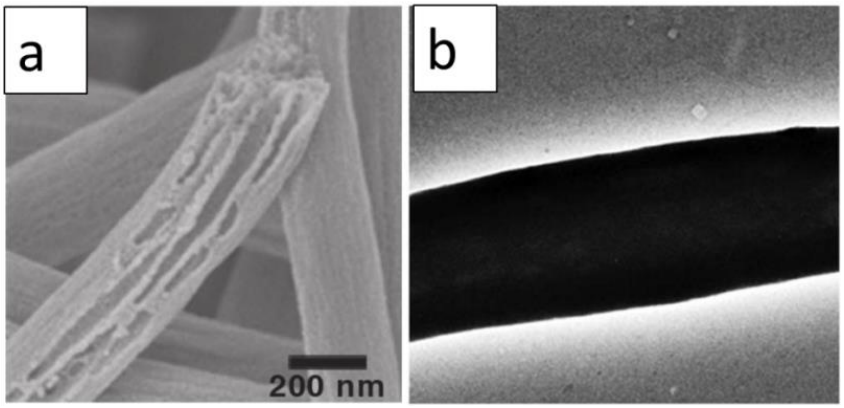

Figure 2.5 (*a) SEM image of porous TiO2 fibre via emulsion electrospinning (adapted from ref [63]); (b) TEM image of core-shell fibre via emulsion electrospinning (image size 2×2 µm, adapted from ref [64]).*

2.2.4 Phase-separation electrospinning

In contrast to emulsion electrospinning, in which phase separation means destabilization of emulsion systems, phase-separation electrospinning is a spinning technique that uses phase separation to fabricate internal structures within fibres. Wang developed core-shell electrospun fibres by spinning homogeneous solutions followed by thermally induced phase separation of PVP/PVDF (Figure 2.6 a) [66]. The core/shell material is determined by component surface energy and blending ratio. Components with lower surface energy are advantageous in the migration to fibre surface during electrospinning. Another approach to achieve porous fibres is known as non-solvent induced phase separation, which involves the use of a combination of a good solvent and non-solvent to induce thermodynamic instability during electrospinning. Katsogiannis et al. electrospun porous PCL fibres using PCL chloroform/DMSO solution [67]. The precipitation of a PCL-rich phase formed the main fibre while the PCL-poor phase formed cavities. Compared with humidity induced porosity, this method has easier control over fibre morphology. Nayani and his group directly electrospun fibres into a non-solvent bath. The solvent exchange between residual solvent in fibre and non-solvent was found to give porous fibres [68]. It was also found that the electrical field could enhance phase separation of electrolyte based solutions during electrospinning. Chen et al. designed glass spinnerets with a high gradient electric potential applied inside the spinneret (schematic shown in Figure 2.6 c), which drove hyaluronic acid molecules towards the opposite direction of the electric

field and formed the core [69]. Using this modified spinneret, they obtained core-shell structured PEO/HA nanofibres. It was also reported that multi-jet structured electrospun fibres were prepared via phase separation [70]. Phase separation electrospinning is a simple way of producing nanostructured fibres which usually does not require specifically designed equipment or complicated processing. By electrospinning homogeneous polymer solutions like conventional electrospinning, nanostructures are achieved. However, according to what has been reported, only limited numbers of morphologies were produced. Moreover, phase separation electrospinning only applies to certain material combinations or solvent systems; while the size of the phase-separated morphology is highly depended on rapid solvent evaporation and usually cannot reach <10 nm.

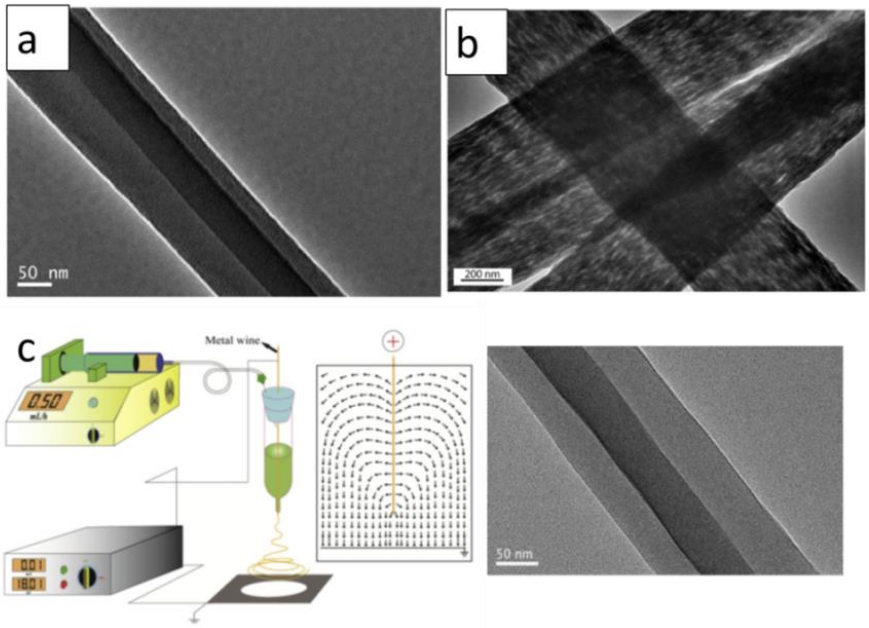

Figure 2.6 (*a) TEM image of PVP/PVDF core-shell nanofibres via electrospinning (PVDF/PVP=1/3) (adapted from [66]); (b) TEM image of highly porous PAN fibres by electrospinning into non-solvent bath (adapted from [68]); (c) schematic showing the electric field induced phase separation during electrospinning and the core-shell PEO/HA fibres (adapted from [69]).*

2.2.5 Electrospinning of block copolymers

Block copolymers (BCP) are polymers which contain two or more chemically distinct blocks. These blocks are connected with each other by covalent bonds and together

they form a BCP. Because of the various properties of each block composing the molecule, BCP shows many special properties and have been used in different areas for a long time. Acrylonitrile butadiene styrene (ABS) is one well-known BCP, where the butadiene block forms the continuous phase while acrylonitrile and styrene blocks form the dispersed phase. This structure brings ABS good impact resistance and toughness and makes it widely used in daily life, such as pipe systems, automotive body panels, kitchen appliance, toys etc. Therefore, an attractive property of bulk BCP is its ability to have phase separation between distinct blocks, resulting in unique internal morphologies. The phase separation is induced by the thermodynamic incompatibility between blocks. If two blocks are immiscible with each other, the incompatibility tends to drive the same blocks to assemble and produce domains made up of one block material. In fact, it is also a procedure to maximize the interaction between the same blocks while minimizing the interaction between immiscible blocks [71]. However at the same time, this process is also prevented by the covalent bonds that connect the blocks. For linear A-B type BCPs, several factors were found to decide its micro-phase behaviour. The most important one is the Flory-Huggins interaction parameter χ, which is related to temperature and describes the free energy cost of contact between distinct blocks [66]. BCP micro-phase separation is proved to be determined by Equation (2.1) [72],

$$\chi_{AB} = \left(\frac{Z}{k_B T}\right)\left[\varepsilon_{AB} - \left({}^{1}/_{2}\right)(\varepsilon_{AA} + \varepsilon_{BB})\right] \tag{2.1}$$

In the above equation, Z represents the number of nearest neighbour monomers to a copolymer cell; ε represents the interaction energy between monomers. A positive χ_{AB} implies the tendency of separation between block A and B; while a negative χ_{AB} implies a mixing tendency of block A and B [72]. In addition, according to the Flory-Huggins equation, high temperature (T) can lead to small χ_{AB} and favours the mixing of two blocks. The degree of polymerization (N) and single block fraction (f) are another two parameters which decide the final microstructure of the material. Based on different conditions, A-B type BCP can generally form structures varying from spherical (S) to cylindrical (C), gyroid (G) and lamellar (L). The morphology transition from S to L is found to be attributed to the combination effect of interfacial energy (enthalpic) and chain stretch (entropic) [73]. A variety of nanostructures have been achieved via BCP bulk self-assembly and applied in energy storage, lithography, etc. [74-76] Self-

assembly of BCP in solution behaves significantly different from that in bulk due to the additional interaction between BCP and solvent. Some commonly reported morphologies include micelle, rod and vesicles [77-79]. There are more complicated structures developed by BCP self-assembly in solution such as large compound micelles, large compound vesicles and hexagonally packed hollow hoops [80-82].

Due to their various self-assembly behaviour and fine size they can reach, electrospinning of BCP is considered as a promising way to introduce nanostructures in electrospun fibres, whose size is otherwise difficult to achieve using phase separation electrospinning methods as described in section 2.4. Kapllani et al. fabricated electrospun conjugated diblock copolymer nanofibres. The BCP self-assembly during electrospinning formed hierarchical structures, with lamellar morphologies oriented along the fibre axis [83]. Some electrospun BCP fibres didn't exhibit phase separation due to fast solvent evaporation, thus annealing (thermal/solvent vapour) is sometimes conducted to enhance molecules' mobility and self-assembly. Kalra et al. reported the confined self-assembly of BCP in co-axial electrospun nanofibres [84]. In their study, BCP was confined in the core layer and highly ordered lamellar morphologies were observed after thermal annealing. By using core-shell structured fibres, the inner BCP was able to be annealed at high temperature without damaging the fibre morphology. Similar work was done by Ma et al., where they observed spherical morphology in electrospun fibre after phase separation [85]. Zhao et al. electrospun photo-cleavable block copolymer PPFP(M)A-*hv*-PEO and annealed fibres in H_2O/THF atmosphere. By removing the PEO block, nanoporous fibres were obtained with elongated pores aligned parallel to fibre axis [86]. Very fine core-shell structured fibres were fabricated by Zhai and his colleagues, using PVA as the shell and anisotropic micellization of amphiphilic PEG-b-PPDO as crystallisable core [87]. According to their paper, direct electrospinning of these BCP dispersions was not possible because of micellization, which significantly decreased solution viscosity. Electrospinning of block copolymers not only produced nanostructured fibres using conventional electrospinning setups, but also provided varieties of nanostructures that either cannot or only complicated be achieved using other methods. Moreover, the fibre diameter or the confined space in core-shell fibres have an impact on phase separation, resulting in interesting morphologies and phase separation kinetics compared to thin films or bulk (see Figure 2.7). The latter, in the meantime, makes block copolymer phase separation in electrospinning more complex than in thin films. Fast solvent evaporation in

electrospinning usually prevents block copolymers from phase separation. Thermal or solvent annealing after spinning can induce phase separation, which however can alter fibre morphology. The use of core-shell structures can preserve fibre morphology but on the other hand also increases the complexity of electrospinning.

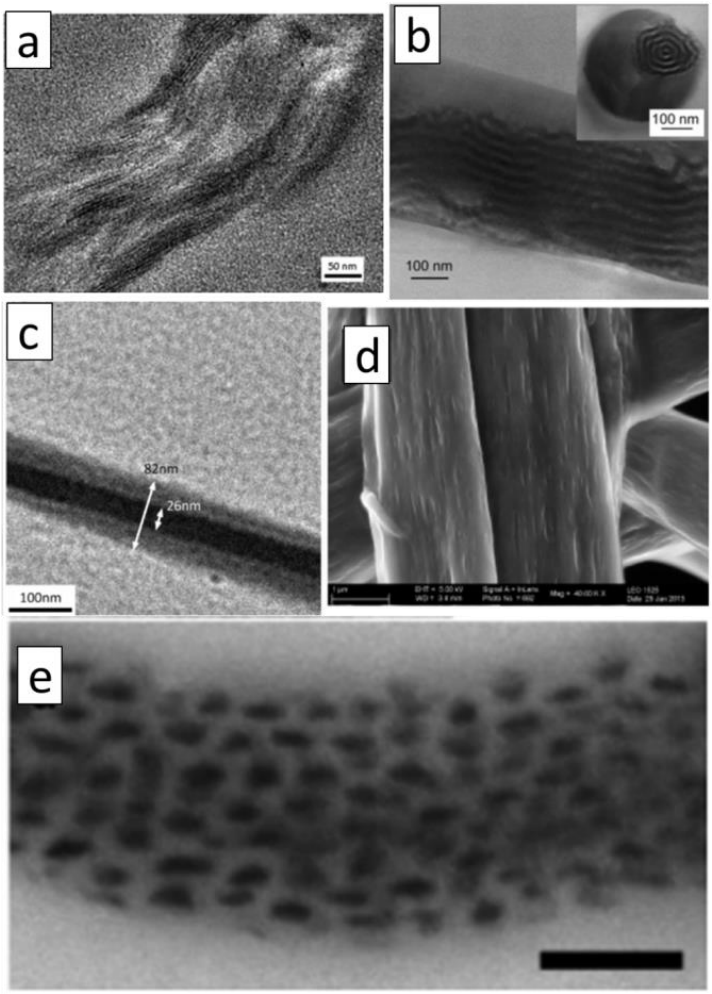

Figure 2.7 (*a) TEM image of conjugated diblock copolymer nanofibres along the fibre axis (adapted from [83]); (b) TEM image of coaxial block copolymer fibre after thermal annealing (adapted from [84]); (c) TEM image of core-shell structure fibre by block copolymer electrospinning (adapted from [87]); (d) SEM image of nanoporous fibre by electrospinning PEG based block copolymer and removing PEG (adapted from [86]); (e) TEM images of block copolymer fibre along fibre axis (scale bar 100 nm, adapted from [85]).*

2.2.6 Short electrospun fibres

In addition to adding secondary features to electrospun nanofibre, it is also of great interests to make discontinuous or short electrospun fibres. Different from electrospun fibres that are continuous, short fibres broaden the potential application area of electrospun fibres. With fewer entanglements, short fibres can be processed and manipulated much easier. For instance in the case of composites, short fibres can be incorporated in liquid formulations, which can be used to make complex geometry via compression or injection moulding; while continuous fibres reinforced composites are limited to simple-curved geometrical shapes [88]. At the right aspect-ratio, short fibres are as effective reinforcements as continuous fibres. Jiang et al. for example found that short polyimide (PI) fibres could provide similar reinforcement as continuous fibres in self-reinforced PI composites [89]. Short fibres were found to be able to control their movement due to the absence of fibre aggregation, which allows for the design of novel devices [90, 91]. In addition, short fibre scaffolds could mimic natural structures with extremely high porosity (more than 99%), which is yet unachievable using continuous fibres [92].

Currently, several methods have been reported for producing short fibres; some of them are shown in Figure 2.8. One of the most commonly used methods is mechanical grinding [93, 94], which was considered to be a highly efficient and easy way to cut electrospun fibres. However, this method is limited to fibres made from 'stiff' materials. For 'soft' polymeric fibres, grinding can break down the fibre network but at the same time it damages the fibre morphology (elongated/crushed) due to fibre stretching and heat generated during grinding. Blender cutting in liquid media is another commonly used option for producing short chopped fibres [95]. In this technique, electrospun fibres are placed in liquid media which was then vigorously mixed using blender/mechanical stirring equipment. Fibres were chopped by a combination of mechanical cutting and shearing. In this way, 'soft' polymeric fibres could be chopped without their morphologies being damaged. One possible issue with this method is fibre aggregation and entanglement during processing even under diluted conditions, which results in a relative high fibre aspect ratio compared with grinding. Other cutting methods include ultrasonication [96, 97], in which electrospun fibres were processed in liquid media using ultrasonic excitation. The ultrasonication generates bubble cavitation followed by bubble implosion. The energy released from this implosion is

considered to cause fibre scission. It was also found that whether fibres could be cut using ultrasonication depended highly on the fibre's ductility; brittle electrospun fibres were more easily to cut than ductile fibres. In addition to mechanical cutting techniques, UV cutting has been proposed [98]. Electrospun fibres made from UV-crosslinkable polymers were exposed to UV light under a mask with aligned slits. Afterwards, the unexposed parts of the fibres were removed, producing fibre fragmentation. It was also reported that short fibres were achieved by controlled degradation followed by fragmentation [99].

Apart from post-processing, some single-step ways to fabricate short electrospun fibres were also developed. By adjusting spinning solution concentration, feeding rate and voltage, discontinuous electrospun fibres were produced instead of continuous fibres [100]. The spinning condition for discontinuous fibres was found in the transition from electrospraying to electrospinning. However, simple as it sounds, the optimal spinning condition is not easy to find since electrospraying or beads-on-string structures usually occur rather than spinning short fibres. Regev et al. found that electrospinning albumin proteins in TFE solution could generate ribbon-like short fibres. They believed that the stiffness of the fibre material could promote the occurrence of dry jet stretching [101]. The use of nanoparticles was also reported to facilitate the formation of short electrospun fibres. The surface charges on nanoparticles were found to enhance the repelling effect on the spinning jet surface, leading to jet fracture and thus discontinuous fibres [102]. Similar to controlling the electrospinning conditions, the addition of positively/negatively charged nanoparticles interrupted the competition between electrical field pull and solution push from an eternal pump. This depends on the combination of polymer solution and nanoparticles; and the addition of nanoparticles changes the fibres' initial properties. Electrospinning setups equipped with specifically designed devices such as electric spark [103] was also developed to make short fibres. The device was reported to produce both continuous and short fibres simultaneously.

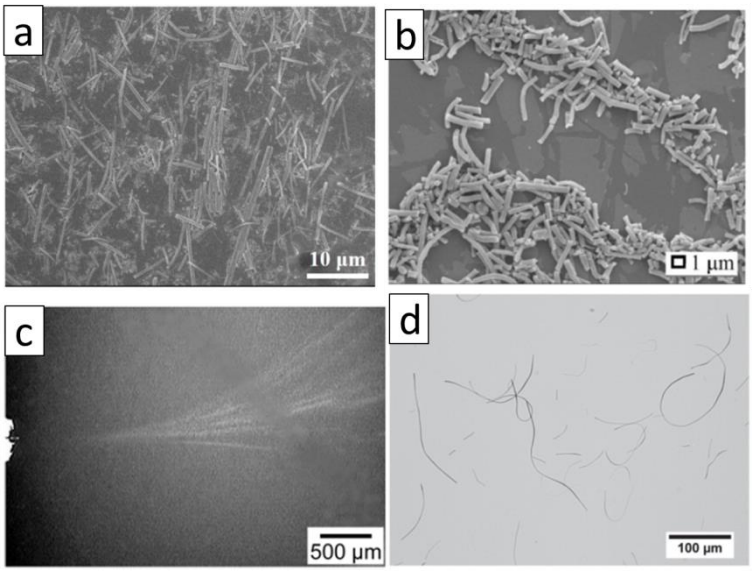

Figure 2.8 (*a) SEM image of short electrospun carbon nanofibres by grinding (adapted from [93]); (b) SEM image of short PS fibres made by ultrasonication aligned electrospun PS fibres in water (adapted from [97]); (c) photograph showing the Taylor cone condition for direct electrospun short cellulose fibres (adapted from [100]); (d) optical microscope image of short PAA nanofibre by mechanical blending (adapted from [95]).*

2.3 Functionalization of Electrospun Fibres

In addition to engineering of electrospun fibre's morphologies, another major research area of electrospinning is the production of functional electrospun fibres. Functional electrospun fibres are becoming a highly influential topic due to their novel properties and potential applications that can hardly be delivered by conventional electrospun fibres. Not only considered as an improvement/addition to conventional electrospinning techniques, functional electrospun fibres also introduced as a huge new area for researchers to explore. Functional electrospun fibres possess various properties include special morphological, chemical and biological features. A common way to achieve functional electrospun fibres is through co-electrospinning polymers with nanoparticles [39]. By incorporating nanoparticles, the properties of the nanoparticles are integrated within the electrospun fibres [104-106]. Meanwhile, the continuity and stability of electrospun fibres makes them suitable carriers for nanoparticles for a wide range of applications. In the previous part of this introduction,

modifications of the fibre's morphology also produced functionalized electrospun fibres such as emulsion electrospinning [107], core-shell electrospinning [108] etc. In this part, functional electrospun fibres using some other methods are introduced and discussed.

2.3.1 Wet chemical treatment

Wet chemical etching is a simple and straightforward technique of functionalization of electrospun fibres. This technique can modify the surface chemical properties of fibres which usually also includes the fibre's surface topography. For instance, Ma et al. [109] immersed electrospun phenolic fibres in KOH solution and finally produced functional carbon fibres after thermal treatment. The treatment of KOH solution not only increased porosity of the carbon fibres but also introduced surface oxygen species, which was considered to be promising for high-performance supercapacitors . Liu et al. surface-hydroxylated ceramic nanofibres using H_2O_2 and incorporated them into poly(vinylidene fluoride) (PVDF) matrix. The surface functionalization enhanced the interaction between fibres and PVDF matrix, which facilitated dispersion of nanofibre and crystallinity of composites [2]. Wet chemical etching is considered to be an easy treatment of electrospun fibres and changes fibre properties. However, the method is also thought to be less controllable; and the hydrophobicity of fibres also sets limitation on the etching effect provided the etchant solution is aqueous. Finally, fibre integrity and continuity can be compromised if harsh etching conditions are applied.

2.3.2 Plasma treatment

Plasma is another commonly used technique for surface modification. It involves reactive gas plasma treatment and inert gas plasma treatment [110-112]. Among reactive gas plasma treatment, oxygen gas is usually used to generate functional group such as –COOH and –OH. Generation of these functional groups not only increases the fibre's surface hydrophilicity but also provides conjugating sites to other functional molecules [112]. Inert gas has also proven to be capable of modifying the fibre surface chemistry. Cheng et al. treated electrospun PLA fibre scaffolds with Ar plasma. The treatment increased the fibre's hydrophilicity without reducing the fibre network integrity. Plasma-treated fibres also showed positive effect on cell migration on fibre scaffolds [111]. Compared with wet chemical etching, plasma etching is considered to be cleaner since it does not leave chemical residuals. Its homogeneity and easy-processing also makes this technique convenient to achieve modifications of the fibre

surface chemistry. However, maintaining the fibre's integrity while delivering sufficient functionalization remains an issue.

2.3.3 Co-electrospinning with functional additives

Functional electrospun fibres can be easily achieved by incorporating additives. Unlike wet chemical etching or plasma treatment, the use of additives not only modifies the surface chemistry but also changes the interior of the fibres. The technique integrates additive specific properties into fibres, providing more flexibility than chemical etching or plasma treatment. By combining various external factors, electrospun fibres can modify their physiochemical properties (wettability, mechanical properties etc.) [113, 114], or further exhibit unique properties like antibacterial activity [115], directive cell adhesion [116], pH-responsive behaviour [58] etc.

The large surface area and continuity of electrospun fibres makes them more suitable and efficient than other functional systems in certain applications that requires high aspect ratios [117]. The limitation of using functional additives may exist when they are not compatible with fibres or not stable during the electrospinning process. Some additives tend to aggregate on the fibre surface instead of being homogeneously distributed. One commonly encountered issue is initial burst release from electrospun fibres when fibres are loaded with drug and used in drug delivery systems [118]. The binding interaction between additives and fibres plays another important role in functional fibre properties. Weak interaction leads to losing functional additives, which means defunctionalisation of electrospun fibres. Measurements to enhance the binding and compatibility between functional additives and fibres involve the use of appropriate spinning conditions and formulations [119], adding specific binding agents [120, 121], or through covalent bonding [122].

2.3.4 Surface physical coating

Surface physical coating of electrospun fibres offers another route to obtain functional fibres. This method can be seen as a post treatment that combines fibres with external functional factors whose functionalization usually remains on the fibre surface (as indicated by their name). Compared with co-electrospinning, physical coatings preserve the fibre properties without being influenced by functional additives. Functional fibres are obtained by conventional electrospinning and following treatment. Issues like destabilization or compatibility between fibre and functional factors are therefore

eliminated. The coating process ranges from simple adsorption in solution or vapour [123] to interfacial polymerization [124], layer-by-layer coating [125], atomic layer deposition [126], etc. By using more complicated technique like layer-by-layer coating or atomic layer deposition, the coating thickness becomes controllable. Schematics showing layer-by-layer coating and atomic layer deposition are presented in Figure 2.9. Protein coating was conducted on electrospun fibres before conducting cell culture; coatings like calcium phosphate are used for promoting specific cell activities [127, 128]. Coating is also commonly used to modify the fibre's surface wettability [129]. However, physical coatings often have weak binding between the coating material and the fibre; and sometimes the functional materials cannot be directly coated. Therefore, effective methods of immobilizing functional materials on the fibre surface without impairing their conformational properties have been studied. A pre-coating or binding agent is often used when the functional materials cannot be directly coated. Here, electrospun fibres were first coated with a layer of binding agent, which will allow the immobilization of the target coating [125, 130]. On the other hand, some of previously discussed methods like core-shell electrospinning, phase-separation electrospinning can also be considered as surface coating but with better robustness.

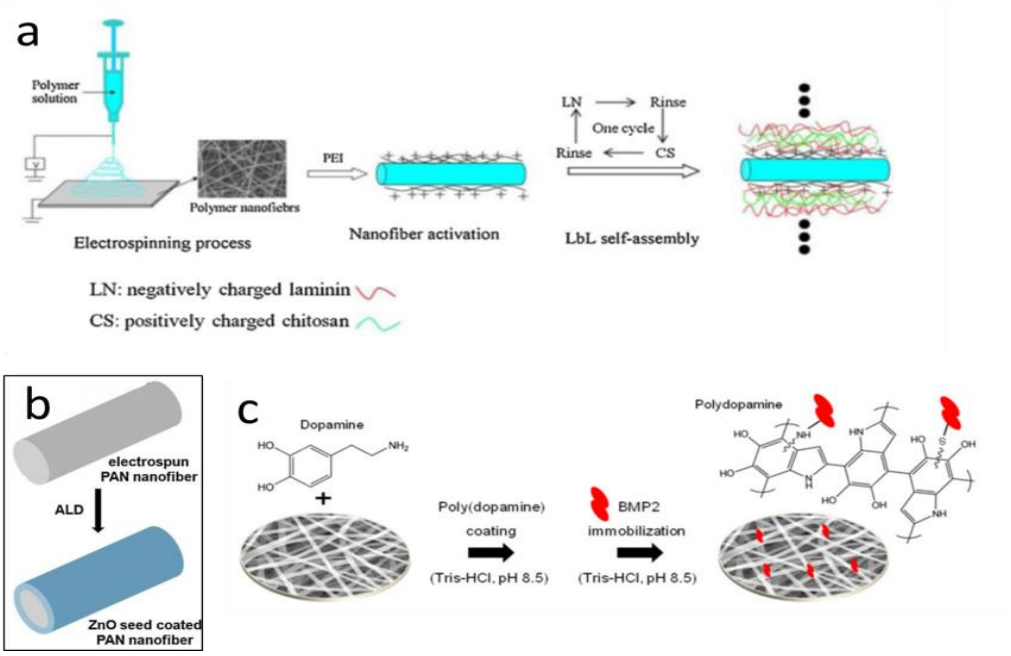

Figure 2.9 *Schematic of layer-by-layer coating laminin protein on PLLA nanofibre (a) adapted from [125]), atomic layer deposition of ZnO seed onto PAN nanofibre; (b) adapted from [126]) and polydopamine coating on PLLA fibre via interfacial polymerization of dopamine; (c) adapted from [130]).*

2.3.5 Surface covalent bonding

Surface graft or covalent bonding provides an alternative but more robust way to functionalize electrospun fibre surfaces compared with surface physical coatings. Instead of coating as-spun fibres with functional materials, this method uses covalent bonding to immobilize active molecules or directly polymerize these on fibre surfaces from small molecules. For instance, both electrospun fibres and functional materials contain reactive chemical groups; then the functional materials can be easily fixed onto the fibre surface through a reaction of fibre and functional materials (Figure 2.10 a) [131]. Alternatively, fibres with initiator groups on the surface can initiate the polymerization of monomers, generating grafted layers that covalently adhere to the fibre surface (Figure 2.10 b) [132]. Surface grafts can also be realised by pre-coating fibres with initiator groups and then polymerizing them to form a functional layer [133]. The advantage of coating via grafting is its higher stability compared to physical coatings. Molecules that are not able to coat fibres via physical interactions can be immobilized on the fibres. Various molecules can be fixed onto fibres, offering versatile

application potentials. By controlling the initiator density/distribution on the fibre surface or polymerization mechanism, the functionalization on electrospun fibres can be precisely and spatially controlled. On the other hand, chemical reaction/polymerization may involve the use of solvent and catalyst or processing under extreme conditions. Solvent and catalyst can easily remain in the fibre scaffold and may prove difficult to remove, creating potential hazard for bio-related applications; and the extreme processing conditions not only introduce difficulties but can also affect the morphological integrity and intrinsic properties of the fibres. To tackle these challenges, mild processing conditions and safe products have to be developed by improving reaction/polymerization mechanism [132, 134].

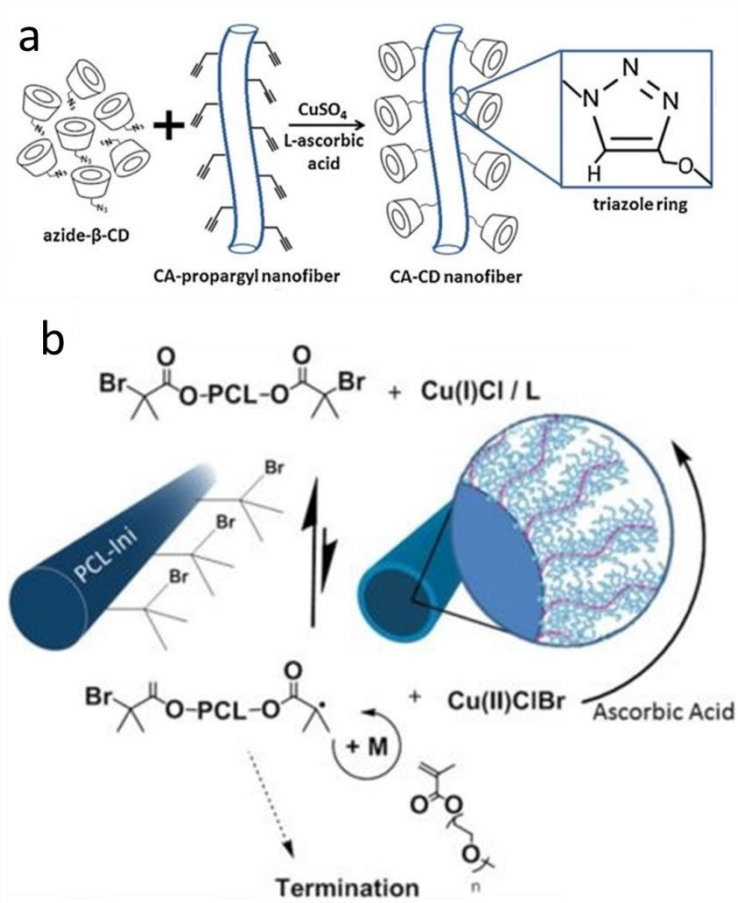

Figure 2.10 *Schematic of electrospun fibre surface modifications: (a) propargyl cellulose acetate fibres grafted with azide-β-cyclodextrins via click reaction (adapted from [131]); (b) PCL electrospun fibres grafted by pOEGMA bottlebrushes via activators regenerated by electron transfer atom transfer radical polymerization (adapted from [132]).*

2.4 Biomedical Applications of Nanoengineered Electrospun Fibres

Due to its facile fabrication, large surface area, intricate structure and other excellent properties, conventional electrospun fibres have been extensively studied and applied to a multitude of areas. A schematic illustrating applications of electrospun fibres by comparing electrospinning-relevant US patents is presented in Figure 2.11 [1]. It can be seen that the majority of patents are related to medical or bio-related areas, with nearly double the total number of patents on filtration, composites, liquid crystal devices and electromagnetic shielding. The reason why electrospinning fibres attract such great interests in bio-related studies is their potential to mimic human body environments. Most human tissues are made up of hierarchical nanofibrous structures; and electrospun fibre scaffolds show great common features with those biological structures. Therefore, electrospinning has become an important tool for biomedical applications. However, conventional electrospun fibres usually only have limited properties. By spinning different materials one can obtain fibres with a variety of properties but this sometimes cannot meet the requirements of novel techniques. Thus, conventional fibres are nanoengineered to either produce various morphologies or modify fibre properties. These nanoengineering of fibres have led to novel properties and applications like self-healing [135], heat storage [136], sensors [137], etc. In the following section, biomedical applications of nanoengineered electrospun fibres are introduced and discussed.

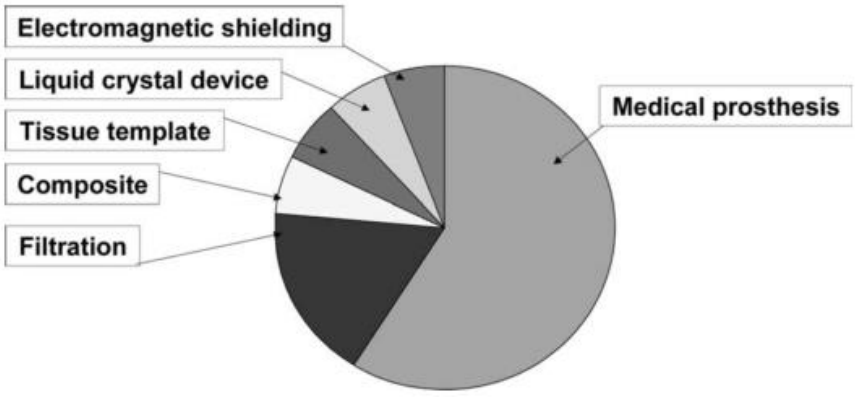

Figure 2.11 *Application of electrospun fibres by application-relevant US patents (adapted from [1]).*

2.4.1 Tissue engineering

Tissue engineering usually involves the use of biocompatible scaffolds to provide sufficient mechanical performance and suitable environment for cell growth during tissue repair [138]. Scaffolds based on electrospun fibres can provide good mechanical durability, while when using biocompatible materials these scaffolds are safe for biomedical use. The large surface area and high porosity of electrospun fibre scaffolds provides large spaces and sites for cell adhesion and growth. Recently, electrospun fibre that exhibit shape memory behaviours were reported, which could potentially produce 'smart' scaffolds [139]. Moreover, electrospun fibre scaffolds with 3D geometries were produced in addition to 2D geometries, which increased the complexity of the scaffolds [140]. Electrospun fibres have been used as scaffolds for various tissue engineering applications such as bone [141], blood vessels [142], nerves [143], cartilage [144], etc. These fibres are usually combined with growth factors to regenerate lost or damaged tissues. The fibrous structure of electrospun fibre scaffolds allows for the nutrition and waste product exchange during cell growth; and it has been quantitively studied that the fibrous architecture can indeed affect cell response [145]. It is less efficient when using conventional electrospun fibres alone as cells only show limited adhesion on scaffolds; while it is also difficult for cells to infiltrate inside these scaffolds. Protein coating/functionalization is usually conducted before seeding cells, which could enhance the adhesion of cells on scaffolds. However, the processing is time-consuming and has less control over the coating homogeneity. Thus core-shell structured electrospun fibres were developed (collagen as shell and synthetic biomaterials core). The one-step technique enabled direct fabrication of biocompatible fibrous scaffolds and more biological sites to be recognized by cells and also enhancement of the infiltration of seeded cells [146]. Hydroxyapatite (HAp) is widely used in bone tissue engineering/substitute due to its good osteoconductive and osteoinductive properties [147]. Electrospun fibres with embedded HAp nanoparticles have been extensively studied for bone tissue engineering. During bone defect repairs, screw holes are usually made and the implanted scaffolds should fit tightly inside these holes. Shape memory fibrous scaffolds have been developed, which given an appropriate trigger, can expand after implantation, enabling a tight fit as well as applying stress on the surrounding tissue (mechano-transduction effects promoting bone repairing) (Figure 2.12 b) [148]. Sometimes physical blending of nanoparticles with electrospun fibres can influence fibre wettability and roughness; while

improvements in fibre mechanical performance are merely moderate. To overcome these issues, in-situ synthesis was reported which is a rapid procedure and does not affect fibre wettability while significantly strengthening the fibre [149]. In addition to modifying the fibre's physicochemical properties, engineering of the fibre morphology is also tried for fabricating scaffolds. Recently, discontinuous gelatin fibre scaffolds with high water adsorption and elasticity were reported. The scaffolds made up of short fibres exhibited good durability in repeating compressive fatigue tests (Figure 2.12 a) [150]. Nanoengineering of electrospun fibres has shown to improve the interaction with cells as well as improve physiochemical properties. However, challenges still exist in terms of cell migration and real tissue environment mimicking. The question how to avoid cell aggregation but create an environment suitable for cells to proliferate and differentiate has to be solved. Meanwhile both sufficient physical and chemical durability of scaffolds should be maintained after engineering the fibres. Moreover, as for any clinical application, scaffolds should be easy to handle and store.

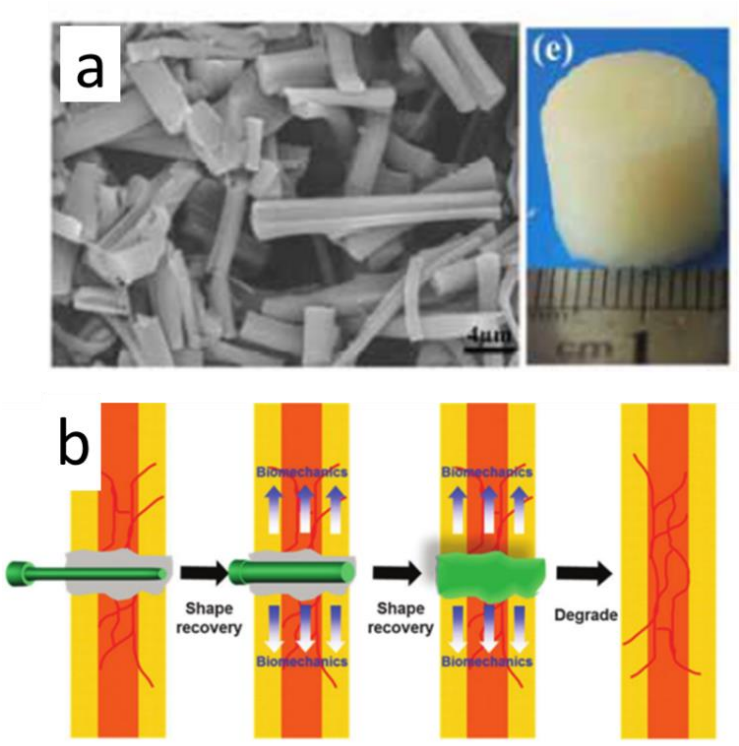

Figure 2.12 (*a) Discontinuous grooved gelatin fibres forming highly water absorption scaffolds for cartilage tissue engineering (adapted from [150]); (b) shape memory electrospun fibre (containing HAp) scaffold expands to fit the screw hole in bone repair (adapted from [148]).*

2.4.2 Drug delivery

Drug release refers to the technology or system that transports therapeutic chemical compounds within patients in a less toxic but more effective and convenient way compared with conventional dosage treatments [151]. Although the application of advanced drug release systems is only starting to become practical reality, the influence on medicine and market requirements are increasing markedly. Electrospun fibres have been widely studied as local or in-situ drug release systems. The aim of using electrospun fibres includes continuously maintaining drug release at therapeutic level over an extended or necessary duration, reducing adverse side effect on the healthy cells or tissues, and decreasing the drug intake by patients [152]. Compared with other drug carriers like liposome, electrospun fibres improved issues such as poor targeting and low drug accumulations [153]. On the other hand, using electrospun fibres for delivery therapeutic agents usually requires surgery, which causes more pain than oral/injection administration. Therefore, using degradable materials is important as they don't need a second surgery to be removed after treatment.

The most common way of preparing electrospun fibre-based drug delivery system is via co-electrospinning main fibre material with drug (one-phase electrospinning). However, as mentioned earlier, this method has potential risks including incompatibility between drug molecules and fibre material, uneven drug molecule distribution, damaging bioactivities by harsh processing conditions, etc. To avoid degradation of drugs during fibre fabrications, the drug molecules are normally loaded onto fibre surfaces after spinning via physical or covalent bonding. Physical coating of bioactive molecules on fibres offers great flexibility and could effectively protect the drug [154]. A concern with this method is that initial burst release can occur. However, according to many clinical cases, a high dosage of drug administration is necessary initially especially for anti-inflammation purposes. Similar drug loading methods includes the use of emulsion electrospinning and co-axial electrospinning [108, 155]. Moreover, drug loading can also be modulated via nanoengineering of fibre surface morphologies. By creating nano-topography on fibres (see Figure 2.13 c), the surface area is further increased, which alters the physical properties of fibres as well as increases drug adhesion sites [156]. Core-shell structured fibres can also lead to controlled drug release rate while at the same time suppressing initial burst release. In addition to changing fibre

morphology, the use of binding agents to absorb drugs or composite fibre structure is another alternative way to achieve more controlled and sustained release [157-159].

Therapeutic molecules can also be entrapped into electrospun fibre scaffolds via grafting. These molecules are immobilised onto the fibre surface via covalent bonding, which is stronger than physical adsorption and thus prevents burst release. This strategy, at the same time, can result in deactivation of therapeutic molecules [160]. In addition, the covalent connection can be cleaved under specific conditions, allowing drugs to be released upon certain environmental triggers [161]. Recently, it was reported that bacteria were grafted on electrospun fibre surfaces for gene delivery [162], which shows the great potential and flexibility of electrospun fibres as drug delivery system (Figure 2.13 b).

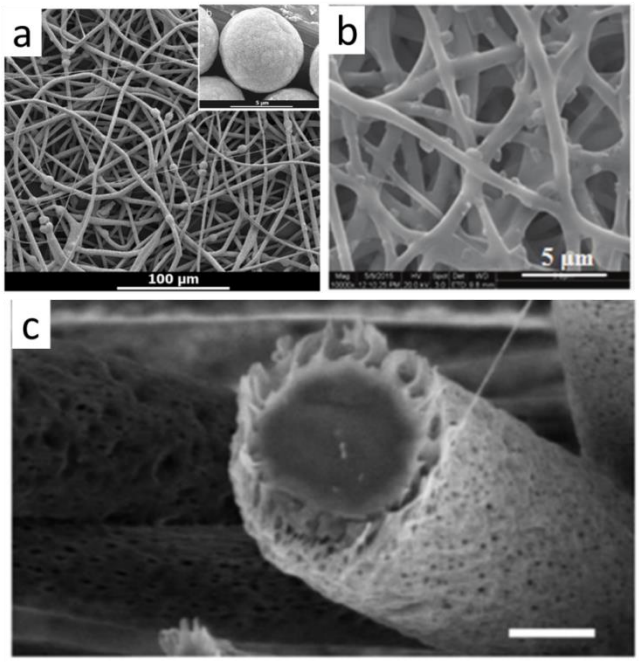

Figure 2.13 (*a) SEM image of electrospun PLGA fibre with 5% protein-loaded $CaCO_3$ particles (inserted are SEM image of protein-loaded $CaCO_3$ particles, adapted from [158]); (b) SEM image of electrospun fibres with bacterial graft for gene delivery (adapted from [162]); (c) SEM image of electrospun fibre with nanoporous superficial layer for drug delivery (scale bar 2 µm, adapted from [156]).*

2.4.3 Wound dressing

Wounds, especially chronic wounds, can be easily contaminated by external environments or sources, thus suffering from persistent inflammatory stimuli and immune response that delay the wound healing process. Wound dressing is a widely-used technique to provide protection of wounds from further mechanical trauma and bacterial infiltration, while at the same time allowing for gas/fluid exchange, which is aimed at accelerating wound healing. Electrospun fibre meshes are particularly interesting as wound dressing candidates due to their large surface area and high porosity. They can provide air/fluid permeability and sufficient physical properties (defined as passive dressing); some of them can even limit bacterial growth and promote cell proliferation (defined as interactive dressing) [163]. To achieve an optimised healing performance, electrospun fibres are usually incorporated or functionalised with anti-bacterial agents such as silver nanoparticles (AgNPs) [26], small molecules [164], polymers [165], antibiotic drugs [166], or growth factors [167], etc. Many of them involve the process of engineering the physiochemical properties of fibres. For instance, by co-electrospinning PLA with anti-inflammatory polymer PLA-b-PDMAEMA, PLA fibre surfaces were functionalized with PDMAEMA blocks. These blocks could be securely fixed onto the fibre surface and exhibit anti-inflammatory effects [165]. Core-shell structured electrospun fibres were fabricated by phase separation or co-axial electrospinning [168, 169]. These fibres usually consist of a relative strong core to provide mechanical stability and an anti-bacterial material shell. In addition, anti-biotic drugs loaded in the core-shell structured fibres could maintain their bioactivity and can be released when applied on a wound bed. It was found that electrical stimulation could promote wound healing as the electrical signal was able to direct epithelium movement. Photosensitive core-shell nanofibrous scaffolds (contain growth factor in the core) were therefore developed which could convert optical energy to electrical energy; the electric signal combined with growth factors enhanced the healing effects [170].

In spite of the progress in wound dressing applications, electrospun fibre meshes are not perfect. Electrospun fibres that target at multiple stages or release various therapeutic agents during the wound healing process are still far from practical implementation. Initial high burst release and high costs can lead to potential human toxicity and restricts large-scale production. An ideal electrospun fibre for wound

dressing should also include sensors that monitor wound healing status and release drug at appropriate concentrations with respect to different status. Therefore, stimuli-responding drug release behaviour is expected to be integrated into future wound dressing systems, while improved reproducibility and scaled-up production of electrospun fibres are also essential tasks that need to be tackled.

2.4.4 Shape memory properties

Shape memory polymers are polymeric materials that can recover from their temporary shape upon certain triggering. They have high level of deformation, light weight and low costs compared with traditional shape memory alloys or ceramics [171]. An implant made of shape memory polymer can be easily programmed into small volume and deployed, which allows for minimum-invasive surgery. When using degradable shape memory polymers, implants can degrade not requiring a second surgery for their removal and making them even more usefulfor certain biomedical applications. Typically reported shape memory polymers include polyurethane, polyimide, polyester, block copolymer, as reviwed eslewhere [171-174].

Electrospun fibres with shape memory properties can be obtained by directly electrospinning the shape memory polymer [139, 175, 176]; it can also be realised by combining them with other materials into a composite structure [177-180]. Nanoengineering or functionalization of electrospun fibres can further introduce additional unique shape memory properties. For instance, Gong *et al.* prepared PCL fibres incorporating Fe_3O_4-loaded multiwalled carbon nanotubes; the fibres' shape memory behaviour could therefore be triggered by alternating magnetic field [181]. Zhang *et al.* developed hollow electrospun fibre with shape memory properties; the nanostructure is also considered to be a potential smart carrier [182]. Tan *et al.* integrated graphene oxide into electrospun shape memory polyurethane fibres; the addition of graphene oxide not only improved thermomechanical properties and stability, but also provided shape memory properties [183]. In addition, shape memory electrospun fibres loaded with HA was able to promote bone healing [148].

2.5 Conclusions

Electrospinning is a potent tool for the fabrication of continuous nano- or micro-scale fibres. Electrospun fibres have received significant interests for various application

areas such as composites and biomedical products due to their large surface area, good continuity, high porosity and many other unique properties. In bio-related applications, electrospun fibres have been used for in-situ drug delivery, tissue engineering scaffolds and wound dressing. They have proven to be able to either allow cell proliferation or sustainable release of therapeutic reagents, making them promising candidates for related applications. But there is an increasing demand for novel electrospun fibres with added functionalities since the physiochemical properties of conventional fibres can no longer meet the needs. However, until now issues such as initial drug burst release, deactivating bioactive molecules and less-reproducible spinning processes are still severely limiting their potential applications.

Nanoengineering of electrospun fibres has introduced many novel micro-and nanostructures and properties. By creating surface nano-topography or multi-channel fibre structures, hierarchical structures can be integrated into electrospun fibres, which further increases their surface area and allows the incorporation of materials that are not spinnable or lose their functional activity during electrospinning. By functionalizing electrospun fibres, their physiochemical properties can be modified. A variety of agents could be immobilized on fibres, offering flexibility and potential for a variety of applications. The future of electrospun fibres will not only focus on developing easier and cost-effective methods for creating engineered fibres, but also produces complex fibrous structures/geometries with highly precise control and reproducibility. Further optimization of processing techniques is essential for industrial-scale production and commercialization of electrospun fibre products in biomedical applications.

Chapter 3 – Electrospun fibre reinforced composites for the design of strong and tough degradable biomaterials

3.1 Introduction

Poly(trimethylene carbonate) (PTMC) is a biodegradable elastomeric material with potential application in tissue engineering. The polymerization of PTMC has been reported since 1932 [184] and is currently most often carried out via the ring-opening polymerisation of 1,3-trimethylene carbonate [7]. Unlike degradable polyesters, due to its poor mechanical properties it has not been extensively used in practical applications. However, its low glass transition temperature and rubber-like properties have made it a good candidate as a soft component in the design of composites or copolymers. PTMC has been incorporated in blends or in the structure of block copolymers with rigid biodegradable polymers such as poly(lactide acid) (PLA) to introduce toughness whilst preserving degradability [185-187]. In addition, Pêgo et al. showed that at very high molecular weight, PTMC can exhibit much improved mechanical properties and dimensional stability [188]. In addition to increasing molecular weight, crosslinking was found to be another way to achieve stable PTMC morphologies. This was achieved, for example, via gamma irradiation [188]. However, high energy irradiation can result in polymer chain scission, which can affect the mechanical performance of the material. To avoid adverse chain scission effects, crosslinkers have been incorporated into the structure of PTMC polymers to produce PTMC networks with improved mechanical properties [189]. Bat et al. incorporated methacrylate groups into PTMC macromers (branched and linear) and crosslinked them in a mixture with PTMC homopolymer upon UV exposure. The resulting material showed excellent dimensional stability and a reduced surface erosion rate compared to linear PTMC [11]. The photo crosslinking technique was considered to be highly efficient and could be completed at room temperature. It was subsequently reported that direct crosslinking of methacrylate-

ended PTMC macromers without linear PTMC could also produce strong and tough materials [190]. On the other hand, incorporating nanoparticles such as tricalcium phosphate into PTMC produced composite materials with improved mechanical properties, displaying improved bone formation [191]. Nevertheless, one potential issue with PTMC/nanoparticle composites is the weak interaction between filler and matrix as weak bonding can potentially trigger failure especially after prolonged usage [192]. In addition, reinforcement can only be achieved at relatively high nanoparticle loading (for β-tricalcium phosphate, 30 vol% loading was reported to increase the flexural modulus of PTMC from 6 to 17 MPa [191]) while the use of fillers with higher shape aspect ratios, such as fibres would be required to reduce the loading requirements.

Electrospinning is a widely used technique for generating micro/nano fibres [38, 193]. The ease of fabrication, large surface area and aspect ratio of electrospun fibres are believed to make them very suitable as reinforcements for soft polymeric materials. However, relatively few reports have presented the use of electrospun fibres to reinforce composites [3, 192, 194-197]. Bergshoef and Vancso incorporated nylon-4,6 electrospun fibres into epoxy resin and produced electrospun fibre reinforced transparent composite [3]. Stachewicz et al. manufactured electrospun nylon 6 fibres-PVA composite with optimized mechanical properties [195]. Yao et al. fabricated high performance unidirectional co-polyimide nanofibre reinforced composites by impregnating fibre mats with styrene-butadiene-styrene block copolymer solutions [196]. Zuo et al. loaded biodegradable electrospun fibres into calcium phosphate [197], with the addition of electrospun polymeric fibres increasing the material's fracture resistance, toughness, porosity and resorption rate. In spite of their interesting properties, the application of electrospun fibres as reinforcement in composites has often been limited because of their relatively poor mechanical properties compared to traditional high performance fibres such as glass or carbon, which is mainly ascribed to the low orientation and chain extension of polymer chains in most electrospun fibres [38]. The limitation of producing high performance electrospun fibre composite is also due to the difficulties of producing highly continuous and oriented electrospun fibres on a large scale [1]. Besides their relatively poor mechanical performance, which is typically limited to 2 to 4 times the Young's modulus of bulk polymer [13], electrospun fibre entanglement is another obstacle in composite fabrication when products of

complex geometry or structure have to be manufactured. Electrospun fibre mats can suffer from poor homogeneity and compatibility with polymer matrices. Moreover, the continuous and entangled fibre mats limit their use in traditional polymer processing techniques like injection moulding, extrusion, 3D printing etc.

Jiang et al. reported the incorporation of short electrospun polyimide (PI) fibres into PI matrix and achieved as good self-reinforcement as when using continuous PI fibres [89]. Unlike conventional short fibres such as glass or carbon fibres [198, 199], short electrospun fibres as reinforcements in polymer composites have received little attention. The use of such short fibres could greatly simplify the procedures associated with fibre integration in composites. In addition, electrospun polymeric fibre properties can be easily modified by changing the polymeric material, coating the fibres or adding functional groups, conferring new properties to the composite material [160]. Most importantly, the use of short fibres enables the creation of composites that have complex shapes and are moulded by traditional flow moulding processes such as extrusion, injection or compression moulding, vastly increasing their potential applications. However, self-reinforced PI/PI short fibre composites exhibited rather limited property improvements. More significant reinforcements can only be realised by using either stronger and stiffer fibres or softer matrices like elastomers or hydrogels.

Poly(lactic acid) (PLA) is a widely studied biodegradable polymer used as food packaging material and for the design of implants [13]. It can be derived from building blocks synthesised using renewable resources and is fully degradable. Moreover, it is much stiffer and stronger than PTMC. The modulus of PLA can be as high as 4 GPa [200], whilst the modulus of drawn PLA fibres and electrospun fibres can reach values as high as 8 GPa [201, 202]. Depending on molecular weight, the Young's modulus of non-crosslinked/crosslinked PTMC for biomedical applications is usually below 10 MPa [190, 191]. Thus, the incorporation of PLA electrospun fibres, with moduli 400 times that of PTMC, can be of interest for the improvement of mechanical properties as well as dimensional stability of PTMC. Meanwhile, the highly porous electrospun fibre network will also ensure that the volume fraction of PLA fibres is minimised when integrated into a composite matrix. By minimising the amount of PLA, the risk of its acidic degradation products accumulating is also reduced, which could otherwise potentially induce tissue inflammatory responses [203]. Moreover, as PTMC is used in 3D printing

for tissue engineering applications [204], the combination of PTMC with short electrospun PLA fibres can potentially enhance the range of applications targeted by this process. In this respect, the development of short PLA fibres is particularly important as it enables 3D processing technologies such as stereolithography and 3D printing to generate polymer-polymer composites with precise, tailored and complex 3D shapes.

In this chapter, we present the formation and characterisation of both long and short PLA electrospun nanofibre-reinforced PTMC composites. A reliable and scalable methodology to generate short PLA fibres from electrospun mats was developed. As a reference, long fibre composites based on electrospun PLA fibre mats were impregnated with tri-functional methacrylate-terminated PTMC macromers, which were then crosslinked under UV to form PTMC/PLA fibre composites. The morphology and mechanical properties of neat PTMC and their long- and short fibre composites were characterized and discussed in relation to fibre length and loading. This work demonstrated the development of PTMC/PLA fibre composites to be used as non-toxic, biocompatible, fully degradable and easily processable materials showing promising features for a variety of tissue engineering applications.

3.2 Experimental

3.2.1 Materials

The three-armed PTMC macromer, methacrylate terminated, with a $\overline{M_w}$ of 10,000 g/mol was prepared as previously described [205]. The chemical structure of the PTMC macromer is shown in Figure 3.1. Poly(lactic acid) (PLA) 2002D was obtained from Natureworks ($\overline{M_w}$ 200,000 g/mol). Chloroform and dimethylformamide (DMF) were purchased from Fisher Scientific. Propylene carbonate and ethanol were purchased from Sigma Aldrich. Irgacure TPO-L and Orasol Orange 247 were obtained from BASF. All polymers and reagents were used as received.

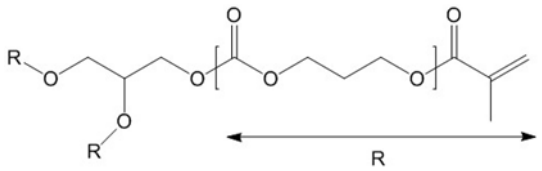

Figure 3.1 *Chemical structure of three-armed PTMC macromer with methacrylate end groups.*

3.2.2 Electrospinning of PLA fibres

PLA 2002D was dissolved in chloroform/DMF mixture with solvent ratio of 3/1. The PLA concentration was prepared at 9 wt% and was stirred until homogeneous. The electrospinning was carried out using an in-house built electrospinning setup. A syringe pump (Kent Genie) was used to continuously supply the PLA solution to the spinning tip at a feeding rate of 1.0 mL/h. A voltage of 18 kV (Glassman EQ) was applied to the spinning tip to charge and generate electrostatic forces, which overcomes the solution's surface tension and ejects a fluid jet. The fluid jet solidified during flight and was collected on aluminium foil. The obtained electrospun PLA fibre mats were left in a vacuum desiccator for 48 hrs to remove residual solvents prior to any further processing.

3.2.3 Fabrication of short electrospun fibres

Two different methods were tested for cutting continuous electrospun fibre mats into short fibres: ultrasonication and mechanical stirring. Both methods were carried out in a series of toluene/petroleum ether (T/P) mixtures as dispersant media. The sonicator (Sonics VCX500) was equipped with a 13 mm probe and had a frequency of 750 kHz. Electrospun fibre mats were placed in the media and sonicated at an amplitude of 40% with 2 sec on and 2 sec off mode. The sonication lasted for 2 min. For the mechanical stirring method, fibre mats were simply placed in the media and stirred at 1500 rpm using a magnetic stirrer (IKA RET basic) for 24 hrs. For both techniques, the resultant fibres were collected first by sedimentation and carefully decanting most of the supernatant. Then the mixture was left to evaporate the media solvent in a fume hood overnight. Finally, the fibres were placed in a vacuum desiccator for 48 hrs to remove residual solvent. During the experiment, one drop of each fibre dispersions was transferred onto a glass slide with a pipette immediately after cutting. The glass slide

was then left in a fume hood to evaporate the solvent and to be used for SEM characterization.

3.2.4 Fabrication of PTMC/PLA fibre composites

PTMC resin was prepared by dissolving PTMC macromer in propylene carbonate, which is a non-volatile, stable solvent, fully compatible with PLA (does not dissolve or swell this material significantly). Three different PTMC concentrations were prepared, 20, 30 and 40 wt%. PTMC was added to propylene carbonate and stirred until fully dissolved. Irgacure TPO-L and Orasol Orange 247 (used to control light intensity) were added to the PTMC/propylene carbonate solution at 5 wt% and 0.15 wt% (with respect to PTMC), respectively. This mixture was continuously stirred to form a homogeneous solution and was carefully transferred into a 90 × 30 × 0.3 mm mould. A quartz plate was used to cover the mould to result in a flat and smooth top surface. The resin was exposed to UV (Omnicure 1500, 15 mW/cm^2) for 90 sec to achieve crosslinking and a high modulus. The cured films were then peeled from the substrate and incubated in propylene carbonate/ethanol media to extract propylene carbonate. The extraction solution was refreshed daily, starting with a ratio of propylene carbonate/ethanol of 50/50 and decreasing the propylene carbonate concentration by 10% steps every day until it was fully removed from the mixture. The extracted composite film was then left in a fume hood to dry and weighed after drying.

The process of making PTMC/PLA fibre composites is shown schematically in Figure 3.2. Pre-weighed electrospun (random) fibre mats with a thickness of 100 µm were cut into 80×20 mm^2 strips and placed on a flat and smooth substrate. 40 wt% PTMC/propylene carbonate solution was then used to impregnate the fibre mat while a quartz plate was placed on top. Gentle pressure was applied on the quartz plate to aid impregnation of the fibres as well as create a smooth surface. Moreover, excessive solution could be removed from the fibre mats to avoid resin-rich areas that could potentially form on the top surface. The impregnated fibre mats were left under pressure overnight to further improve fibre wetting and impregnation. Next, the samples were cured by UV and extracted in the same way as described above. PTMC/short fibre composites were prepared by UV curing the PTMC/short fibre mixtures (short PLA nanofibres dispersed into PTMC/propylene carbonate solutions). Different amounts of short PLA nanofibres (5 and 30 wt% with respect to PTMC) were mechanically blended with PTMC/propylene carbonate solution (PTMC/propylene carbonate solutions were at a concentration of 40

wt%). The mixture was cast into a 90×30×0.3 mm mould and crosslinked under UV. The composites were then extracted in the same way as the long fibre composites based on continuous fibre mats.

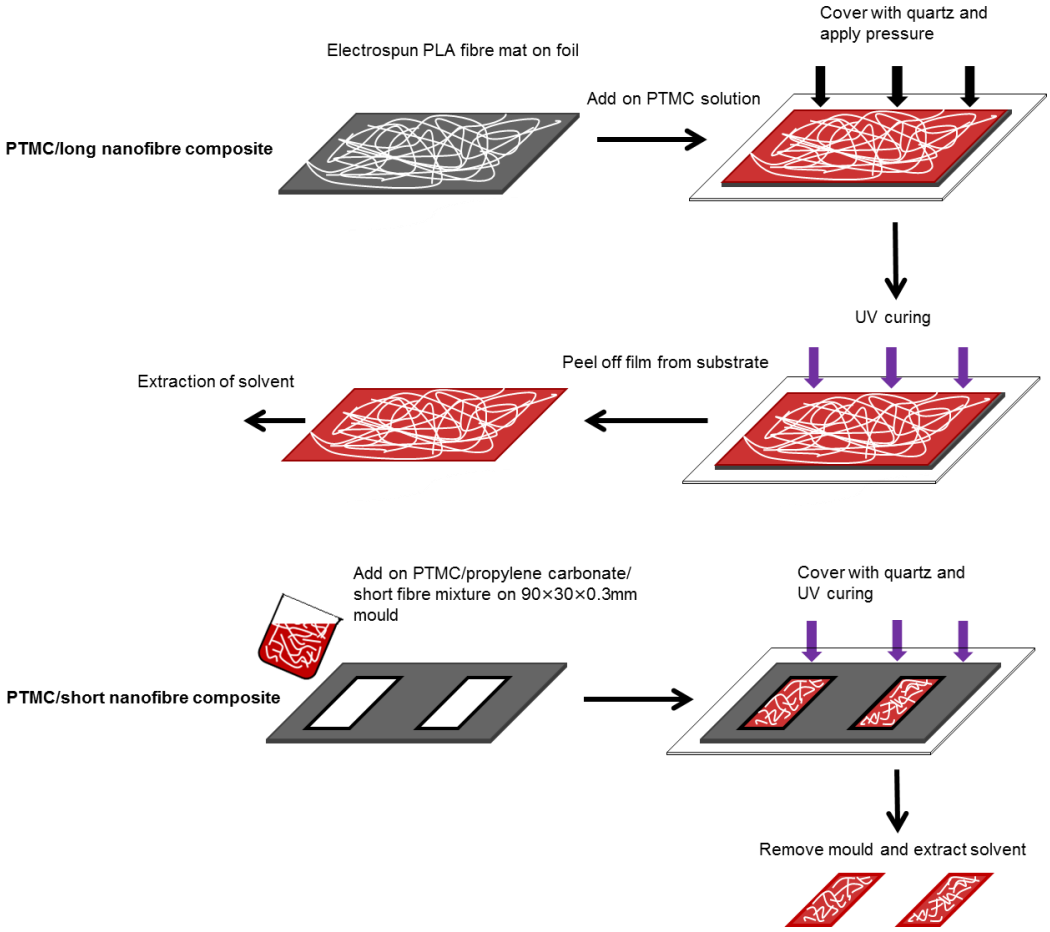

Figure 3.2 *Schematic representation of the fabrication process of long- and short PTMC/PLA fibre composite films.*

3.2.5 Characterization

Scanning electron microscopy (SEM) (FEI Inspect F) was used to characterize both long and short electrospun PLA fibres. All SEM samples were coated with a thin gold layer before imaging. The imaging was performed at 10 mm distance and a voltage of 10 kV. Image J software was used to analyse the average fibre diameter and length. To observe the interaction between fibres and matrix, samples were immersed and cold fractured in liquid nitrogen. The fracture surface was then coated with a thin gold layer and characterized using SEM.

Rheology was carried out with a rheometer (TA instruments DHR-3) to characterize rheological properties of the PTMC/propylene carbonate solution during UV exposure. The PTMC solution was placed between parallel plates of 20 mm diameter and a gap of 0.5 mm. The test was performed at a frequency of 1 Hz, a strain of 0.1% and a UV intensity of 15 mW/cm^2. Tensile tests were carried out using an Instron 5967 equipped with a 1 kN load cell at room temperature. All samples were cut into dumbbell shapes with a size of 65×13 mm^2 and a thin centre part of 30×3 mm^2. Strain was taken from the displacement of the grip. Tensile tests were performed at a rate of 50 mm/min. Young's moduli were calculated from the slope of the stress-strain curve at low strain (from 0-2%). For each sample, three specimens were tested. In addition to tensile tests, dynamic mechanical analysis (DMA) (TA instruments Q800) was used to investigate the storage modulus of PTMC/PLA fibre composites at different temperatures ranging from -50 ˚C to 170 ˚C. DMA was carried out at a heating rate of 3 ˚C/min with a frequency of 1 Hz and a strain of 0.1%. Thermal properties were tested by differential scanning calorimeter (DSC, Perkin-Elmer DSC 4000). Electrospun PLA fibres and PTMC/PLA fibre composites were heated from 25 ˚C to 180 ˚C at a rate of 10 ˚C/min. Neat PTMC was heated from -50 ˚C to 180 ˚C at a rate of 10 ˚C/min. T_g is determined by the mid-point temperature of the materials' glass transition in first heating cycle. The crystallinity of the PLA fibres is calculated using,

$$X_c = \frac{\Delta H_m}{\Delta H_{ref}} \times \frac{1}{w} \times 100 \quad (3.1)$$

where X_c is the crystallinity, ΔH_m is the experimental heat of fusion at melting point determined by DSC, ΔH_{ref} is the theoretical heat of fusion of fully crystalline PLA (93 J/g) [206] and w is the weight fraction of PLA in the composites.

3.3 Results and Discussion

3.3.1 Electrospinning of PLA and short nanofibre fabrication

In this study, two different routes were explored for the cutting of PLA electrospun nanofibres. SEM images of long and short electrospun PLA fibres are shown in Figure 3.3 and Figure 3.4. The electrospun fibres ranged in diameter from 300 nm to 1300 nm with an average diameter of 625 ± 280 nm. Fibres are continuous and smooth with no obvious defects (such as beads) present (see Figure 3.3 a1 and a2). A number of

methods have been reported for the cutting of electrospun fibres, including ultrasonication [96, 97], UV cutting [98], cryogenic-cutting [89, 90], direct spinning by tuning concentration and voltage [207], spinning with nanoparticles [102] or the use of a specific electrospinning setup [103]. Cryo-cutting is an up-scalable method of fibre cutting however we found that the PLA fibres remained relatively ductile even at low temperature, making the cutting difficult. Ultrasonication is easy to operate, with relatively standard equipment. The mechanism of this cutting method involves bubble cavitation and implosion, releasing energy that can result in the rupture of fibres. The method proved successful for the cutting of carbon nanotubes [208], however, its effectiveness was significantly reduced when using ductile polymer fibres. Hence, fibre pre-treatment such as irradiation has been used to generate weak points before ultrasonication in order to promote cutting [97]. In our work, we used a media composed of toluene and petroleum ether to facilitate the fragmentation of electrospun fibres. As PLA is hydrophobic, water was considered not suitable for ultrasonic cutting because of the poor interaction between water and fibres. Since fibre-fibre bonding is energetically favoured over fibre-water interactions, less water can infiltrate into the electrospun network, leading to less bubble cavitation and implosions [96]. Surface modification of the PLA fibres could improve its hydrophilicity but may affect its mechanical properties. The combination of toluene and petroleum ether is hydrophobic and readily wets the PLA fibre mat. Moreover, PLA is neither dissolving nor degrading in these two solvents at room temperature, thus the nature of fibres will not be affected. Water was also avoided to prevent hydrolytic degradation of PLA and to ensure that hydrophilic drugs that may be loaded in PLA fibres would not diffuse out prior to their incorporation in the PTMC matrix. Figure 3.3 b to d presents SEM images of PLA fibres processed by sonication in toluene/petroleum ether (T/P). They show that cutting of the PLA fibres is promoted when the toluene concentration increases. This could be explained by partial swelling of PLA in toluene. At a low volume fraction of toluene (T/P=3/7), the surface of the PLA fibres becomes rougher and pitted but no fracture was observed. Increasing the toluene concentration raised the swelling of PLA fibres in the media. Fibres started adhering to each other and the network began to break down (T/P=6/4), finally leading to the collapse of the fibres. Fibre morphology was severely damaged at 80% toluene (T/P=8/2). Short fibres are generated at this T/P ratio however fibres' mechanical properties are significantly

influenced due to morphological damage. Thus these fibres were considered not suitable for PTMC reinforcement.

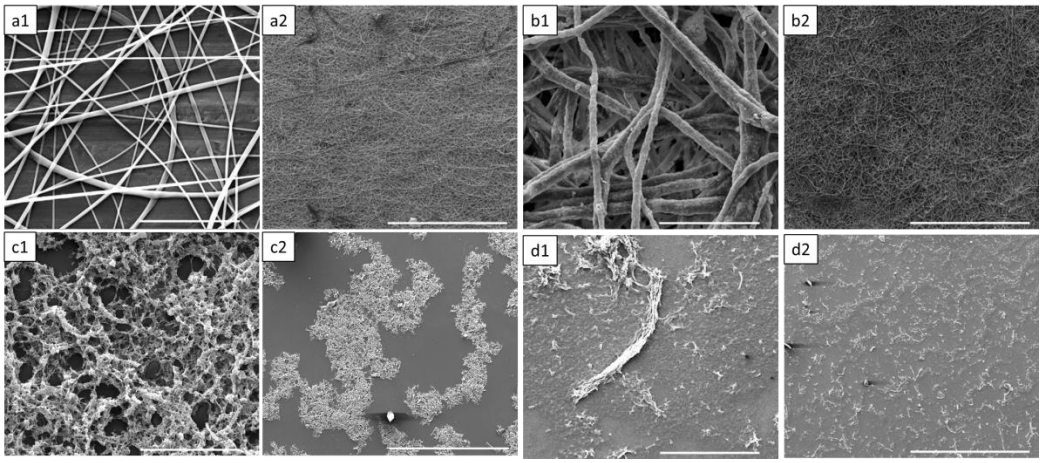

Figure 3.3 *SEM images of PLA electrospun nanofibres and cut short PLA fibres produced by ultrasonication: (a1-a2) as-spun PLA fibres; (b1-b2) sonication of PLA fibres in T/P=3/7; (c1-c2) sonication of PLA fibres in T/P=6/4; (d1-d2) sonication of PLA fibres in T/P=8/2. (scale bars: a1, b1, c1, d1, 20 µm; a2, b2, c2, d2, 400 µm).*

To maintain the morphology of cut fibres, mechanical stirring was used which generates less local heating than ultrasonication. The impact of solvent composition (10-100% toluene in petroleum ether) used to suspend nanofibres during mechanical stirring was studied. It was found that at toluene concentrations approaching 80%, the electrospun fibre mats started to disentangle as well as fragment (see Figure 3.4 a). In addition, fibres maintained their structure rather than collapsed and there was little sign of solvent-induced damage, despite the high toluene concentration. Stirring in 100% toluene led to swelling and partial dissolution of the PLA fibres and distortion. Stirring in 80% toluene media produced fibre lengths ranging from 50 µm to 700 µm. The characterisation of the length distribution obtained is summarized in Figure 3.4. The average length of the PLA fibres made by this method is 220 ± 112 µm with the majority of the cut fibres between 100 and 200 µm in length. Compared with ultrasonication, mechanical stirring could cut these ductile electrospun PLA fibres without damaging their structure or requiring any pretreatments. Compared to other techniques such as UV or cryogenic milling, mechanical stirring is simple, accessible and

scalable. Moreover, this technique did not lead to the degradation of PLA as in the case of UV or laser processing, preserving the properties of the fibres.

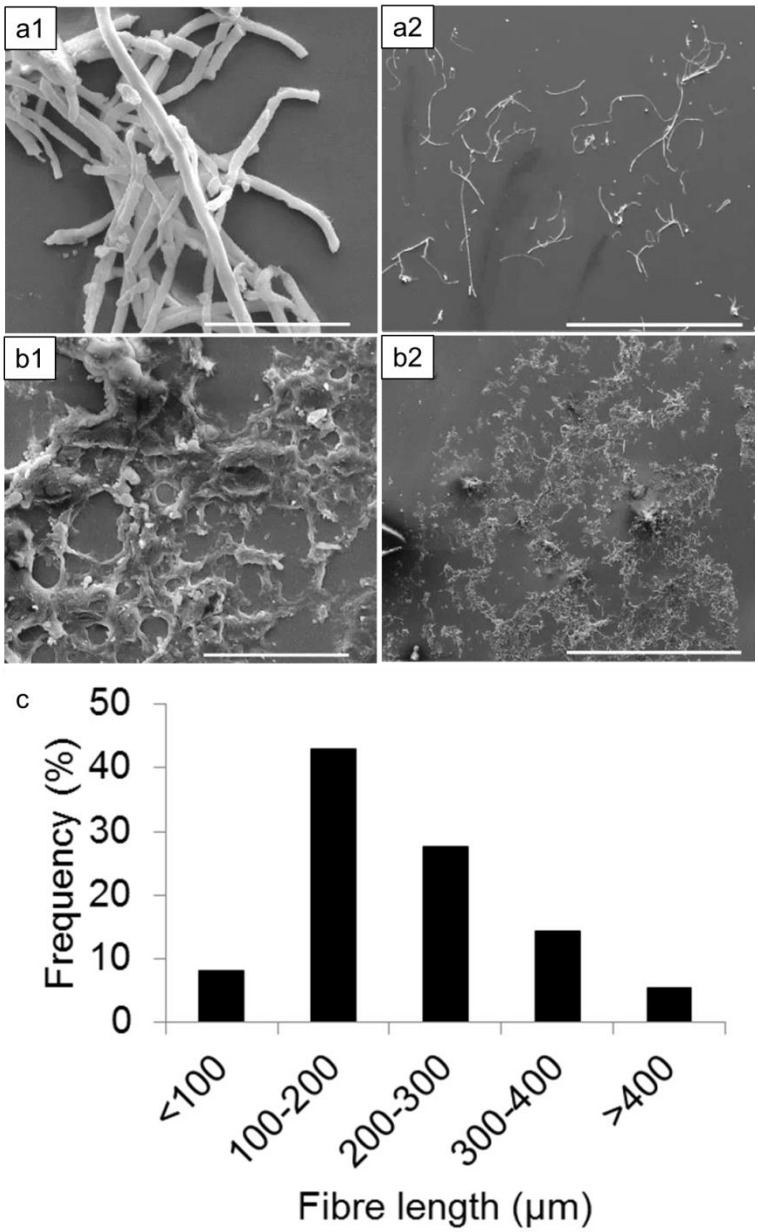

Figure 3.4 *Characterisation of fibres cut by mechanical stirring. SEM image of cut PLA fibres produced by mechanical stirring: (a1-2) stirring of PLA fibres in T/P 8/2; (b1-2) stirring of PLA fibres in T/P 10/0; scale bars: a1, b1, 20 µm, a2, b2, 400 µm. (c) length distribution of cut fibres produced by mechanical stirring in T/P=8/2 with average length at 220 ± 112 µm.*

3.3.2 Fabrication of PTMC and PTMC/PLA fibre composites

The PTMC and PTMC/PLA fibre composites were prepared by the crosslinking of the methacrylate end groups under UV irradiation. Photo-rheology was performed to study the rheological behaviour of the PTMC macromers in propylene carbonate resin during UV curing before the preparation of the PTMC composites. Three different concentrations of PTMC in propylene carbonate were tested (20, 30 and 40 wt%). To achieve optimal viscosity of the solutions for impregnation of the electrospun PLA fibre mats and the dispersion of the short electrospun fibres, the PTMC concentration was maintained below 40 wt%, above which the viscosity was found to be too high for effective impregnation and processing. Too low concentrations, on the other hand, resulted in delayed curing, low crosslink densities and poor mechanical properties. The rheological profile of PTMC resin during curing is presented in Figure 3.5. In these experiments, UV exposure was started at 20 sec and lasted for 90 sec. For all three concentrations, loss modulus G'' was initially higher than storage modulus G', indicating a viscous fluid behaviour. With increasing UV exposure time, both G' and G'' increases and crossed over at the gelation point. It was observed that the time to sol-gel transition for the 20 wt% resin was longer than for 30 and 40 wt% resins. This is attributed to the lower density of crosslinking groups and potentially stronger impact of oxygen concentration at lower concentrations. Afterwards G' overtook G'' and continued to increase although at a slower rate. It reached a plateau at around 90 sec of exposure and stopped progressing further as photoinitiation was not maintained. Thus, the optimal UV exposure time for preparing the PTMC resin and its composites was set at 90 sec in all further experiments. In addition, resins formed from 40 wt% solutions displayed a higher G' and a lower degree of shrinkage than those prepared from 30 wt% solutions. Therefore, the optimal concentration of PTMC in solutions used to impregnate fibres and prepare composites was set at 40 wt%.

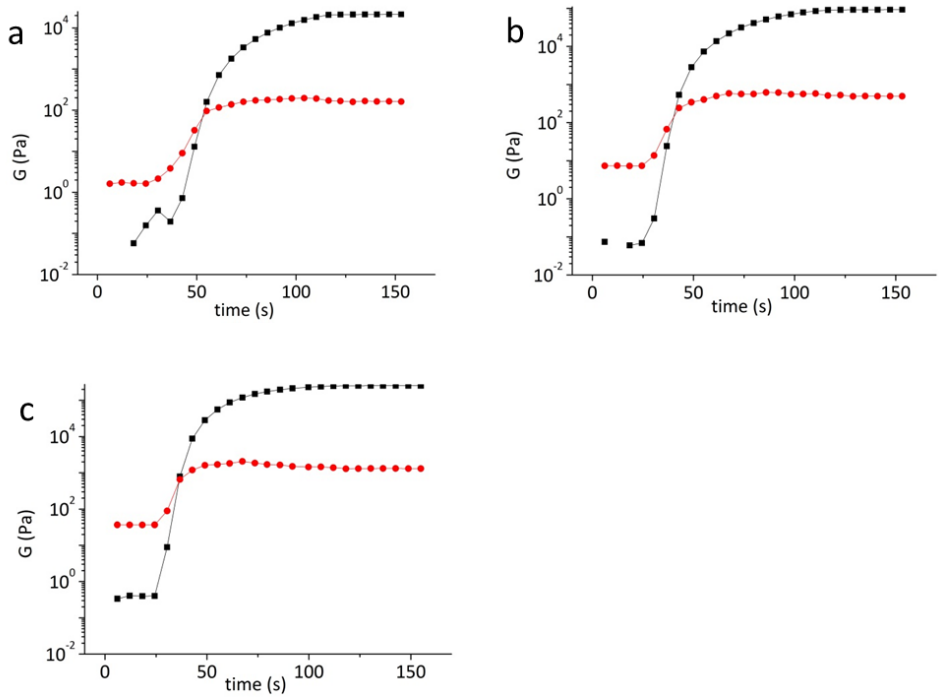

Figure 3.5 *Rheological profiles of PTMC/propylene carbonate solution cured under UV, as a function of time: (a) 20 wt% PTMC, (b) 30 wt% PTMC and (c) 40 wt% PTMC (UV started at 20 sec for 90 sec at an intensity of 15 mW/cm^2, frequency 1 Hz, strain 0.1%). Black squares, shear storage modulus; red circles, shear loss modulus.*

Neat PTMC and PTMC/PLA fibre composite samples were produced using 40 wt% macromer solutions. SEM images of these composites are presented in Figure 3.6. During processing, it was noticed that the matrix solution readily impregnated the PLA fibre mats, implying excellent wetting ability, presumably favoured by the high porosity of the fibre network [203, 209]. However, considering the low volatility of propylene carbonate, this solvent had to be removed after UV curing through extraction using a diluted propylene carbonate/ethanol solution. By reducing the propylene carbonate/ethanol ratio, propylene carbonate trapped in the crosslinked PTMC slowly diffused out. The removal of propylene carbonate resulted in shrinkage of PTMC by 70±5 vol%. Gradual reduction in propylene carbonate content was important to control stress accumulation during extraction, especially for the PTMC/PLA fibre composites and avoid loss of the sample's integrity. After extraction, the PTMC-rich areas that were not fully incorporated into the PLA fibre mat (on the side of samples) were removed. This protocol resulted in composite films with a thickness of around 110 µm (measured

for each sample). By comparing the mass of the electrospun fibre mats with that of the PTMC/PLA fibre composites, the weight fraction of fibres in the composite was calculated varying from 17 to 23 wt% with average value of 20 wt%. In the case of continuous electrospun fibre mats, the interconnected pores were completely filled with PTMC resin and no obvious voids were present in SEM, which suggests good wetting and impregnation of the PTMC resin into the electrospun PLA fibre mats. Only a thin layer of PTMC was observed at the composite surface; this layer was formed during the fabrication process and did not contain any fibres. The roughness of the PTMC fracture surface was increased with the incorporation of PLA fibres. All fracture surfaces indicated good levels of adhesion and a strong interaction between the electrospun PLA fibres and the PTMC matrix with little evidence of fibre pull-out. This suggests good stress transfer between PLA fibres and PTCM matrix and a high reinforcing efficiency of the electrospun fibres.

PTMC/short fibre composites were also characterized using SEM. By increasing the content of short fibres, the fracture surfaces of the PTMC composites became rougher. Again very few voids or fibre pull-outs could be observed after fracture, indicating a good dispersion, wetting and interaction of the fibres and matrix. Compared to composites based on continuous electrospun mats, short fibres provide additional processing flexibility. The amount of fibres in the composite can be easily tuned by adding more or less fibres in the resin, while for mat-based composites, the amount of fibres is limited by the porosity of the mat. Simply casting more resin onto the electrospun fibre mats may to some extent alter the fibre/matrix ratio but will ultimately result in PTMC-rich layers on the surface of the composite. More importantly, short fibre reinforced PTMC composites can be easily moulded into complex shapes via injection or compression moulding or 3D printing, while continuous fibre composites can only be made into simple double curved shapes due to the 2D mat structure. Issues with short fibres composites and particularly nanofibre composites are often related to an uneven distribution of fibres in the matrix and aggregation. Some fibres were found to aggregate while also some PTMC-rich areas were observed. This fibre aggregation is due to the interaction between nanofibres. The average length of the short electrospun fibres is 220 µm while some were as long as 700 µm. Similar to other high aspect ratio nanoparticles such as carbon nanotubes, the high aspect ratio of these fibres (which

can be as high as 300) will inevitably induce also some entanglements or network formation due to fibre-fibre interactions [210, 211].

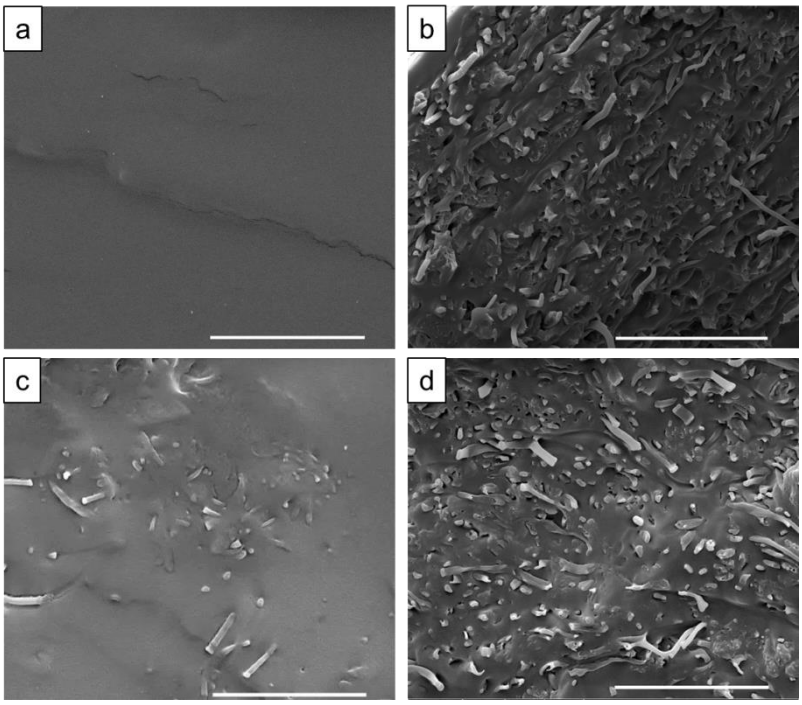

Figure 3.6 *SEM images of the cold fractured surface of neat PTMC and fibre-incorporated PTMC composites: (a) neat PTMC; (b) PTMC/PLA continuous fibre composite (20 wt%); (c) PTMC/PLA short fibre composites (5 wt%); (d) PTMC/PLA short fibre composites (30 wt%) (scale bar: 20 µm).*

3.3.3 Thermomechanical properties of PTMC and PTMC/PLA fibre composites

Thermal properties of PLA electrospun fibres, PTMC/PLA continuous fibre composites and PTMC/PLA short fibre composite were characterized by DSC and presented in Figure 3.7. T_g of PTMC is measured at -13.5 ˚C (graph not shown) and was not affected by the incorporation of PLA fibres. A second polyester-associated T_g was observed for as-spun PLA fibres and PLA fibres in PTMC composites, near 60 ˚C, which is slightly lower than the T_g of bulk PLA (63.9 ˚C). This decrease of T_g can be explained by polymer chain orientation during electrospinning, which leads to internal stresses and drives molecules to become mobile at lower temperature [212]. T_g of short PLA fibres is 53 ˚C, presumably due to small traces of residual solvents from the cutting process. All samples showed melting points near 154 ˚C. In addition, as-spun PLA fibres showed cold crystallization, which is not observed for other samples. The crystallinity of bulk

PLA, electrospun PLA fibres, short PLA fibres, long and short PLA fibres in PTMC are 34.4%, 3.4%, 35.1%, 55.6% 32.8% respectively. The increase of PLA crystallinity after processing into short- and/or PTMC/PLA fibre composites is due to the solvent treatment [213]. The crystallinity of short fibres was found to be lower than that measured for continuous fibre mats in composites, possibly as a result of a reduced PLA chain orientation.

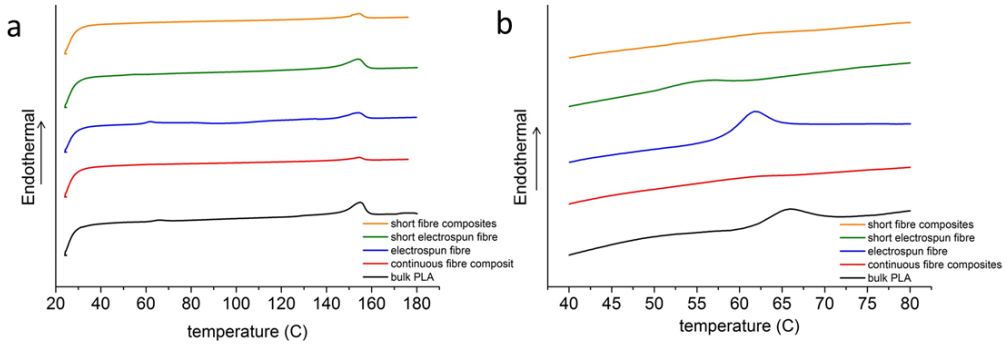

Figure 3.7 *(a) DSC thermal scan of bulk PLA (black), continuous electrospun PLA fibres (blue), short PLA fibres (green), PTMC/PLA continuous fibre composite (red) and PTMC/PLA short fibre composite (orange) from 20 to 180 ˚C; (b) the glass transition region of all samples.*

The stress-strain profiles recorded for pure PTMC, electrospun fibre mats and composites are shown in Figure 3.8. Both PTMC and PTMC loaded with 5 wt% short fibres exhibit elastic properties. All other samples exhibit low yield strain. Electrospun fibre mats and PTMC/continuous fibre composites also show strain-hardening due to orientation of PLA molecules during stretching. Quantification of mechanical data is listed in Table 3.1. Electrospun PLA fibre mats have poor mechanical properties due to random fibre orientation, fibre bending and fibre-fibre sliding when stretched. Compared with neat PTMC, the Young's modulus of the PTMC composites reinforced with continuous PLA fibre mats (20 wt%) is improved by more than two orders of magnitude. Tensile strength was increased 5-fold and toughness was doubled. The increase in Young's modulus, tensile strength and toughness implies an efficient mechanical reinforcement of the PTMC by the electrospun PLA fibres. As expected, the elongation at break of PTMC decreased after incorporating the electrospun PLA fibre mats. The low failure strain of these composites can be attributed to the low failure

strain of PLA fibres. According to the tensile test results, electrospun PLA fibre mats exhibited a low failure strain (near 20%), which is however higher than the failure strain of bulk PLA (near 9%) [214], due to the deformation mechanisms in these nonwovens. SEM images of tensile fracture surfaces are shown in Figure 3.9. Neat PTMC samples exhibit a smooth fracture surface while long fibre reinforced PTMC has a rough fracture surface. Some fibre protrusions can be seen at the surface but most fibres were strongly embedded in the matrix (Figure 3.9b). This again suggests a strong bonding between the PLA fibre and PTMC matrix.

PTMC composites based on short PLA fibres also showed an improvement in mechanical properties. With the addition of merely 5 wt% short fibres, the elastic modulus, tensile strength and toughness of PTMC were improved by a factor of 3. Interestingly, in the case of short fibre composites the elongation of break was not affected by the addition of PLA fibres. Moreover, unlike long fibre composites, composites with 5 wt% short PLA fibres didn't show the marked non-linear behaviour at low strain. Instead they maintained a good level of ductility similar to neat PTMC. The improvement in Young's modulus and tensile strength is again an indicator of the effective reinforcement of the PTMC by the PLA fibres. Compared with self-reinforced PI/PI short fibre composites [89], at similar fibre loading level, reinforcement in the PTMC/PLA short fibre composites was found to be more significant due to the greater property mismatch between PLA and PTMC. As the short fibre loading increases, the composite's Young's modulus increased linearly (see Figure 3.8). At 30 wt% PLA fibres, the modulus increased by a factor of 20. Tensile strength increased 4.5 times but at a much slower rate than the Young's modulus. Interestingly, the toughness of these composites was similar to those of low fibre loadings. The elongation at break however decreased significantly in comparison with short fibre composites incorporating 5 wt% PLA fibres. There is little evidence of fibre pull-out in the short fibre composites; instead, a failure mode involving fibre breakage was observed, suggesting that the PLA fibre length is well beyond the critical length [215]. The fibre critical length (L_c) is defined by $L_c = \sigma_f \cdot D/2\tau$, where σ_f is the fibre strength, D is fibre diameter and τ is the interfacial shear strength [216]. When perfect adhesion between fibre and matrix is assumed, the maximum interfacial shear strength (τ) is equal to the shear yield stress of the matrix which can be estimated from the tensile strength of the matrix (1.3 MPa) using Von Mises yield criterion ($\sigma_y / \sqrt{3}$ MPa) [217]. A fibre strength of 53 MPa (data

provided by supplier for bulk PLA) and diameter (600 nm) were used together with τ (1.3 / $\sqrt{3}$ MPa) to estimate L_c. The critical fibre length is calculated at 21 µm, which is one order of magnitude below the average fibre length of the cut fibres (220 µm), indicating a high reinforcement efficiency of these short fibres as the actual fibre length is more than 10 times the critical length.

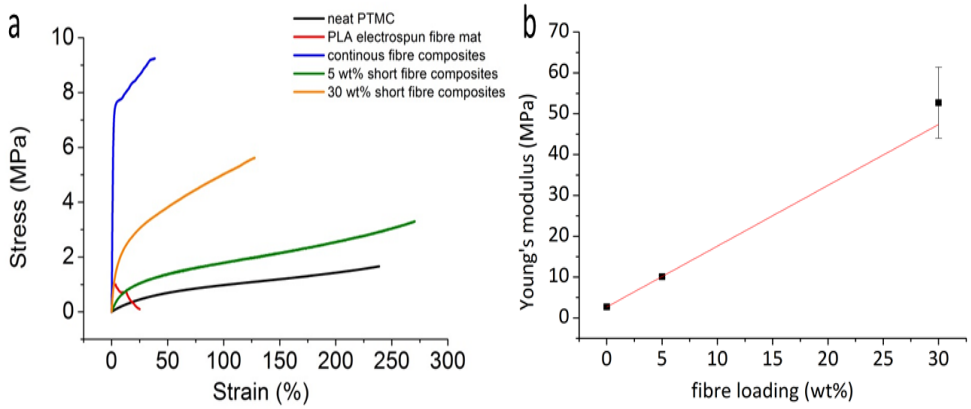

Figure 3.8 *(a) Representative stress-strain curve of neat PTMC (black), electrospun PLA fibre mat (red), PTMC/PLA continuous fibre composite (20 wt%) (blue), PTMC/PLA short fibre composite (5 wt%) (green) and PTMC/PLA short fibre composite (30 wt%) (orange). (b) Dependence of composite Young's modulus on short fibre loading (for each sample, the average modulus was based on three specimen measurement's results).*

Table 3.1 *Summary of tensile test results of neat PTMC, electrospun PLA fibre mat and PTMC composites*

Sample	Young's modulus (MPa) [a]	Tensile strength (MPa)	Elongation at break (%)	Toughness (MPa)
PTMC	2.7±0.1	1.3±0.1	199±31	1.6±0.4
PLA fibre mat	46.2±8.8	1.2±0.4	20±8	0.2±0.1
PTMC/PLA continuous fibre composite (20 wt%)	310±87	7.5±1.7	46±4	3.3±0.7
PTMC/PLA short fibre composite (5 wt%)	10.1±0.3	3.4±0.1	289±30	5.9±0.7
PTMC/PLA short fibre composite (30 wt%)	52.7±8.7	5.9±0.7	141±19	6.1±1.5

[a] Young's modulus were calculated by the slope of the stress-strain curve at 0-2% strain.

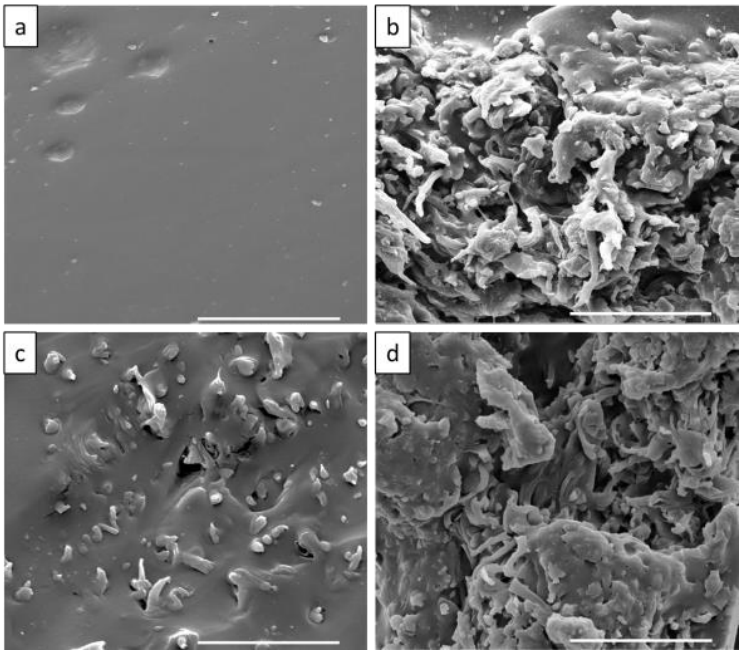

Figure 3.9 *SEM images of the fracture surface of neat PTMC and fibre-incorporated PTMC composites after tensile testing: (a) neat PTMC; (b) PTMC/PLA continuous fibre composite (20 wt%); (c) PTMC/PLA short fibre composite (5 wt%); (d) PTMC/PLA short fibre composite (30 wt%) (scale bar: 20 µm).*

A modified rule of mixture (MROM) was used to evaluate the experimental data of the electrospun fibre reinforced composites [215, 218]. In such analysis, perfect interfacial adhesion between fibres and matrix as well as a homogeneous distribution of fibres in the matrix were assumed. The MROM equation predicting the Young's modulus of a composite is:

$$E_c = \chi_1 \chi_2 V_f E_f + V_m E_m \quad (3.2)$$

In this equation, χ_1 and χ_2 represent the fibre orientation and length efficiency factors, respectively. E_c, E_f and E_m are the Young's modulus of the composite, PLA fibres and PTMC matrix material, respectively. The volume fractions V_f and V_m are derived from the weight fractions of the PLA fibres and PTMC matrix. A density of 1.247 g/cm^3 was measured for PTMC, using a density meter. The density of PLA was taken as 1.24 g/cm^3, based on the product data provided by the supplier for bulk PLA. Hence, for continuous fibre composites (20 wt%), the volume fractions of fibre and matrix are calculated as 20.1% and 79.9%, respectively. The length efficiency factor χ_2 for continuous fibre mat composites is 1 and can be ignored. The orientation factor χ_1 is defined as 3/8 for in-plane (2D) randomly distributed fibres [219, 220]. Thus Equation (3.2) can be transformed into;

$$E_c = \frac{3}{8} V_f E_f + V_m E_m \quad (3.3)$$

In this equation, E_m (2.7 MPa) was directly obtained from tensile tests of PTMC. E_c of continuous fibre mat composite (310 MPa from tensile tests) was used in Equation (3.3) and a PLA fibre modulus E_f of 4.1 GPa was back-calculated, being slightly higher than that of bulk PLA (3.5 GPa as provided by supplier). A slightly higher modulus can be expected because electrospinning will, to some extent, align the polymer chains within fibres. Ultra-thin electrospun fibres (< 200 nm in diameter) typically show a three-fold increase in Young's modulus compared to that of bulk polymer. However, thicker fibres (>300 nm in diameter) will often show properties similar to those of bulk polymers [221]. However, earlier studies have shown that the Young's modulus of single electrospun PLA fibres with diameters of 350 nm can even reach values as high as 8 GPa [201]. In our case, fibres had an average diameter of 600 nm, which is expected to have little effect on E_f. This is supported by the back-calculated Young's modulus for the fibre of 4.1 GPa, which is comparable to that of bulk PLA (3.5 GPa).

For short fibre composites, the fibre length efficiency factor χ_2 has also to be considered. Here, the orientation factor χ_1 is defined as 1/5 because the fibres are considered to be randomly (3D) distributed throughout the matrix [219, 220]. The length efficiency factor χ_2 can be estimated using Equation (3.4) [222];

$$\chi_2 = 1 - \frac{\tanh(a \cdot \frac{L}{d})}{a \cdot \frac{L}{d}} \tag{3.4}$$

with

$$a = \sqrt{\frac{-3}{2 \ln V_f} \cdot \frac{E_m}{E_f}} \tag{3.5}$$

In this equation, L is the mean length of the discontinuous fibres; d is the average fibre diameter; a is a coefficient. The value of χ_2 is then calculated and the composite modulus E_c can be predicted using Equation (3.2), in which E_m (2.7 MPa) was obtained from tensile test and E_f (3.5 GPa) was provided by the supplier for bulk PLA. The results are listed in Table 3.2.

Table 3.2 *Comparison of theoretical predictions using MROM with experimental data.*

Sample	Fibre volume fraction V_f (%)	Matrix volume fraction V_m (%)	E_f (MPa) ×10^{-3}	E_m (MPa)	Fibre orientation factor χ_1	Fibre length factor χ_2	E_c[a] (MPa)	E_{cE}[b] (MPa)
PTMC/PLA short fibre composite (5 wt%}	4.8	95.2	3.5	2.7	1/5	0.86	31.5	10.1
PTMC/PLA short fibre composite (30 wt%)	23.3	76.7	3.5	2.7	1/5	0.90	149	53

[a] E_c is the short fibre composite modulus derived from the MROM; [b] E_{cE} is the composite modulus obtained from the experimental tensile tests.

In our PTMC/short fibre composites, the mean fibre length is around 220 µm compared to a critical length of 21 µm for the PTCM/PLA fibre system. The calculated fibre length efficiency factors χ_2 are therefore close to χ_2= 1 (0.86 and 0.90, respectively) as the

fibre length is well above the critical length ($L \approx 10.L_c$) [215]. For short fibre reinforced composites, the theoretical predictions overestimate the experimental data. This can be explained by some of the fibre aggregation in these systems as observed by SEM. The MROM assumes a homogeneous distribution of fibres in matrix. Fibres should be uniformly and randomly dispersed throughout the matrix and each fibre should be fully surrounded by matrix [223]. In the case of fibre aggregation, the fibre orientation factor χ_1 is also affected. The interfacial contact area between fibres and matrix is inhibited and therefore the stress transfer between fibres and matrix becomes less efficient. Moreover, aggregation also changes the fibre aspect ratio. Thus the fibre length efficiency factor χ_2 is reduced [224]. Meanwhile, aggregation of fibres will also introduce stress concentrations, which will be accompanied by a decrease in composite strength. Another issue to consider is the effect of the fibre cutting procedure on fibre properties, such as a decrease in crystallinity. All of these effects may lead to an overestimation in composite properties.

3.3.4 Temperature dependence of mechanical properties of PTMC/PLA fibre composites

DMA was performed on both neat PTMC and its continuous PLA fibre composites. The evolution of the storage modulus (G') and tan δ as a function of temperature is presented in Figure 3.10. Experiments began at -50 ˚C and ended at 170 ˚C. At low temperatures, well below the PTMC glass transition temperature (T_g), the storage modulus of both samples was initially very high (2.3-2.7 GPa). With increasing temperatures, the modulus decreased slowly until a rapid drop occurred at 7.5 ˚C. Meanwhile the tan δ of both samples also reached its peak value, corresponding to the glass transition temperature of the PTMC matrix. With increasing temperatures, a second drop in storage modulus is observed for the PTMC/PLA fibre composite. A second peak also appeared in the tan δ curve of the composite, indicating the glass transition of the electrospun PLA fibres. Upon further heating the storage modulus of the composite continues to decrease until reaching the PLA melting point while the crosslinked PTMC matrix maintains a rubber plateau modulus of around 1.0 MPa. Furthermore, the storage modulus for crosslinked PTMC and PTMC/PLA fibre composite at body temperature (37 ˚C) are 1.8 MPa and 190 MPa, respectively. Hence, these results demonstrate the benefit of using electrospun PLA fibres as reinforcement for PTMC matrices, in terms of material stiffness, improving the mechanical properties

and dimensional stability of PTMC in conditions typically experienced for tissue engineering applications.

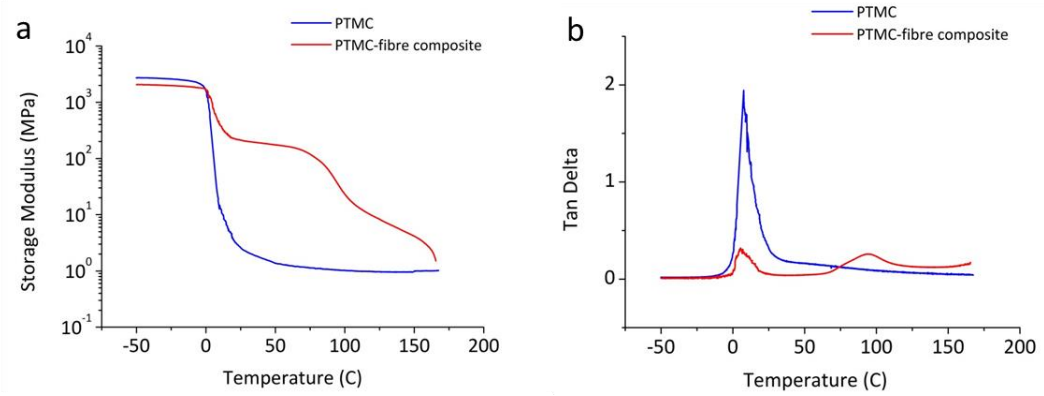

Figure 3.10 *DMA results of neat PTMC (blue) and PTMC/PLA fibre composites (red): (a) storage modulus as a function of temperature; (b) tan δ as a function of temperature.*

3.4 Conclusions

Electrospun PLA fibre reinforced PTMC composites were successfully prepared and characterized. A new method of cutting electrospun PLA fibres with lengths ranging from 50-700 µm using solvent-assisted mechanical stirring was reported. These short PLA nanofibres were then incorporated into PTMC matrix to produce short fibre reinforced composites. Their mechanical properties were tested and compared with those based on electrospun continuous PLA fibre mats, and were analysed using a simple micromechanical model. The mechanical properties of PTMC were improved for both long (continuous) and short PLA fibres. PTMC is found to be significantly enhanced by the incorporation of continuous fibre mats (more than 100 times increase in Young's modulus). However, the ductility and toughness of these composites are significantly decreased compared to short fibre composites. However, composites based on short fibres also exhibited a good reinforcing efficiency. Even with the addition of a small amount (5 wt%) of short PLA fibres, the Young's modulus and tensile strength improved significantly without compromising the ductility of PTMC.

Besides interesting mechanical characteristics, the developed short fibre composites are of particular interest due to their potential processing advantage over traditional

electrospun fibre reinforced composites based on veils or mats. Short fibre composites can be processed into complex shapes using liquid formulations, injection or compression moulding, and 3D printing or stereolithography.

The developed electrospun PLA fibre reinforced PTMC composites, being based on materials already well-established for biomedical applications, are expected to be nontoxic and biodegradable. Their improved mechanical performance and dimensional stability makes them interesting candidates for many tissue engineering applications. For example, short PLA fibres can be incorporated in PTMC resin and used to create complex scaffolds by stereolithography or 3D printing. Moreover, the electrospun PLA fibres could be loaded with a drug which when embedded in a PTMC matrix can lead to novel drug release systems.

Chapter 4 – Shape memory polymer composites based on degradable polymers with controlled properties, easy processing and flexible design

4.1 Introduction

Shape memory polymers (SMPs) are a group of polymeric materials which are capable of recovering from their temporary shape to a memorized permanent shape when triggered by an external stimulus. Compared to conventional shape memory alloys (SMAs) and ceramics, SMPs exhibit significant advantages including high flexibility and strain, high compliance, softness, low density and low cost [225]. Moreover, SMPs are capable of responding to various external stimuli (e.g., light, moisture, electrical etc.) in addition to temperature [226-229]. Polyuretane, polyester, polyaramide and polyimide are among the most commonly reported SMPs [171-174]. Their shape memory behaviour is mostly realised via the thermal-induced rubber-glass or melting-crystallization transitions. In spite of their excellent properties, SMPs on the other hand are considered to have low strength and modulus [230]. Thus reinforcement fillers have been added into SMPs, leading to shape memory polymer composites (SMPCs), which not only improved SMPs' mechanical properties and shape-fixing efficiency, but also introduced non-thermal stimuli-responsive effect [179, 231, 232]. Recently, SMPCs based on non-SMPs have been developed, in which an elastomer is combined with a fixing phase, providing shape memory effects. Luo and Mather [233] reported the fabrication of SMPCs by integration of crystallisable poly(carprolactone) (PCL) electrospun fibres into elastic silicone rubber matrix. The shape fixing and recovery was completed by the reversible crystallization and melting of PCL fibres respectively. Zhang et al. [234] reported the fabrication of SMPCs by direct melt blending of styrene-butadiene-styrene block copolymer (SBS) and PCL. Robertson et al. prepared SMPCs by electrospinning interwoven PCL and polyurethane (PU) elastomer followed by compression into films [235]. The occurrence of these SMPCs has offered a new concept to obtain shape memory effects with regular polymers.

Advances in SMPs and SMPCs have gained them great interests for potential applications in intelligent medical devices. However, many SMPs and SMPCs are limited by either their biocompatibility or degradability. Multiblock degradable copolymers that offer shape memory effects have been synthesized [236-239]. Nevertheless, these SMPs involve specific polymer synthesis that restricts large-scale production. Recently, Lawton et al. reported fully degradable SMPCs based on polyanhydride elastomer and PU-PCL electrospun fibres, which allowed for reconfiguration of the material's permanent shape [4]. However, similar to other previously reported biodegradable SMPs, its innovative potential is subjected to complicated and time-consuming procedures of obtaining FDA approval for use in medical devices. Moreover, the material's geometry is limited to simple-curved shapes due to manufacturing technique restrictions.

The aim of the current work is to fabricate fully degradable one-way SMPCs by incorporating poly(lactic acid) (PLA) electrospun fibres into a crosslinked poly(trimethylene carbonate) (PTMC) network. Both PLA and PTMC are commercially available and well-established polymers that have been used in medical applications [240]. The crosslinked PTMC network was previously used to build scaffolds for cartilage tissue engineering via stereolithography [204]. In our SMPCs, crosslinked PTMC matrix acts as the 'net point' that determines permanent shape; while PLA electrospun fibres act as the 'switching phase' that provides shape fixing and recovery via their glass-rubber transition. The large interfacial area between fibres and matrix enables an efficient transfer of stress induced during shape fixing and recovery [88]. When composites are deformed at temperature above T_g of PLA, PLA molecule chains are mobile and re-organize. As composites are cooled down to below T_g of PLA, PLA molecule chains become less mobile while the elastic PTMC cannot generate sufficient retraction force to recover the deformation. Thus, the temporary shape is obtained. Upon heating to temperature above T_g of PLA, the PLA molecule chains become mobile again and the elastic PTMC recover its orginial shape as a result of entropic energy release.

In addition to continuous electrospun fibres, we also produced SMPCs based on short electrospun PLA fibres. The use of short fibres allows for easy control over the amount of fibres incorporated through which the shape memory effect can be tailored. More importantly, short fibre composites can be processed into complex shapes by

traditional moulding techniques like injection moulding, compression moulding, extrusion, etc.), vastly broadening SMPCs potential applications. Shape memory properties were adjusted by modifying the PTMC matrix properties using PTMCs of different molecular weight. Finally, poly(ethylene glycol) (PEG) was co-electrospun with PLA, which acts as an easy and non-toxic plasticiser, allowing the modification of the glass transition temperature (T_g) of PLA [241, 242]. By integrating these PLA-PEG fibres into PTMC composites, the shape memory transition temperature can be tuned, offering SMPCs more flexibility to practical conditions.

4.2 Experimental

4.2.1 Materials

Three-armed methacrylate-ended PTMC macromer with $\overline{M_w}$of 5,000 g/mol, 10,000 g/mol and 17,200 g/mol were synthesized as reported in [205]. PLA 2002D ($\overline{M_w}$200,000, density 1.24 g/cm^3, tensile modulus 3.5 GPa) was purchased from Natureworks. PEG ($\overline{M_w}$8,000), propylene carbonate and ethanol were purchased from Sigma-Aldrich. Chloroform, dichloromethane (DCM) and dimethylformamide (DMF) were obtained from Fisher Scientific. Irgacure TPO-L and Orasol Orange 247 were supplied by BASF. All polymers and reagents were used as received.

4.2.2 Electrospinning and short fibre preparation

Electrospinning was carried out using in-house built equipment. For PLA electrospinning, PLA 2002D was dissolved in a mixture of chloroform and DMF (mass ratio 3/1) at a concentration of 9 wt%. A syringe pump (Kent Genie) was used to continuously supply PLA solutions at 1.0 ml/h to the blunt spinning needle through a PTFE tube. For PLA/PEG co-electrospinning, 10 wt% PEG was added to the PLA. The blends were dissolved in DCM at a total polymer concentration of 9 wt%. The PLA/PEG solution was supplied to the spinning needle at 2.0 ml/h using a syringe pump. The spinning distance was 15 cm (from needle to collector). Voltage of 20-25 kV (Glassman EQ) was applied to the needle during spinning. Random fibre mats were collected on a grounded foil sheet, which were kept in a vacuum desiccator for 48 hrs to remove residual solvent after spinning.

Short PLA fibres were prepared as previously described in Chapter 3 and [88]. Briefly, electrospun PLA nanofibres were mechanically stirred in toluene/petroleum ether media ($V_{toluene}/V_{petroleum\ ether}$ 80/20) at 1,500 rpm for 24 hrs. Fibres with different lengths were achieved by mechanically stirring as-spun fibres in $V_{toluene}/V_{petroleum\ ether}$ 70/30 at 1,500 rpm for 24 hrs. For easy description, these two short fibres are named as fibre L1 and fibre L2, respectively in the chapter. The resultant fibres were achieved by filtering. Recovered fibres were dried in fume hood overnight and then transferred into vacuum desiccator for 48 hrs to remove residual solvents.

4.2.3 Fabrication of SMPCs

PTMC/PLA continuous fibre composites were fabricated by casting PTMC/propylene carbonate solution onto electrospun PLA fibre mats [88]. PTMC concentration was prepared at 40 wt%. Photoinitiator Irgacure TPO-L and Orasol Orange 247 (for controlling light intensity) were added to PTMC/propylene carbonate solution at the concentration of 5 wt% and 0.15 wt% respectively, with regards to PTMC. The solution was slowly cast onto the electrospun fibre mats (50×20×0.10 mm). A quartz plate was placed on top with gentle pressure applied to facilitate solution impregnation as well as creating a flat and smooth composites surface. The whole system was then exposed to UV (Omnicure 1500) at 15 mW/cm^2 for 90s to crosslink the matrix. The cured composite films were then extracted using propylene carbonate/ethanol to remove propylene carbonate. A daily-refreshed propylene carbonate/ethanol media with decreasing propylene carbonate ratio (10 vol% decrement daily) was used for extraction, which started from $V_{propylene\ carbonate}/V_{ethanol}$ 50/50 and finished until 0/100. The fully extracted composites were left in a fume hood for 48 hrs to dry. PTMC/PLA short fibre composites were prepared by first blending short fibres with 40 wt% PTMC/propylene carbonate solution and then casting the mixture into 50×20×0.15 mm^3 mould, which was then exposed to UV for crosslinking and extracted in the same way as PTMC/PLA continuous fibre composites. Four different fibre L1 amounts (5, 10, 30 and 50 wt% with respect to PTMC) were loaded into PTMC composites. PTMC composites with 10 and 30 wt% fibre L2 were prepared in the same way as fibre L1. For comparison, neat PTMC samples were produced by casting 40 wt% PTMC/propylene carbonate solution into a 50×20×0.15 mm^3 mould, followed by the same UV crosslinking and extraction process.

4.2.4 Morphological characterization

Scanning electron microscopy (SEM, FEI Inspect F) was used to characterize both fibres and composites. All samples were sputter coated with gold before analysis. The imaging was performed at 10 mm distance and voltage of 10 kV. For the characterization of short PLA fibres, a drop of fibre dispersion at the end of mechanical stirring was transferred onto a coverslip and dried in a fume hood. For observing fibre-matrix integration, composites were immersed and cold fractured in liquid nitrogen. Image J software was used to calculate the average diameters of the electrospun fibres as well as the lengths of the cut fibres.

4.2.5 Thermomechanical analysis

The thermomechanical properties of PTMC and PTMC/PLA fibre composites were characterized using dynamic mechanical analysis (DMA, TA instruments Q800). The test was carried out using multi-frequency-strain mode at pre-load of 0.05 N, frequency of 1 Hz and strain of 0.1%, with 125% force track applied. Samples were cut into 20×5 mm^2 rectangular films (thickness 0.1-0.15 mm depending on different samples) and mounted onto DMA clamp. Temperature was first equilibrated at -50 ˚C and then ramped to 100 ˚C at 3 ˚C/min. Storage modulus (E') and tensile loss tangent (tan δ) as a function of temperature are analysed. T_g is determined by the temperature point when tan δ reaches its maximum value. Differential scanning calorimetry (DSC, Perkin-Elmer DSC 4000) was used to investigate the thermal properties of PLA and PLA-PEG fibres, PTMC matrix and fibre composites. A temperature scan was performed from 25 ˚C to 180 ˚C at a rate of 10 ˚C/min rate. T_g is determined by the mid-point of the glass transition. The crystallinity of PLA fibres is calculated by:

$$X_c = \frac{\Delta H_m}{\Delta H_{ref}} \times \frac{1}{w} \times 100\% \quad (4.1)$$

where X_c is the crystallinity, ΔH_m is the experimental heat of fusion at melting point determined by DSC, ΔH_{ref} is the theoretical heat of fusion of fully crystalline PLA (93 J/g) [206] and w is weight fraction of PLA.

4.2.6 Shape memory test

Shape memory tests were conducted using a DMA (TA instruments Q800) with samples cut into 20×5 mm rectangular films (thickness 0.1-0.15 mm depending on different samples). Controlled force mode was used in the tests. First, a stress-strain test of each sample at T_g+20 ˚C (T_g of PLA or PLA-PEG blend) was performed to determine the

suitable static force to be used for the shape memory test. Samples were preloaded by 0.01 N and run at 0.1 N/min force ramp until sample failure or reaching maximum equipment displacement. The schematic of the shape memory test programme is presented in Figure 4.1. In each single cycle of the shape memory test, samples were preloaded by 0.01 N and equilibrated at T_g+20 ˚C. They were then stretched to 30-50% strain at a force ramp of 0.1 N/min. The final static force used here was determined by the earlier stress-strain test at T_g+20 ˚C. After holding the load at this temperature for 5 min, samples were cooled down to T_g-20 ˚C at -10 ˚C/min while maintaining the static force. The static force was quickly released at T_g-20 ˚C and samples were allowed to relax for 5 min. The temperature was finally raised back and equilibrated at T_g+20 ˚C, triggering sample shape recovery. Another three consecutive loading cycles were performed on each sample. For comparison, SME tests on neat PTMCs were programmed in the same way as PTMC/PLA fibre composites at T_g+20 ˚C (T_g of PLA or PLA-PEG blend).

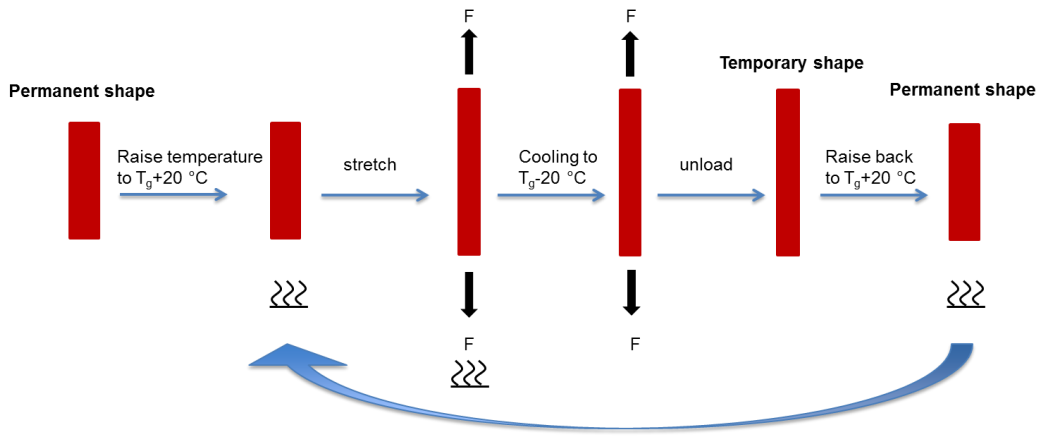

Figure 4.1 *Schematic showing the shape memory tests cycle: sample is heated and stretched at T_g+20 ˚C; it is cooled down to T_g-20 ˚C while holding the load, during which the temporary shape is fixed; the original shape is recovered when sample is heated back to T_g+20 ˚C. Four consecutive loading cycles were performed on each sample.*

4.3 Results and Discussion

4.3.1 PTMC/PLA continuous fibre composites

Electrospun PLA fibres are characterized using SEM (see Figure 4.2 a). Fibres are continuous and smooth with few defects being present. Some PLA fibres are found to

be adhering to each other, which is due to the incomplete solvent evaporation during electrospinning, leading to fusion of fibre surfaces. PLA electrospun fibres have diameters ranging from 0.4 µm to 3 µm with an average diameter of around 1.2 µm. The SEM images of cold-fractured PTMC/PLA continuous fibre composites are shown in Figure 4.2 b. By measuring the mass of the electrospun fibre mat before and after PTMC infiltration, the mass ratio of continuous PLA fibre in PTMC composites is estimated at 29.8±2.8%. The absence of widespread fibre pull-out is indicative for a strong interaction between PLA fibres and PTMC matrix. For continuous fibre composites, the interconnected space between the electrospun fibres is completely filled by PTMC matrix and no cavities are observed, suggesting excellent impregnation of PTMC solution into the electrospun fibre mat during the fabrication process. Together with the strong adhesion between fibres and matrix, it implies efficient stress transfer in these continuous fibre composites. DSC and DMA were performed to study their thermo-mechanical properties and to determine the temperature range for the shape memory tests. DSC thermograms of PLA fibre and PTMC/PLA fibre composites are shown in Figure 4.3. T_g at 60 ˚C and T_m at 154 ˚C are observed for both as-spun PLA fibres and PTMC/PLA fibre composites. In addition, the crystallinity of continuous PLA fibres is increased from 3.4% to 37.1% after incorporation into PTMC composites due to solvent induced crystallization [213]. The storage modulus (E') and tan δ as a function of temperature are presented in Figure 4.2 c. At low temperature (below -20 ˚C), both PTMC and PTMC/PLA fibre composites are stiff, with an E' at around 2 GPa. As temperature increases, a first drop in E' occurred to all samples. Meanwhile, tan δ reached its first peak, corresponding to the T_g of PTMC (around -4 ˚C). PTMC/PLA fibre composites exhibited another distinct peak in tan δ at 78 ˚C due to the glass transition of PLA. Since the shape memory test was conducted in a DMA, T_g=78 ˚C was used as the shape memory transition temperature in the following experiments. To determine the force needed for the shape memory tests, stress-strain tests of PTMC and PTMC/PLA fibre composites at 98 °C (T_g+20 °C) were conducted in a DMA. The representative stress-strain curve is shown in Figure 4.8. The Young's modulus and tensile strength of PTMC is increased from 1.7 to 16.6 MPa and 0.6 to 2.0 MPa respectively by the introduction of the continuous PLA fibres. Failure strain is also improved three-fold from 51% to 176%.Thus electrospun PLA fibres can be considered as efficient reinforcements for PTMC in biomedical applications.

Representative temperature-stress-strain plots of a shape memory test cycle of PTMC and PTMC/PLA fibre composite are shown in Figure 4.2 d. To quantify the shape memory properties of each sample, the strain fixity (R_f) and strain recovery (R_r) are introduced, calculated by;

$$R_f = \frac{\varepsilon_u(N)}{\varepsilon_m} \tag{4.2}$$

and

$$R_r(\mathrm{N}) = \frac{\varepsilon_m - \varepsilon_p(N)}{\varepsilon_m - \varepsilon_p(N-1)} \tag{4.3}$$

where N is the number of cycles tested, ε_m is the maximum strain that the sample is stretched to, ε_u is the strain of the sample after relaxing at 58 °C (T_g-20 °C) and ε_p is the strain of the sample after recovering at 98 °C. 100% of R_f and R_r means complete shape fixing and recovering, respectively. R_f and R_r of each sample against the test cycle number (N) are presented in Figure 4.2e. The detailed quantification of R_r and R_f in each test cycle can be found in Table 4.2. Continuous PTMC/PLA fibre composites are seen to have excellent shape fixity with an average R_f of 94%. In its first test cycle, a permanent strain of 20% was not recovered and R_r (1) was calculated at 53%. This unrecovered strain can be explained by PLA chain relaxation at 98 °C as well as processing history [172]. The PLA chains were initially oriented due to the extensional flow in electrospinning [38]. This molecular orientation turns into disorder when the composites are heated at 98 °C, resulting in the unrecovered strain. The strain recovery ratio R_r increased to 87% in the second cycle and reached 95% in the fourth cycle. Compared to SMPCs with discrete phases [234], a continuous network as in the case of electrospun fibre mats is more efficient in transferring stresses, offering a better shape fixity ratio R_f. Neat PTMC samples exhibited excellent elasticity. No shape fixing was observed for PTMC as samples recovered to their original dimension immediately upon releasing the load in all four test cycles (see black curve in Figure 4.2 d).

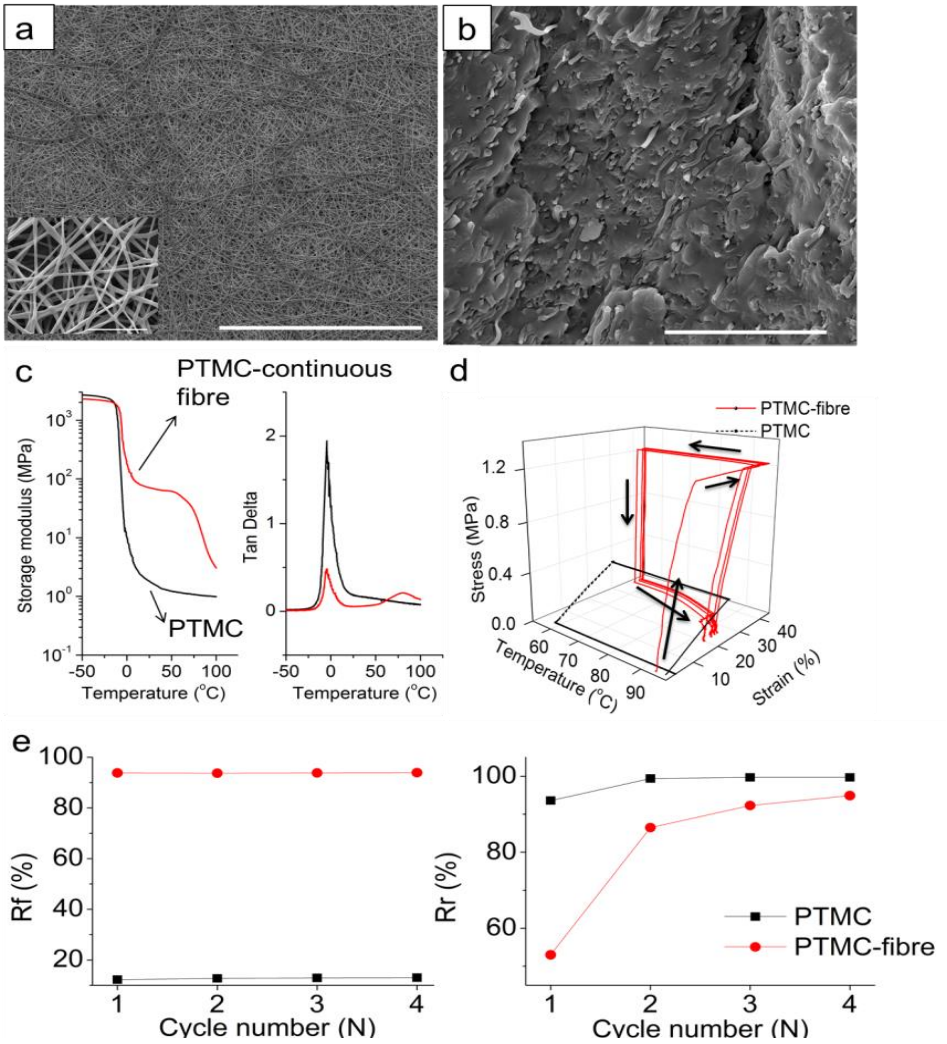

Figure 4.2 *(a) SEM images of electrospun PLA fibres (scale bar 400 μm), inset shows an electrospun PLA fibre mat at higher magnification (scale bar 20 μm); (b) SEM images of cold-fractured PTMC/PLA continuous fibre composites; (c) storage modulus and tan δ of PTMC and PTMC/PLA continuous fibre composites as function of temperature tested by DMA; (d) representative temperature-strain-stress plots showing shape memory test cycles (1 to 4) of neat PTMC (black dashed) and PTMC/PLA continuous fibre composites (red solid); (e) shape fixity ratio (R_f) and shape recovery ratio (R_r) against testing cycle number (N).*

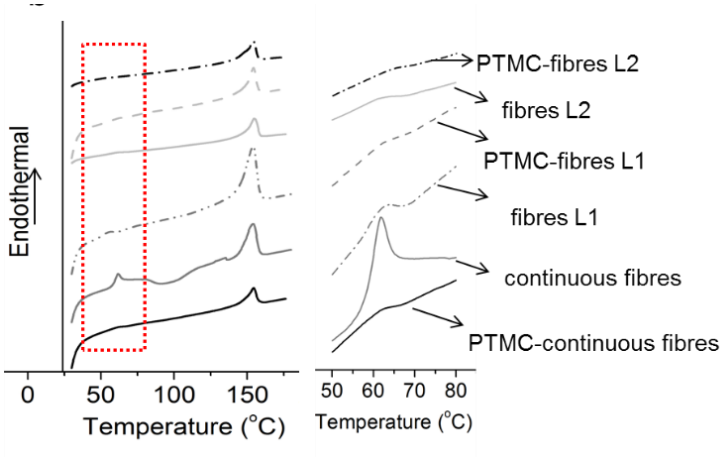

Figure 4.3 *DSC thermograms of PLA fibres and PTMC/PLA fibre composites.*

4.3.2 PTMC/PLA short fibre composites

Continuous electrospun PLA fibres were successfully cut into short fibres by stirring in toluene/petroleum ether 80/20 (named as fibre L1) and their SEM images are presented in Figure 4.4 a and b. Fibre L1 has lengths ranging from 50 to 700 µm, with an average length of 220±110 µm. Different short fibre loadings (5, 10, 30 and 50 wt%) are mixed separately with the PTMC/propylene carbonate solution and crosslinked to form the short fibre composites. SEM images of cold-fractured PTMC/PLA fibre L1 composites are presented in Figure 4.4 c-f. Also in the case of short fibre composites, fibre pull-outs are rarely observed after fracture, indicating a strong bonding between the discontinuous PLA fibres and the PTMC matrix. According to Chapter 3 and our previous report [88], the critical length L_c of short PLA fibres in PTMC was calculated at 21 µm, which is one order of magnitude below the average length of the discontinuous PLA fibres. This, on the other hand, indicates that these short fibres are still highly efficient in transferring stresses [215]. DSC and DMA were performed on PTMC/PLA short fibre composites in the same way as PTMC/PLA continuous fibre composites. DSC thermograms of short PLA fibre and PTMC/PLA short fibre composites are shown in Figure 4.3. T_g and T_m are not changed compared to continuous fibre composite samples, calculated at 60 ˚C and 154 ˚C, respectively. The crystallinity of PLA is increased from 3.4% to 35.1% (fibre L1) and finally to around 33% (in PTMC composites). This increase in crystallinity is due to solvent induced crystallization [213]. Representative storage modulus (E') and tan δ as a function of temperature are presented in Figure 4.5 (obtained from composites containing 30 wt% fibre L1). A second peak of tan δ at 78 ˚C

indicates that PTMC/PLA short fibre composites have T_g at 78 ˚C. Thus shape memory tests are conducted at 78±20 ˚C, i.e. the same temperature as for PTMC/PLA continuous fibre composites.

To determine a suitable force to be used in the shape memory tests, stress-strain tests of PTMC/PLA fibre L1 composites at 98 °C was performed using DMA. The representative stress-strain curve and quantified results can be found in Figure 4.8 and Table 4.1 respectively. Composites with 5, 10 and 30 wt% short PLA fibre show good ductility with strains varying from 105% to 128% at 98 ˚C. Young's modulus and tensile strength are improved after incorporating fibre L1, however these values were lower than for continuous fibre composites due to less fibre continuity and reduced fibre efficiency [219]. As fibre L1 loading is increased from 5 to 50 wt%, composite modulus increased up to eight times that of neat PTMC. However, continuing increasing fibre loading to 50 wt% resulted in a decrease in both composite strength and ductility. This decrease in failure stress and strain can be explained by the low yield strain of PLA and stress concentrations arising from fibres and fibre aggregates [88, 201].

In the shape memory tests of PTMC/PLA short fibre composites, all samples (except for 50 wt% fibre loading) showed a high shape recovery ratio R_r but a low shape fixing ratio R_f compared to continuous fibre composites. With 5 wt% fibre L1 incorporated, the material has the lowest R_f. This is because when only a few fibres are present in the composites, they are not able to bear the contraction force from the PTMC matrix necessary to maintain the deformation after removal of the external stress, resulting in a similar behaviour as neat PTMC. By increasing the amount of short PLA fibres, composites maintained good a shape recovery ratio R_r but showed an increase in their shape fixing ratio R_f. The improvement in R_f is a result of the improvement in the fibres' abilities to bear the entropic contraction stress of the PTMC. When 50 wt% fibre L1 are incorporated, the composites exhibit good shape fixing with R_f reaching 86% in the 4th test cycle. At this high fibre loading, the composites are still showing good recovery properties (R_r = 94%). It is found that at similar fibre loading (30 wt%), short fibre composites are still less shape-fixing than continuous fibre composites.

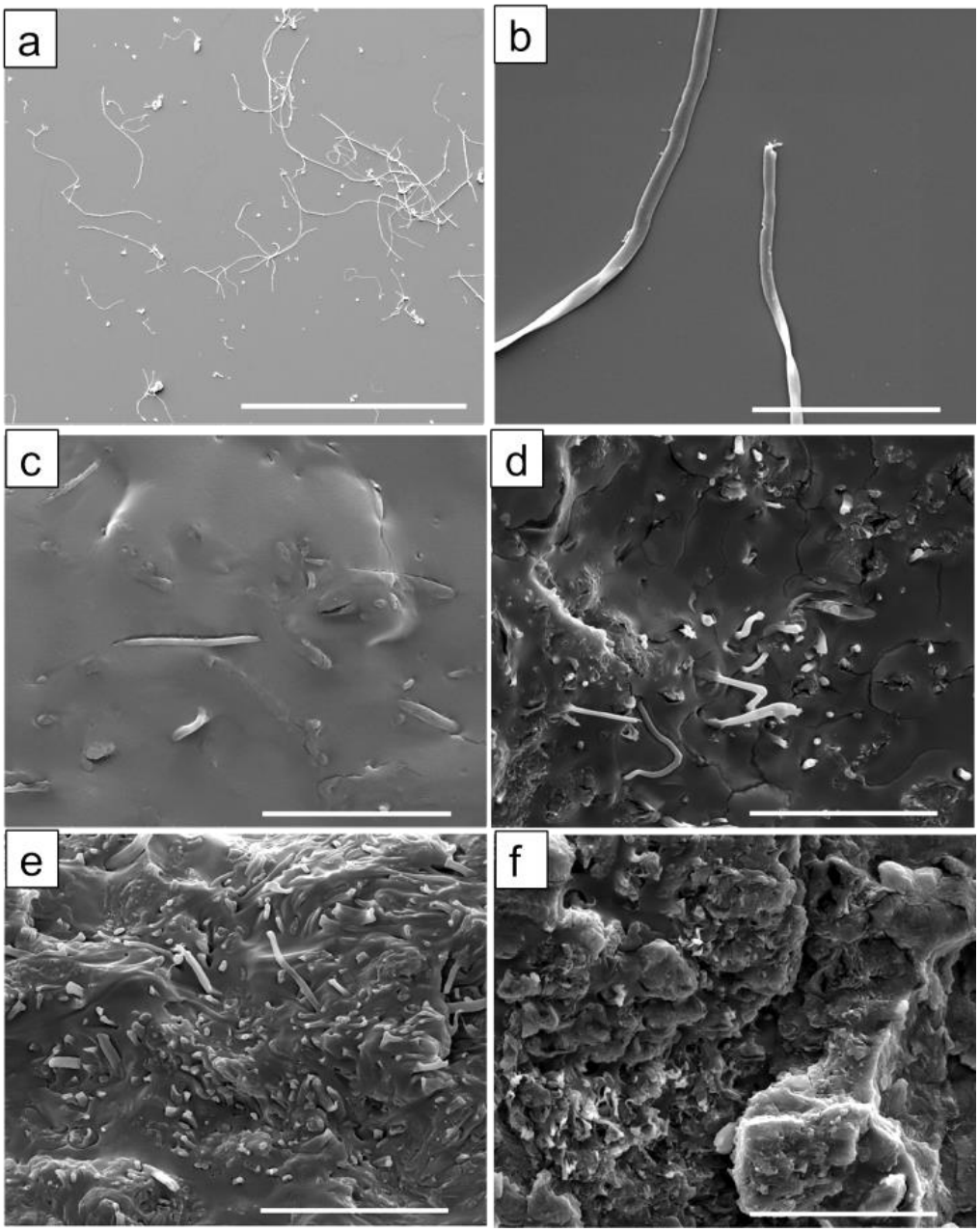

Figure 4.4 (*a, b) SEM images of electrospun PLA fibre L1 (scale bar a, 400 µm; b, 20 µm); (c-f) SEM images of cold-fractured PTMC containing; (c) 5 wt%, (d) 10 wt%, (e) 30 wt%, and (f) 50 wt% PLA fibre L1 (scale bar 20 µm).*

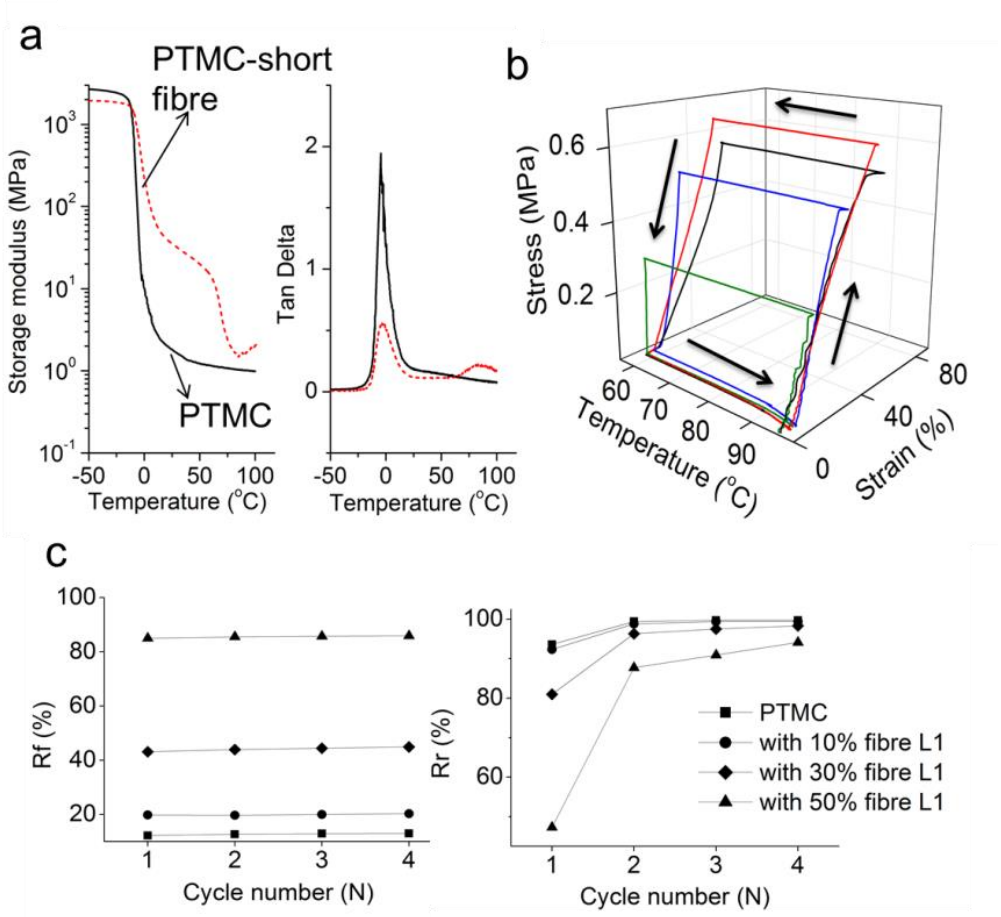

Figure 4.5 (*a) Representative storage modulus and tan δ of PTMC and PTMC/PLA 30 wt% short fibre composites as function of temperature tested by DMA; (b) representative temperature-stress-strain plots showing shape memory test cycle of PTMC with different short PLA fibre loadings (black: 5 wt%, red: 10 wt%, blue: 30 wt%, green: 50 wt%); c. shape fixity ratio (R_f) and shape recovery ratio (R_r) against test cycle number (N).*

To investigate the importance of a continuous fibre phase on composites' shape memory behaviour, short fibres with slightly longer average lengths were prepared by mechanical stirring as-spun fibres in toluene/petroleum ether 70/30 (named as fibre L2). Fibre L2 lengths ranged from 100 to 850 µm, with an average length at 270±140 µm. The length distribution of fibre L1 compared to fibre L2 is presented in Figure 4.6. By decreasing the toluene fraction during mechanical stirring, the average fibre length was increased slightly due to less swelling of PLA [88]. Two different loadings of fibre L2 (10 and 30 wt%) were incorporated into PTMC composites. Composites containing 50

wt% fibre L2 are difficult to prepare due to fibre entanglements and relatively poor dispersion. By observing cold-fractured samples, fibre L2 showed excellent adhesion with PTMC as most PLA fibres remained embedded within the matrix. SEM images of PTMC/PLA fibre L2 composites can be found in Figure 4.6a-b. Because fibre L2 has an average length which is also one order of magnitude higher than the critical length of PLA in PTMC (L2 ≈ 13·L_c), these discontinuous fibres are expected to show comparable reinforcing efficiencies as fibre L1 (L1 ≈ 10·L_c) [215]. Thermo-mechanical tests show no difference in T_g between fibre L2 and fibre L1 based composites, which is at 60 ˚C (by DSC) and 78 ˚C (by DMA), respectively. The crystallinity of fibre L2 increases from 3.4% to 10.8% (as short fibre), which is lower than fibre L1 (35.1%) and finally to around 33% (in PTMC composites). The difference in solvent-induced crystallization between fibre L2 and L1 is due to different swelling ratios of PLA under each processing condition. Stress-strain tests on PTMC/PLA fibre L2 composites at 98 °C (T_g+20 °C) was performed using DMA. The detailed quantified test results are listed in Table 4.1. The Young's modulus and tensile strength of PTMC is enhanced by loading fibre L2. Composites also showed good ductility at 98 ˚C, with a failure strain near 150%. Composites containing 10 wt% fibre L2 and L1 have comparable mechanical properties because both fibres have average lengths which are much longer than the critical length (≥ 10·L_c), hence leading to similar reinforcing efficiencies of fibre L2 and L1 [215]. Composites containing 30 wt% fibre L2 exhibit a lower modulus and tensile strength than fibre L1 based composites due to fibre entanglement and heterogeneity. In shape memory tests of PTMC/PLA fibre L2 composites, at 10 wt% fibre loading the composites shape fixing ratio is increased three-fold (R_f from 20 to 61%); at 30 wt% fibre L2 loading, the composites shape fixing is also improved from 45% to 64%. Composites based on fibre L2 showed more training effects in the first test cycle but eventually excellent shape recovery was obtained (both near 95%). The difference in shape fixing ratio between composites based on fibre L1 and L2 is due to the different aspect ratios of the PLA fibres, which results in differences in fibre entanglements, dispersion and network formation. At the same fibre loading, fibres of higher aspect ratio are found to offer stronger shape fixing properties due to more fibre entanglements [211].

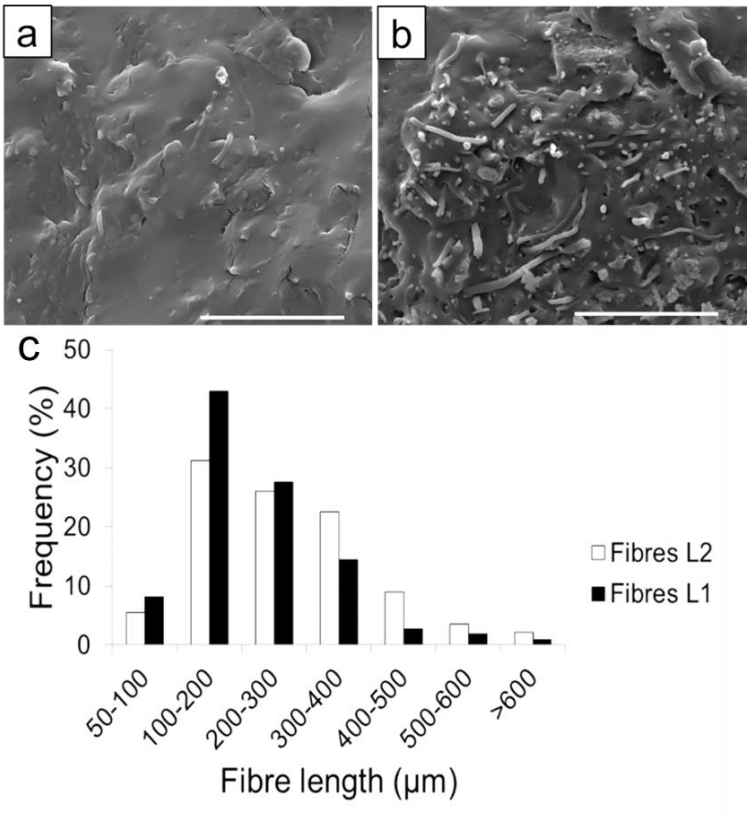

Figure 4.6 *SEM images of cold-fractured PTMC/PLA fibre L2 composites: (a) PTMC/10 wt% fibre L2, (b) PTMC/30 wt% fibre L2. (c) Length distribution of fibre L1 and L2. A total number of 300 short fibres were randomly picked from SEM images and their length is analysed using Image J software. The average length of fibre L1 and L2 are calculated at 220±110 μm and 270±140 μm, yielding aspect ratios of 340 and 430, respectively.*

To further support the importance of fibre entanglements in the polymer materials' shape memory behaviour, a suspension of fibre L1 after mechanical stirring was deposited into a 50x20×1 mm^3 mould and rectangular fibre mats were formed after evaporation of the media solvents. It is expected that in this way more fibre-fibre contacts and entanglements are formed. Fibre L1 loading in the composites is calculated at around 30 wt%. PTMC/propylene carbonate solution was cast onto a short fibre mat using the same protocol as for continuous electrospun fibre mats. Stress-strain tests indicated no significant effect on composite mechanical properties. However, shape memory tests showed a significant improvement in shape fixing ratio R_f, increasing it from 45 to 75%, while composites also remained an excellent shape

recovery ratio (R_r at 97% in 4th test cycle). Thus by increasing the fibre loading or fibre aspect ratio, more fibre entanglements are realised, which finally leads to a stronger fibre network and better shape memory properties of the composites.

4.3.3 Modulating elastomeric phase (PTMC) properties

The impact of the properties of the elastomeric phase on composites' shape memory behaviour is also investigated by varying PTMC macromer molecular weight. PTMC macromers of $\overline{M_w}$5,000 and 17,200 were used to substitute PTMC 10,000. The composites were prepared and tested in the same way as for PTMC 10,000 based samples. PTMC 5,000 matrix shows again strong adhesion with PLA fibres as no fibre pull-out is observed in cold fractured composite samples. Some cavities are found in PTMC 17,200 based composites but also here most fibres are still well embedded within the polymer matrix (Figure 4.7). By observing the peak of tan δ using DMA, T_g of PTMC 5,000 and 17,200 shifted to -1.9 ˚C and -8.8 ˚C, respectively, compared with -4 ˚C for PTMC 10,000. Stress-strain tests at 98 ˚C showed that neat PTMC 5,000 is stiffer with a lower failure strain while neat PTMC 17,200 is softer with a considerably high failure strain (see Table 4.1**)**. The difference in T_g and mechanical properties are the result of molecular chain mobility and changes in crosslink density. With fibre reinforcement, all composites exhibit similar mechanical behaviours. In the shape memory tests, no shape memory effect was observed for neat PTMC 5,000 samples. Some unrecovered deformation is seen for neat PTMC 17,200 samples as a result of viscoelastic creep. Due to the increased stiffness for PTMC 5,000, composites, shape fixing property is decreased due to PLA fibres that are less competent to withstand the contraction force from the PTCM matrix. However, its recovery ratio is thus improved as expected. In contrast, composites' shape recovery property for PTMC 17,200 is decreased as this matrix is softer and a lower recovery force can be generated (see Table 4.2).

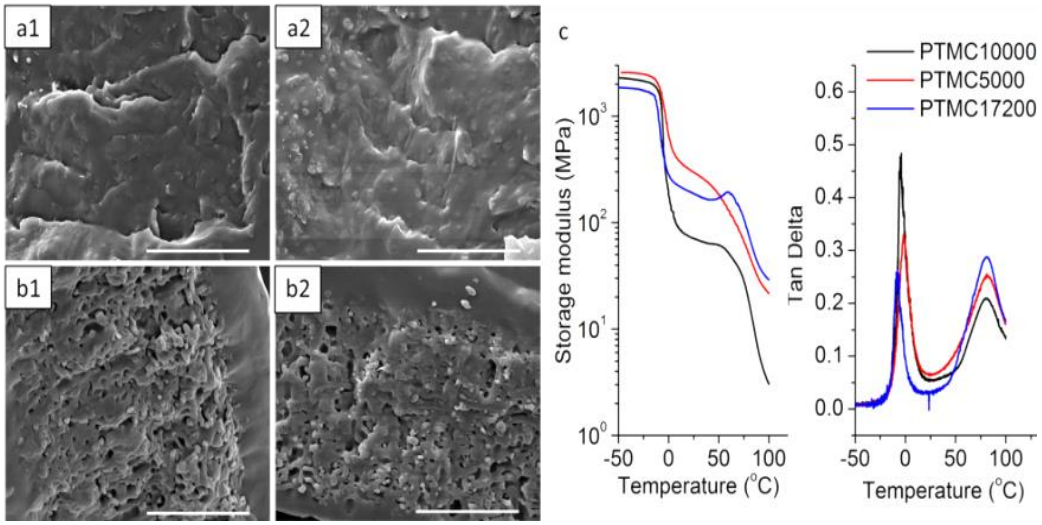

Figure 4.7 *SEM images of PTMC 5000 fibre composites before (a1) and after (a2) shape memory testing; SEM images of PTMC 17200 fibre composites before (b1) and after (b2) shape memory testing. The scale bar for a and b is 20 µm. (c) storage modulus and tan δ of PTMC/PLA continuous fibre composites as function of temperature by DMA (black: PTMC 10,000, red: PTMC 5,000, blue: PTMC 17,200).*

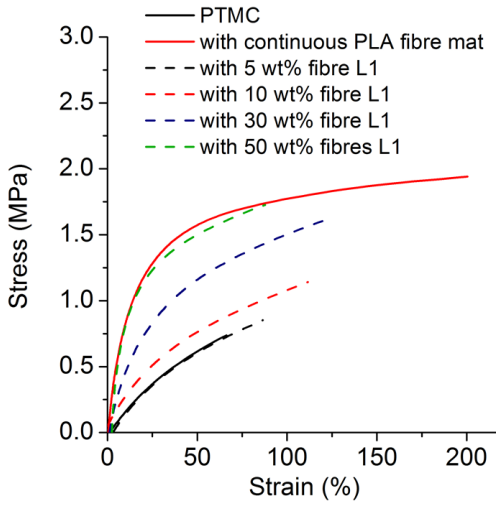

Figure 4.8 *Representative stress-strain curve of PTMC and PTMC/fibre composites at 98 ˚C: (black) neat PTMC, (red) PTMC/continuous fibre composites, (black dash) PTMC/5 wt% fibre L1 composites, (red dash) PTMC/10 wt% fibres L1 composites, (blue dash) PTMC/30 wt% fibres L1 composites, (green dash) PTMC/50 wt% fibres L1 composites*

Table 4.1 *Summary of strain-stress tests of PTMC and PLA fibre reinforced PTMC composites at 98 ˚C using DMA.*

Sample	Young's modulus (MPa)*	Tensile strength (MPa)	Yield strain (%)
PTMC	1.69±0.13	0.58±0.08	51±7
PTMC5000	2.12±0.15	0.59±0.09	37±3
PTMC17200	1.15±0.08	0.56±0.03	276±3
PTMC continuous fibre	16.63±4.46	1.97±0.36	176±41
PTMC5000/continuous	11.40±0.59	2.10±0.07	199±11
PTMC17200/continuous	11.49±1.27	1.43±0.07	209±18
PTMC/5 wt% fibre L1	2.50±0.13	0.98±0.07	105±16
PTMC/10 wt% fibre L1	2.38±0.20	1.17±0.02	128±12
PTMC/30 wt% fibre L1	7.33±0.87	1.68±0.18	116±25
PTMC/50 wt% fibre L1	12.46±6.93	1.19±0.36	85±20
PTMC/10 wt% fibre L2	2.79±0.62	0.82±0.19	146±45
PTMC/30 wt% fibre L2	4.39±0.20	1.24±0.06	169±13
PTMC/fibre L1 mat	6.61±1.55	1.44±0.42	122±22

*Young's modulus is calculated by the slope of stress-strain curve at 0-3% strain

Table 4.2 *Quantification data of R_r and R_f of different samples.*

Sample	*Rf1 (%)*	*Rf2 (%)*	*Rf3 (%)*	*Rf4 (%)*	*Rr1 (%)*	*Rr2 (%)*	*Rr3 (%)*	*Rr4 (%)*
PTMC	12.2	12.7	12.9	13.0	93.6	99.4	99.7	99.7
PTMC5000	12.2	14.0	14.5	14.9	94.4	97.8	99.1	99.5
PTMC17200	38.3	42.4	44.3	45.4	77.8	87.9	92.3	94.3
PTMC continuous fibre	93.8	93.7	93.8	93.9	53	86.5	92.3	94.9
PTMC5000 continuous	66.9	67.0	67.4	67.8	65.3	93.9	96.8	97.7
PTMC17200 continuous	86.5	88.4	89.5	90.3	43.8	72.2	82.7	86.9
PTMC/10% fibre L1	19.8	19.7	20	20.3	92.3	98.8	99.4	99.4
PTMC/30% fibre L1	43.1	43.9	44.4	44.9	81	94.1	96.2	97.4
PTMC/50% fibre L1	85	85.5	85.7	85.9	47.3	87.7	90.9	94.1
PTMC/10% fibre L2	54.5	57.7	59.6	61.1	69.5	91.5	93.7	95.3
PTMC/30% fibre L2	58.1	60.8	62.6	63.7	66.2	89.2	92.5	94.2
PTMC/fibre L1 mat	74.7	75.7	75.2	75.3	72.2	94.1	96.2	97.4
PTMC/PLA-PEG fibre	96.3	96.5	96.7	96.8	52.0	77.3	84.1	87.7

The SEM images of PTMC and PTMC/PLA fibre composites after shape memory tests are shown in Figure 4.9. A strong bonding between PLA fibres and PTMC still exists as no fibre pull-out occurred, indicating a good mechanical stability of the SMPCs. Photographs demonstrating the composites' shape memory behaviour are presented in Figure 4.10. For this a 20×3×0.12 mm^3 rectangular sample (permanent shape) was cut out of the continuous fibre composite film and placed on a hot plate heated at 100 ˚C. The sample was then deformed around a glass rod and quickly quenched in cold water. After removing the glass rod, the sample remained curved (temporary shape). The single curved sample was then transferred back onto the hot plate at 100 ˚C, which showed a quick recovery back to the sample's original flat shape (full recovery within 15 sec). For short fibre composites, a spring-shaped (permanent shape) sample was produced using a spiral tube mould. The temporary spiral shape was obtained by compressing the spring-like sample in a water bath at 90 ˚C followed by quenching in cold water. Shape recovery was achieved within 3 sec by placing the compressed spiral back in the water bath at 90 ˚C.

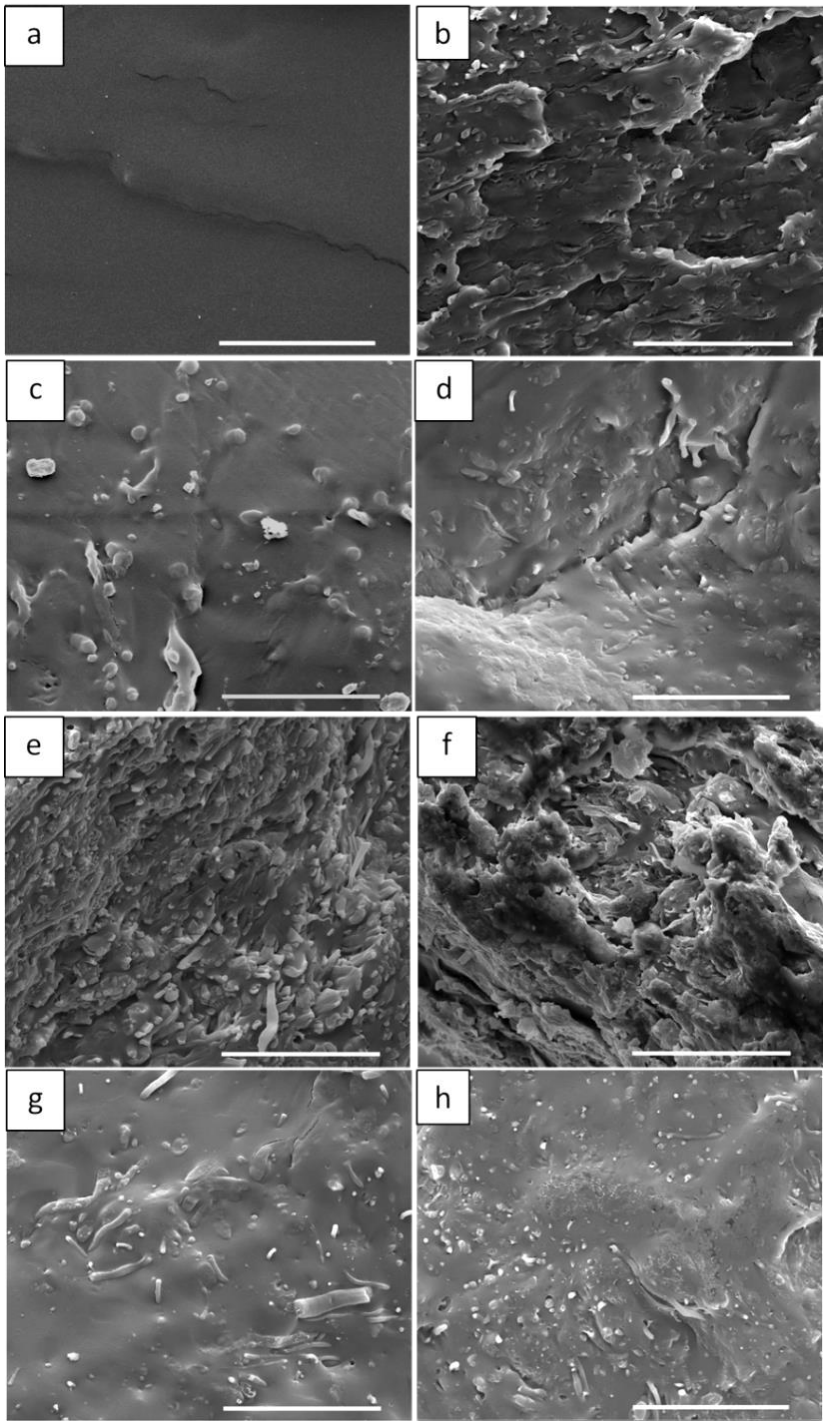

Figure 4.9 *SEM images of cold-fractured cross-sections of PTMC and PLA fibre reinforced PTMC composites after four shape memory test cycles: (a) neat PTMC, (b) continuous PTMC/PLA fibre composite, (c) PTMC/5 wt% fibre L1 composite, (d) PTMC/10 wt% fibre L1 composite, (e) PTMC/30 wt% fibre L1 composite, (f) PTMC/50 wt% fibre L1 composite, (g) PTMC/10 wt% fibre L2 composite, (h) PTMC/30 wt% fibre L2 composite (scale bar 20 µm).*

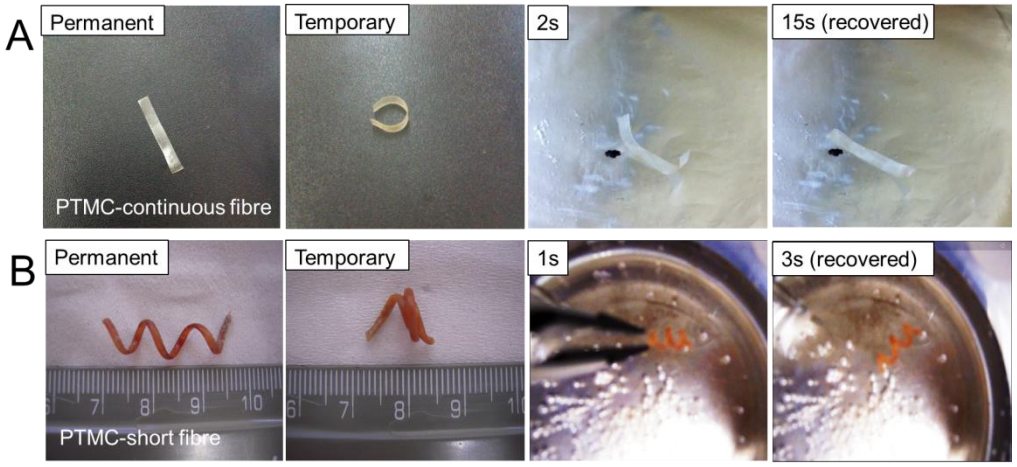

Figure 4.10 *Photographs demonstrating PLA fibre reinforced PTMC composite shape memory behaviour: (A) Rectangular PTMC/PLA continuous fibre composite sample was bended around a glass rod at 100 ˚C and then quenched. The shape recovery was triggered by heating at 100 ˚C; (B) a spring-shaped sample of PTMC/50 wt% fibre L1 composite was compressed in a water bath (90 ˚C) and quenched in cold water. By heating the sample back to 90 ˚C, shape recovery was achieved.*

4.3.4 Modulating shape memory transition temperature

In addition to tuning the composites' shape fixing and recovery properties by adjusting the PLA fibre loading and aspect ratio, PEG was blended into PLA to modify the shape memory transition temperature. PTMC/PLA-PEG blend fibre composites were prepared and tested in the same way as PTMC/PLA continuous fibre composites. SEM images of electrospun PLA-PEG fibres and cryo-fracture surfaces of these composites are shown in Figure 4.11. Fibres are continuous and defect-free. The average diameter is calculated at 1.2±0.6 µm with some very thin fibres present (150 nm). The change in fibre morphology is due to the change in viscosity of the electrospinning solution with the addition of PEG. Fibres are still adhering firmly to the PTMC matrix, implying good stress transfer and reinforcing efficiency.

Thermo-mechanical tests were performed using the same conditions as for PTMC/PLA continuous fibre composites. DSC tests show that the T_g of electrospun PLA fibre is shifted from 60.0 ˚C to 46.1 ˚C after blending with 10 wt% PEG. Meanwhile the cold crystallization peak becomes more narrow and decreased from 95.4 ˚C to 81.8 ˚C. The crystallinity is calculated at 14.8%, higher than for pristine PLA fibre (3.4%). After

integration into the PTMC network, the cold crystallization peak disappeared, with crystallinity increasing to 41.6% while T_g is increased to 50 ˚C. This is believed to be caused by the diffusion of PEG during the fabrication process. A melting point is measured at 155 ˚C for all samples. DMA tests were performed to study the transition temperature for the shape memory effect. The tan δ peaks of PTMC and fibre phase are shifted from -4 ˚C to -19 ˚C and 78 ˚C to 68 ˚C, respectively (see Figure 4.11), indicating that PEG exists in both the PTMC matrix phase and PLA fibre phase. Thus shape memory tests were performed at 68±20 ˚C. Stress-strain tests at 88 ˚C showed good mechanical properties of composites with Young's moduli of 12.0±0.5 MPa, tensile strengths at 1.48±0.03 MPa and yield strains at 191±10%, compared with 1.7±0.2 MPa, 0.74±0.02 MPa and 74±8% for neat PTMC. PTMC/PLA-PEG blend fibre composites showed excellent shape fixity properties (average 97%). A training effect of 48% unrecovered strain is observed in the first test cycle. The recovery ratio R_r gradually increased and approached 90% in four cycles. The detailed quantification on R_r and R_f is listed in Table 4.2. Neat PTMC under this condition still presents significant elasticity with no shape fixity (average R_r at 99.5% and R_f at 9.6%). For comparison, shape memory tests at 68 ˚C were also performed on PTMC/PLA fibre composites without PEG, whose T_g was initially measured at 78 ˚C. The average shape fixing ratio R_f is decreased to 71.3%, which is due to a decreased polymer chain mobility. Thus, this proves that the addition of PEG is effective in altering the shape memory behaviour temperature.

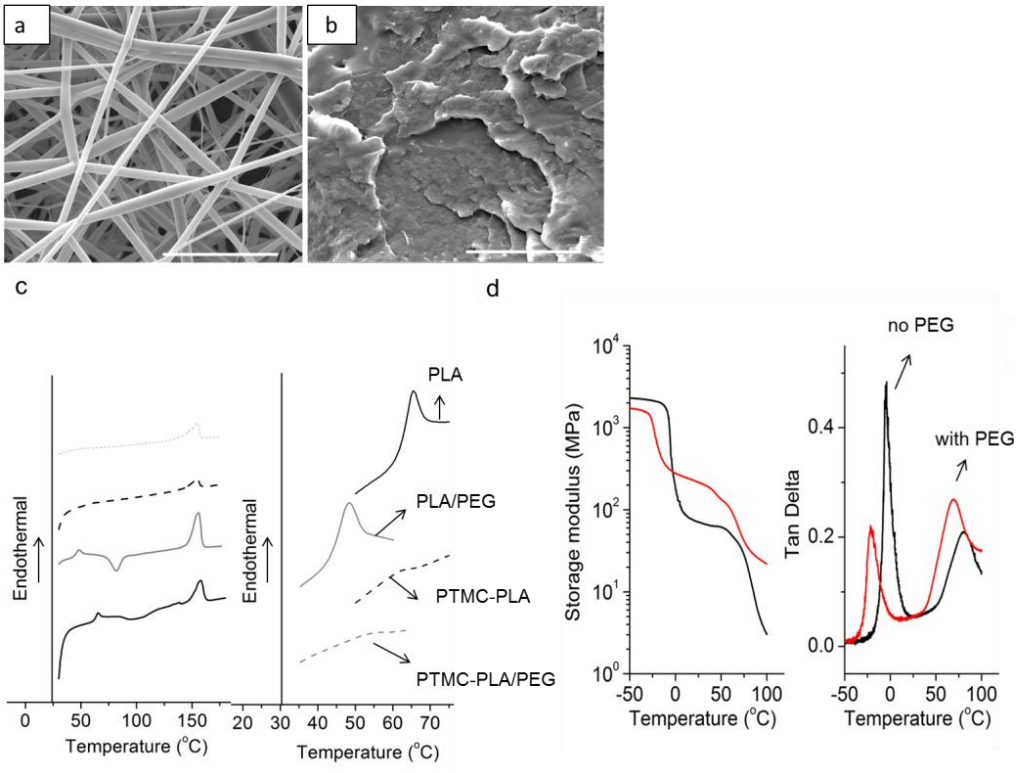

Figure 4.11 *SEM images of electrospun PLA/10% PEG blend fibres (a) and their cold-fractured PTMC composites before shape memory test (b) (scale bar 20 µm); (c) DSC thermograms of electrospun PLA/10% PEG blend fibres and their PTMC composites; (d) storage modulus and tan δ of PTMC/PLA fibre composites as a function of temperature (with and without PEG).*

Composite samples after shape memory tests are characterized by SEM and DMA. Fibres remained well embedded in the PTMC matrix (see Figure 4.12), showing the stability of the composites after repeated usage. The storage modulus increased after the shape memory test, which is a result of polymer chain orientation by stretching during the test. The tan δ peak of the composites remained unchanged, indicating that no aging effects occurred during the test. Therefore, it can be concluded that these shape memory composites are both mechanically and thermally stable.

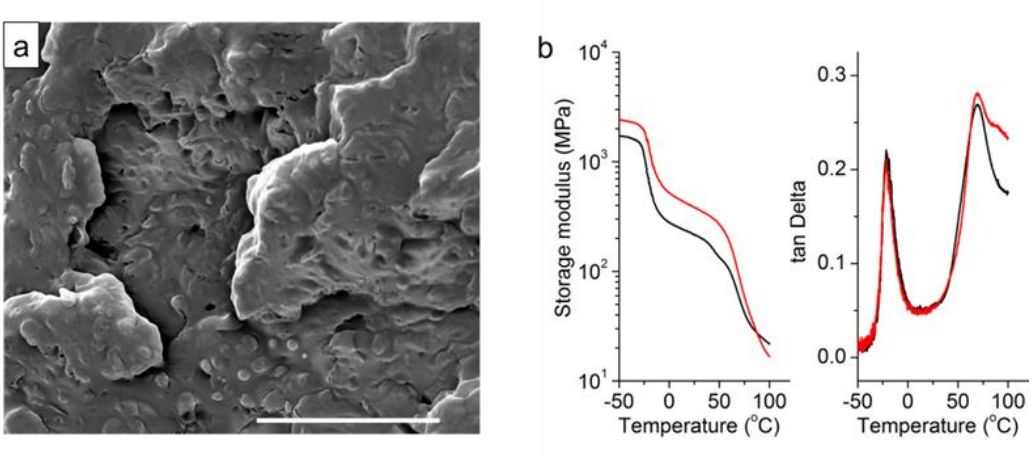

Figure 4.12 *SEM image of cold-fractured PTMC/PLA-PEG fibre composites after shape memory test (scale bar 20 µm); (b) storage modulus and tan δ of PTMC/PLA-PEG composites as function of temperature tested by DMA (black-before shape memory test; red-after shape memory test).*

4.4 Conclusions

Biocompatible and degradable one-way SMPCs were successfully developed by incorporating both continuous and discontinuous electrospun PLA fibres into a crosslinked PTMC network. These fibres not only act as reinforcing fillers but also as a 'switching phase', which in combination with the elastic PTMC network demonstrates shape memory properties. The large interfacial area and strong bonding between PTMC matrix and PLA fibres indicate a highly efficient stress transfer mechanism. With the integration of continuous electrospun PLA fibre mats or 50 wt% short PLA fibres, the Young's modulus of PTMC was increased by one order of magnitude without compromising the material's elasticity under experimental conditions. Continuous fibre composites exhibited good shape memory properties (R_f= 94%, R_r= 95%), while discontinuous fibre composites loaded with 50 wt% short PLA fibres also proved to exhibit good shape fixity and recovery (R_f=86%, R_r=94%). By controlling the short PLA fibre loading and aspect ratio, composite shape memory properties can be tailored. It was found that by increasing the short fibre's aspect ratio and loading, the composites' strain fixing behaviour is improved while good strain recovery is maintained. Moreover, by using short fibres, composite fabrication processes such as injection moulding and compression moulding become feasible, opening up the possibility to create complex

3D geometries. Finally, it was is found that by adding PEG as a plasticizer into the PLA fibres, the composites' shape memory transition behaviour can be performed at different temperatures, significantly increasing the SMPCs' potential applications. The biocompatible and degradable nature of the developed SMPCs in combination with the potential of easy processing and flexible designs can therefore make these materials interesting candidates for smart medical devices.

Chapter 5 – Advanced drug delivery systems based on drug-loaded electrospun PLA fibres in photo-crosslinkable PTMC matrix

5.1 Introduction

Poly(trimethylene carbonate) (PTMC) is a biocompatible and degradable polymer material that can be synthesized via ring-opening reaction of 1,3-trimethylene carbonate [7]. Its degradation mediated by a surface-erosion mechanism, is characterized by an extremely low level of non-enzymatic hydrolysis and non-acidic degradation by-products, which makes PTMC an attractive material and polyesters alternative for biological applications [8]. However, PTMC is usually considered to have poor mechanical performances, which restricts it from certain usages that require good dimensional stability. Efforts have been endeavoured to enhance the mechanical properties of PTMC, by increasing molecular weight [188], blending with other stiffer polymers or inorganic particles [191, 243, 244], copolymerizing with 'hard' polymer blocks [245] or crosslinking [189]. Recently, Schüller-Ravoo et al. synthesized three-armed PTMC macromers and functionalized the arm with methacrylate ends. The photo-crosslinking of the functionalized macromer produced flexible and tear-resistant elastomeric materials [190]. Stereolithography (SLA) is a common additive manufacturing technique, employed to build PTMC-based structures with unprecedented degree of precision for the control of three-dimensional architectures. Despite the great potential of SLA-fabricated scaffolds, very few examples of PTMC drug delivery systems fabricated using photo-fabrication can be found in the literature. Indeed, SLA requires successive layer-by-layer photoreactions of the resin compounds, containing methacrylated-ended macromers and photo-initiators. This intrinsically restricts the potential of the SLA-fabricated scaffolds to be used as drug delivery carriers, due to chemical UV cross-reaction and incompatibility between the therapeutics and the photoreaction, and due to the light sensitivity of a great majority of active compounds. So far, only Vitamin B12 (as model system) has been

incorporated into PTMC photo-crosslinkable matrix, in the form of non-soluble micro-granules to prevent any degradation [197].

In Chapter 3, reinforcement of PTMC was achieved by incorporating electrospun poly(lactic acid) (PLA) fibres in methacrylate-ended PTMC macromer followed by UV crosslinking [88]. The improvements in mechanical properties of PTMC combined with potential biological features has brought interests in designing composite drug delivery systems, which is the focus of the current chapter using Dexamethasone (Dexa) as a model drug. Dexa is a synthetic glucocorticoid with several therapeutical applications, such as anti-inflammatory, immunosuppressant and decongestant [246]. It also shows potent stimulation effects on the proliferation and osteogenic differentiation of mesenchymal stem cells (MSCs) in the presence of β-glycerol phosphate and ascorbic acid/ascorbate [247, 248], with optimal concentrations ranging from 10 to 100 nM [249].

Since then, various platforms have been developed as Dexa carriers, allowing for a sustained release, such as implant dispensers [250], nanoparticles/hydrogel complexes [251], self-assemblies of nanofibre gels [252], electrospun fibres [118], macroporous scaffolds [253], additive manufacturing fabricated structures [249] etc. Among those, Dexa-charged nanoparticles are easy to administrate as injectable system but have low drug loading efficiency and it is difficult to prevent their dispersion in the body following their administration for local treatment. Hydrogel/fibre reinforced composites are more suitable for local delivery and showed controlled release profiles according to previous reports; nevertheless their poor mechanical performance restricts their potential applications. Electrospun polymer fibres have gained great interest as drug carriers due to their ease of fabrication, high drug encapsulation efficiency, large surface area and highly porous fibrous structure [254]; but a burst release usually occurred as a result of drug accumulation at the fibre surface [212, 255]. The initial burst release can be alleviated by improving drug-polymer compatibility and drug solubility in polymer solution during electrospinning (i.e. employing surfactants, although this gives rise to problems of cytotoxicity). A sustained release is also realized by fabricating complex structures that encapsulate drug in core-shell structures, modifying the fibre's chemical properties or using drug-binding agents [8, 157, 256-258]. Most of these methods are inevitable to either modify the fibre or drug chemical/physical properties or involve complicated fabrication processes.

The objective of current work is to fabricate a PTMC/PLA fibre composite system that enables the controlled release of Dexa. PLA was chosen for the fabrication of electrospun fibres since it is commercially available, biocompatible, degradable and much stiffer than PTMC. Additionally, the combination with PTMC is also improving the ductility of the rather brittle PLA material, as shown in Chapter 3 [88]. PLA fibres loaded with Dexa were electrospun and incorporated into PTMC matrix. Such hybrid materials will bring various advantages in terms of tailoring mechanical properties, preservation of drug stability and control of diffusion rates, compared to direct drug-loaded PTMC strategies. In order to validate this approach, the biological activity of Dexa-loaded PTMC/PLA fibre composite films was assessed by investigating its osteogenic effect on human stem cells.

PTMC-based scaffolds have already shown great versatility and promising potential in terms of biomedical applications [7], while its ability to incorporate therapeutics into the PTMC-photocrosslinked structure without affecting its activity is of major importance.

5.2 Experimental

5.2.1 Materials

Poly(lactic acid) (PLA 2002D, $\overline{M_w}$200,000 g/mol, density 1.24 g/cm^3) was obtained from Natureworks. PTMC (three-armed methacrylate-ended, $\overline{M_w}$10,000 g/mol) macromer was synthesized as reported [205]. Chloroform, dimethylformamide (DMF), methanol, dichloromethane and acetonitrile (HPLC grade) were obtained from Fisher Scientific. Poly(ethylene glycol) methacrylate (PEG-methacrylate, average Mn 360 g/mol), dexamethasone (powder, BioReagent, ≥97%, chemical structure shown in Figure 5.1), 2-Hydroxy-4'-(2-hydroxyethoxy)-2-methylpropiophenone (Irgacure 2959, I2959) were purchased from Sigma-Aldrich. Phosphate buffered saline (PBS) was prepared by dissolving one tablet of PBS (Sigma-Aldrich) in 200 ml deionized water. All materials and reagents were used as received.

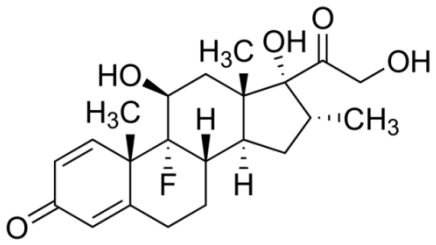

Figure 5.1 *Chemical structure of dexamethasone (Dexa)*

5.2.2 Electrospinning and composite preparation

Electrospinning was performed using the in-house built electrospinning equipment described in Chapter 3. To spin PLA and Dexa-loaded PLA fibres, a PLA solution with a concentration of 9 wt% in chloroform/DMF (chloroform:DMF=3:1) was first prepared. For low Dexa-loaded fibres (0.7 wt% with respect to PLA), Dexa was added to the PLA solution and stirred until fully dissolved. For higher Dexa loadings (2.4 wt% with respect to PLA), methanol was used to replace DMF while preparing the PLA solution in order to increase the drug solubility. The PLA or PLA-Dexa solution was supplied through a PTFE tube at 1.0 ml/h to the electrospinning spinneret. The spinning was carried out at a voltage of 18-20 kV and a distance of 15 cm. Random fibre mats were collected on a grounded sheet of aluminium foil. Finally three different PLA fibre mats (neat PLA (PLA 0), PLA-low Dexa (PLA 1) and PLA-high Dexa (PLA 2)) were obtained and they were evaporated in a vacuum desiccator for 48 hrs to remove residual solvent.

Hot-pressing was used to incorporate the electrospun fibres into PTMC matrix. To perform hot-pressing, PTMC macromer was first dissolved in dichloromethane at 50 wt% concentration together with 0.67 wt% of I2959 (with respect to PTMC). After dissolution, the PTMC/dichloromethane solution was transferred into a vacuum desiccator for 48 hrs to remove the dichloromethane. The dried PTMC/I2959 mixture was then ready to use for hot-pressing (Dr. Collin P300E). 40 mg of PLA fibre mats (size 50×50×0.08 mm^3, referred to as PLA 0, PLA 1 and PLA 2, loaded with 0, 0.68 and 2.42 wt% of Dexa respectively) was placed in a 60×60×0.15 mm^3 mould, which was then transferred into the hot-press. 160 mg of PTMC macromer (containing I2959) was placed on top of the fibre mats. Fibres and PTMC were pre-heated to 60 ˚C for 5 min and then pressed under 25 bar pressure. The compression moulded films had a thickness of 0.06 mm and were removed from the mould after cooling to room

temperature. This was followed by exposing these composite films to UV (Omnicure 1500) for 100 sec at 15 mW/cm^2 to cure the PTMC (UV intensity is higher than in SLA due to the composite structure). The composite films were then stored in a nitrogen box for further experiments. For comparison, PTMC samples without fibres were prepared by casting PTMC/I2959 dichloromethane solution into a 50×5×1 mm^3 mould followed by evaporation of the solvent. PTMC was UV-cured using the same parameters as described above. Four different sets of samples were prepared, named PTMC (for neat PTMC without PLA fibre), PTMC/PLA 0, PTMC/PLA 1 and PTMC/PLA 2 for composites reinforced with PLA fibres loaded with 0, 0.7 and 2.4 wt% of Dexa, respectively.

5.2.3 Electrospun fibre and PTMC/PLA fibre composite characterization

The morphology of the electrospun fibres and PTMC/PLA fibre composites were characterized using scanning electron microscopy (SEM, FEI Inspect F). All samples were mounted onto a SEM specimen stub and sputter-coated with a thin gold layer. To examine PTMC infiltration and fibre-matrix interaction, composite samples were cold-fractured in liquid nitrogen and the fracture surfaces were characterized using SEM. Thermal properties of electrospun fibres were measured using differential scanning calorimetry (DSC, Perkin-Elmer DSC 4000). Samples were first equilibrated at 25 ˚C and then ramped to 180 ˚C at 10 ˚C/min. Glass transition temperature (T_g) was determined by the mid-point of the glass transition. The crystallinity of PLA was calculated by,

$$X_c = \frac{\Delta H_m}{\Delta H_{ref}} \times 100\% \quad (5.1)$$

where X_c is the crystallinity, ΔH_m is the experimental heat of fusion at melting point determined by DSC, ΔH_{ref} is the theoretical heat of fusion of fully crystalline PLA (93 J/g) [206]. Tensile tests of electrospun fibre mats and PTMC/PLA fibre composites were performed using dynamic mechanical analysis (DMA, TA Q800) in a controlled force mode. Samples were cut into 20×5×0.06 mm^3 rectangular strips before being mounted into clamps. A preload of 0.05 N was applied and the specimens were stretched at a rate of 0.1 N/min until failure at room temperature. The Young's modulus was derived from the slope of the stress-strain curve at a low strain (0-2%) and three tests were performed for each type of sample.

5.2.4 In vitro measurement of Dexamethasone release

Dexa concentration in phosphate-buffered saline (PBS) was determined using high performance liquid chromatography (HPCL, Waters e2695) equipped with UV detector and a Kinetex column (Phenomenex, C18, 100 Å, 5 µm, 150×4.6 mm^2). The mobile phase was 50/50 v/v acetonitrile/PBS, eluted at 1.0 ml/min. The detection was performed at 256 nm UV adsorption wavelength with 50 µl injection for each solution. Before injection, a series of Dexa/PBS solutions at concentrations ranging from 8×10^{-6} to 5.6×10^{-4} mg/ml were prepared for contructing a calibration standard curve (HPLC peak area against Dexa concentrations). To evaluate the Dexa elution from electrospun PLA fibres and PTMC/PLA fibre composites, 15×15 mm^2 specimen were cut from each sample and immersed in 3 ml PBS into an incubator at 37 ˚C for a period of five weeks. At different time intervals, each specimen was removed from the media and transferred into 3 ml fresh PBS. The recovered media was then analysed using HPLC and again three tests were conducted per sample group. The Dexa concentration released in the media is calculated by first integrating the HPLC peak and then derived from the standard calibration curve.

5.2.5 Gel permeation chromatography analyses

Gel permeation chromatography (GPC) technique was employed to investigate the possible coupling between Dexa and the methacrylate-ended PTMC macromers, in the presence of a photoinitiator, during UV curing. We examined the refractive index (RI) signal of methacrylate and Dexa before and after UV curing. Instead of PTMC-methacrylate, a model of macromer PEG-methacrylate was used and dissolved in tetrahydrofuran (THF) at a concentration of 2.0 mg/ml. Dexa and I2959 were added at 0.20 mg/ml and 0.17 mg/ml respectively. The solution was degassed in nitrogen for 30 min and divided into two portions, one of which was UV treated at 15 mW/cm^2 for 100 sec. For reference, THF solutions of Dexa and I2959 were also tested separately to identify their signals. The GPC tests were performed using Agilent Technologies 1260 infinity equipped with a UV detector at 308 nm wavelength. Tetrahydrofuran (with 2.0 vol% triethylamine) was used as the eluent at a flow rate of 1.0 ml/min.

5.2.6 Cell experiments

PTMC/PLA fibre composite films (PTMC/PLA 0, 1 and 2) were punched into discs with a diameter of around 6.0 mm (each disc weighs around 1.5 mg). These discs were then placed in a 96-well plate and sterilized in ethanol 70% for 10 min.

Human bone marrow mesenchymal stem cells (hBMSCs) were isolated from vertebral body bone marrow aspirates (obtained from donors undergoing spinal fusion with informed consent and full ethical approval (KEK Bern 126/03)). hBMSCs of two donors were expanded individually and seeded separately (at passage 3) onto the films at a density of 20,000 cells/cm^2. In order to investigate the biological activity of Dexamethasone released from the composite structures (PTMC/PLA 0, 1 and 2), the cells were cultivated in osteogenic media depleted of any Dexamethasone (called "OM-") based on basic low glucose DMEM (GIBCO) supplemented with 10% serum (SeraPlus), 1% penicillin/streptomycin (GIBCO), 50 µg/mL ascorbic acid and 5 mM glycerol-2-phosphate (all from Sigma-Aldrich). The osteogenic differentiation of hBMSCs in the described groups were compared to cells seeded on PTMC/PLA 0, cultivated under non-osteogenic condition (negative control in basal medium, called "BM", based on basic low glucose DMEM supplemented with 10% serum and 1% penicillin/streptomycin) and complete osteogenic medium (positive control, called "OM+" similar to "OM– " composition but supplemented with 10 nM Dexamethasone (from Sigma-Aldrich). After seeding, the 96-well plates were filled with 200 µL of the different media and were changed three times a week for the 28 days of the osteogenic experiment. For all the *in vitro* investigations, control surfaces based on tissue culture polystyrene (TCPS) was used (96-well plate TPP, Trasadingen, Switzerland).

The cytocompatibility of the different PTMC/PLA composite films and the cell proliferation kinetic was evaluated using CellTiter Blue assay (Promega, Dübendorf, Switzerland) at 2, 6, 14, 21 and 28 days post-seeding (n=5 per group), following the supplier's recommendation. The resulting fluorescence intensity was read with a multi-plate reader (Viktor^3, 1420 Multilabel Count, Perkin-Elmer) and values were corrected using cell-free condition.

For DNA quantification, samples were first incubated in lysis buffer made of Triton X-100 at 0.1% in 10 mM of Tris-HCl, pH=7.4 (all from Sigma-Aldrich) and followed by one freezing-thawing cycle. Then, the DNA content was estimated using fluorescent CyQuant® GR Dye assay, according to the supplier's recommendation (Invitrogen), (n=3 per group). Alkaline phosphatase activity (ALP) from the cell-lysis solution was determined using colorimetric quantification. Briefly, samples along with a set of standard solutions (*p*-nitrophenol of concentrations from 0 to 1000 µM) were incubated with alkaline buffer solution (2-amino-2-methylpropanol 1.5 M pH=10.3,

from Sigma-Aldrich) and then ALP substrate buffer was added (phosphatase substrate dissolved in diethanolamine buffer at 1 M in 0.5 mM $MgCl_2$ adjusted pH=9.8). After mixing, and heating (at 37 ˚C for exactly 15 min), a solution of NaOH at 0.1 M was added to each tube in order to stop the reaction. Then, the intensity of *p*-nitrophenol formation was monitored at 405 nm. The total ALP contents were expressed as enzyme activity units in nmol/min (n=3 per group), as a function of total DNA (ng) per well measured using CyQuant® assay. ALP staining was performed after washing the cell monolayers with PBS (3 times), fixation (with ice cold ethanol 90% for 4 min), washing with deionised (DI) water and later, staining with Fast Blue dye solution for 1 hr wrapped in tin foil (Naphthol AS-MX, according to Sigma-Aldirch recommendation). After incubation, samples were washed 3 times with DI water and imaged by light microscopy (Macrofluo™ from Leica).

Presence of mineralization was detected using Alizarin Red Staining (ARS, Sigma-Aldrich), with TCPS as control films. The cell monolayer was washed with PBS, fixed with formaldehyde 4% and further washed with DI water. Then, 40 mM ARS solution at pH=4.2 was added to each well for 1 hr and thoroughly washed with DI water for 5 days. Finally, samples were imaged by light microscopy (Macrofluo™ from Leica) and a quantification of the ARS was performed by acid extraction thereafter. Briefly, acetic acid (at 10%) was added to each well for 30 min, and the loosely attached monolayer of cells was transferred to Eppendorf tubes, heated to 85 ºC for 10 min, and then placed on ice for 5 min. After centrifugation at 20,000 g for 15 min, ammonium hydroxide was added to the supernatant (final pH of 4.1-4.5) and absorbance was recorded at 405 nm and compared to ARS standard solutions ranging from 0 up to 2000 µM (n=3 per group). For all the mentioned assays, background values obtained from cell-free conditions are subtracted from the final values.

SEM analyses required the fixation of the samples overnight in buffered paraformaldehyde at 4%, dehydration with gradual concentration of ethanol up to 100% followed by immersion in hexamethyldisilazane (Sigma-Aldrich). After complete drying, the samples were sputter-coated with C and investigated using a Hitachi S4700 FESEM instrument.

5.2.7 Statistical analyses

Statistical analysis of data was performed using Prism software (GraphPad Software, La Jolla, CA, USA). We assumed normal distribution of data. One way ANOVA with Tukey's multiple comparison test was applied to detect significant differences between experimental groups (with $p < 0.05$). Data presented are means ± standard deviation (SD) unless stated otherwise.

5.3 Results and Discussion

5.3.1 Physical properties of PTMC/PLA fibre composites

The morphologies of electrospun fibres (with and without Dexa) were characterized using SEM (see Figure 5.2 top). Interestingly, the incorporation of Dexa into PLA produced more uniform and thinner fibres, with an average diameter for PLA fibres decreasing from 1.23±0.47 µm (PLA 0) to 0.39±0.14 µm and 0.74±0.15 µm for PLA 1 and PLA 2, respectively (Figure 5.2 bottom). Some heterogeneity (e.g. beading) was observed on fibres with 0.7 wt% Dexa, which is ascribed to the reduced viscosity of the spinning solution. However, no beading was observed for fibres with 2.4 wt% Dexa, whose surfaces were smooth. The difference is attributed to the increased solubility of Dexa when using methanol instead of DMF for electrospinning. Moreover, the fact that electrospinning using methanol (for fibres with high drug loading) produced larger diameter fibres than by using DMF (for fibres with low drug loading) is explained by the faster evaporation rate of methanol compared to DMF, which resulted in quicker solidification of the fluid jet and thus less stretching.

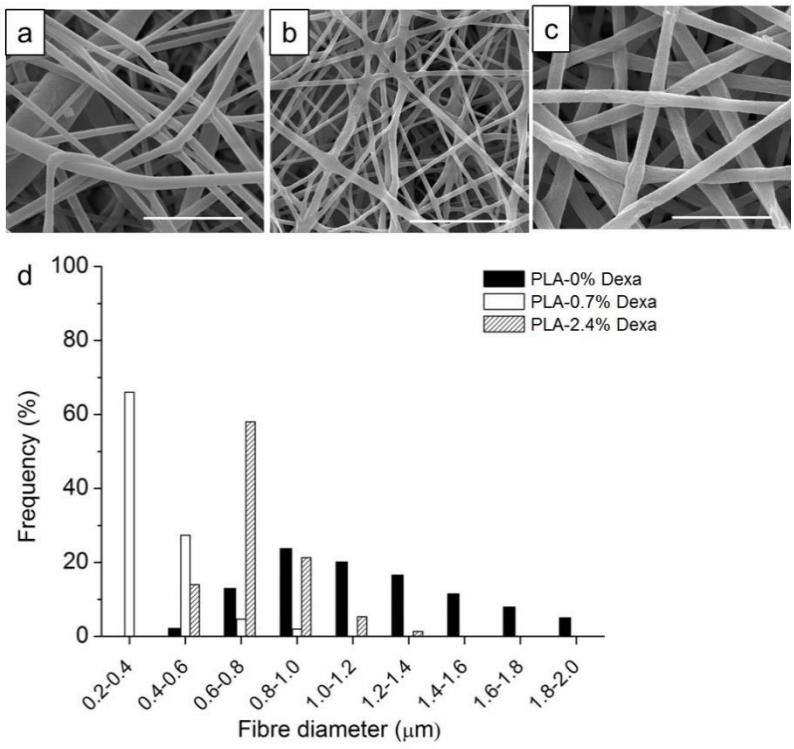

Figure 5.2 *SEM images of electrospun fibres (scale bar 5 μm): (a) PLA-0% Dexa, (b) PLA-0.7% Dexa and (c) PLA-2.4% Dexa (A); (d) fibre diameter distribution of PLA-0% Dexa, PLA-0.7% Dexa and PLA-2.4% Dexa.*

Thermal properties of electrospun fibres are then characterized using DSC (Figure 5.3). A melting point (T_m) of 154 ˚C is measured for all samples except for PLA 2 (153 ˚C). Glass transition temperature (T_g) of bulk PLA (63.9 ˚C) is decreased after electrospinning (PLA 0, 60.0 ˚C) and further decreased to 59.2 ˚C (PLA 1) and 59.0 ˚C (PLA 2), respectively, with the addition of Dexa. This decrease in T_g after electrospinning is caused by the inner stress stored in electrospinning, which makes molecules become more mobile at lower temperature [212]. Small molecules, such as Dexa, are considered to act as plasticizer and lower the T_g of PLA. Cold crystallization is observed for all electrospun PLA fibres. The cold crystallization peak becomes sharper and cold crystallization temperature (T_{cc}) is shifted to lower temperatures (from 95.4 ˚C to 87.9 ˚C) after incorporating 2.4 wt% Dexa. The crystallinity of bulk PLA is decreased from 34.4% to 3.4% after electrospinning and further decreased to 2.1% after adding 0.7 wt% Dexa. However, the crystallinity is increased slightly to 5.7% when using methanol instead of DMF. The changes in PLA crystallinity are considered to affect the fibre's mechanical properties, which is evaluated later by tensile tests.

a

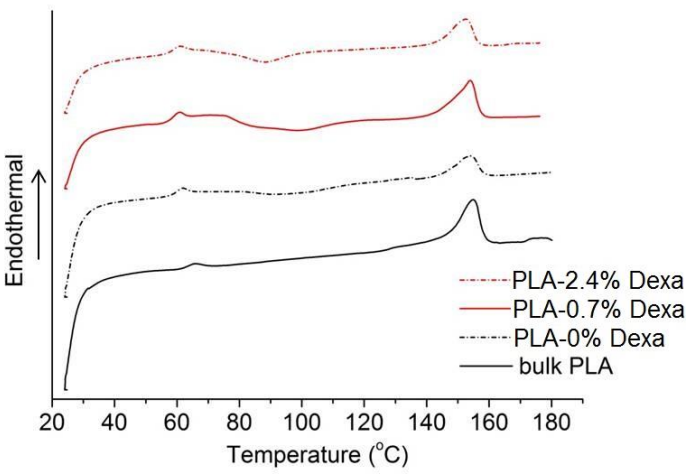

b

sample	T_g (°C)	T_m (°C)	T_{cc} (°C)	crystallinity (%)
Bulk	63.9	154	N/A	34.4
PLA 0	60.0	154	95.4	3.40
PLA 1	59.2	154	97.6	2.10
PLA 2	59.0	153	87.9	5.70

Figure 5.3 *(a) DSC thermograms of the different PLA materials without Dexa (bulk PLA and PLA 0) and with Dexa loading (PLA 1 and 2). (b) Quantification of the PLA fibres' thermal properties depending on the processing and presence of Dexa.*

The SEM images of PTMC/PLA fibre composites are presented in Figure 5.4, where both the morphology of surfaces (a1, b1, c1) and cross-sections (a2, b2, c2) are presented. The composite surfaces are PTMC rich, with only some PLA fibres exposed. We observed a good compatibility between PLA and PTMC, as fibres are well wetted by PTMC matrix with very few voids and debonds being present (Figure 5.4 b2 and c2). PTCM matrix seem to adhere well to PLA fibres as most fibres are well embedded within the matrix with little fibre pull-out visible at the cryo-fracture surface, indicating a good level of interaction and interfacial bonding between fibres and PTMC matrix.

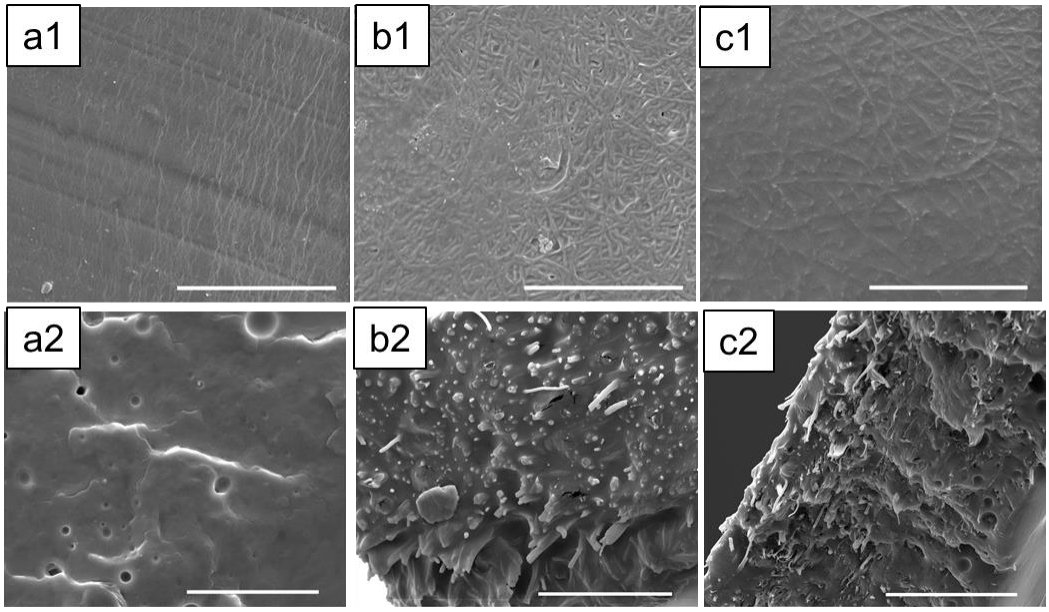

Figure 5.4 *SEM images of PTMC ((a1) surface, (a2) cross-section); PTMC/PLA 1 ((b1) surface, (b2) cross-section) and PTMC/PLA 2 ((c1) surface, (c2) cross-section), respectively (scale bar 20 µm).*

The mechanical properties of both electrospun fibres and PTMC/PLA fibre composites are quantified and the results are presented in Figure 5.5 and Table 5.1. PTMC exhibited elastic properties with decreased failure strain compared with solution processed PTMC described in the Chapter 1. It is found that the Young's modulus and strength of the electrospun fibre mat is much weaker than bulk PLA (3.5 GPa, provided by supplier). Previous studies showed that electrospun nanofibres with diameters ≤ 200 nm can typically exhibit a three-fold increase in Young's modulus compared to bulk polymer properties [221]. Despite a potential increase in fibre properties due to molecular orientation, the reason of the low Young's moduli of electrospun fibre mats is due to their lack of fibre orientation, high mat porosity, and weak fibre-fibre interactions enabling sliding during stretching. PLA 2 mats have a higher Young's modulus than PLA 0 because of their higher crystallinity (5.7% compared to 3.4%). Meanwhile, PLA 1 exhibits a lower failure strain, which is explained by its more heterogeneous structure, with the presence of beads (see Figure 5.2), which can act as potential defects, resulting in a low failure strain. The mechanical properties of PTMC are significantly improved by the addition of the electrospun fibres. Young's modulus of PTMC is increased by more than one order of magnitude and tensile strength is

increased 3-4 folds, indicating a highly effective mechanical reinforcement effect due to the integration of electrospun PLA fibres within the PTMC matrix. In addition, it is also observed from the stress-strain curve that the yield strain/stress, ultimate tensile strain/stress of electrospun fibre mats are increased after integrating into PTMC, indicating good improvement on electrospun PLA fibre by composite structure.

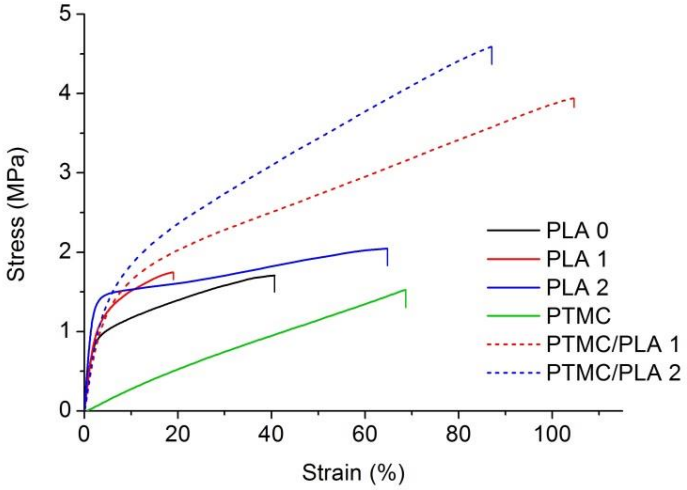

Figure 5.5 *Representative stress-strain curves of electrospun PLA fibre mats and PTMC/PLA fibre composites.*

Table 5.1 *Results of the tensile tests of electrospun PLA fibre mats and PTMC/PLA fibre composites.*

Sample	Young's modulus (MPa)	Strength (MPa)	Failure strain (%)
PLA 0	45.3±5.4	2.31±0.94	50±27
PLA 1	49.7±5.3	2.14±0.36	21±4
PLA 2	65.9±21.9	2.18±0.82	72±6
PTMC	2.7±0.5	1.31±0.43	62±11
PTMC/PLA 1	30.9±6.8	4.61±1.19	107±9
PTMC/PLA 2	33.9±19.3	3.86±1.41	82±13

5.3.2 Investigation of the crosslink-reaction between Dexa and methacrylated-PEG during UV curing

To study possible cross-reactions between methacrylate end-groups and Dexa, GPC tests were first run on Dexa and photoinitiator to identify their RI signal. A signal at 18.9 min is identified to be Dexa while a signal at 20.3 min belongs to I2959 (see Figure 5.6 a).The RI signal against elution time of Dexa and PEG-methacrylate before and after UV curing is presented in Figure 5.6 b. After UV curing, the intensity of the Dexa peak (eluted at 18.9 min) is significantly reduced. In the meantime, the peak corresponding to PEG-methacrylate (17.9 min) is shifted to lower elution times (17.7 min) with increased signal intensity. The shift of the PEG-methacrylate signal peak, the decreased signal intensity of Dexa and the increased signal intensity of PEG-methacrylate are all indicators of the coupling between Dexa and PEG-methacrylate. The reaction between Dexa and methacrylate-ended macromers shows the instability of Dexa when exposed to UV-curing processes and its potential deactivation when directly integrated into PTMC. It is therefore crucial to integrate them within electrospun fibres to protect their properties and functions.

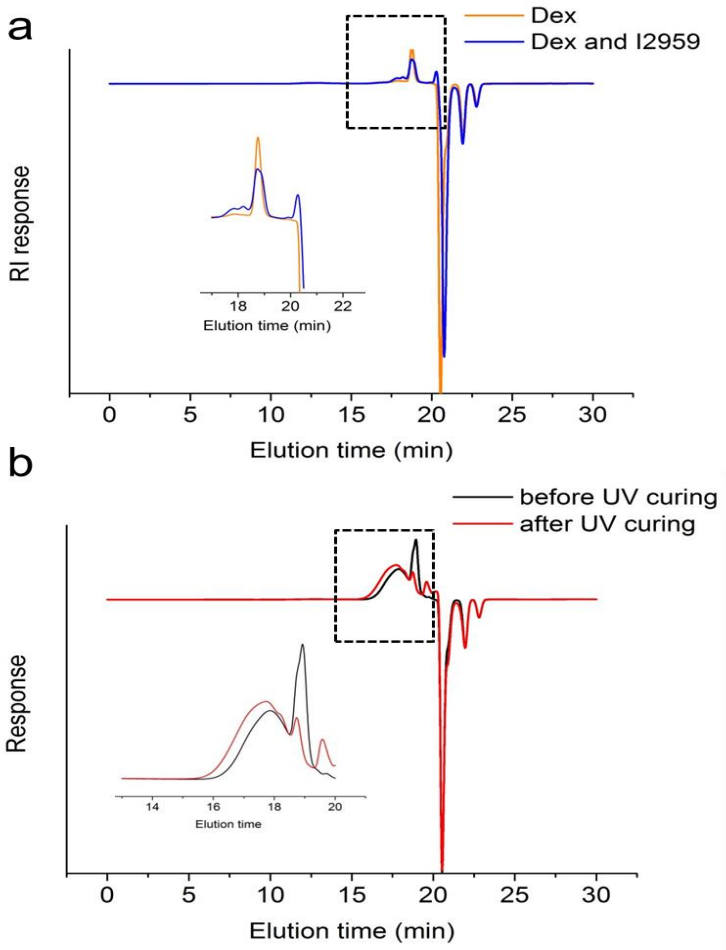

Figure 5.6 *(a) Refrective index detector (RI) signal against elution time of Dexamethasone and photoinitiator; (b) RI signal against elution time of Dexa and PEG-methacrylate before (black) and after (red) UV curing.*

5.3.3 In vitro release of Dexa from electrospun PLA fibres and PTMC/PLA fibre composites

To determine Dexa concentration released during the *in vitro* tests, a series of standard Dexa/PBS solutions were injected into HPLC (the representative chromatogram of standard Dexa/PBS solution at 3.2×10^{-4} mg/ml is shown in Figure 5.8a) and a calibration curve of Dexa concentration against HPLC peak integration was drawn (Figure 5.7). A distinctive peak at 2.4 min elution time was observed for all standard Dexa/PBS solution, which corresponds to Dexa; a linear relationship between Dexa concentration and HPLC peak integration was observed.

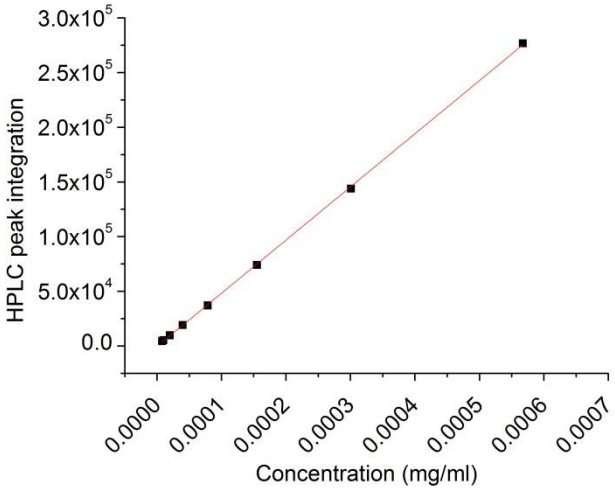

Figure 5.7 *Calibration curve of standard Dexa/PBS solution ranging from 8.0×10^{-6} to 5.6×10^{-4} mg/ml: a linear relationship between Dexa concentration and HPLC peak integration was observedwithin this range*

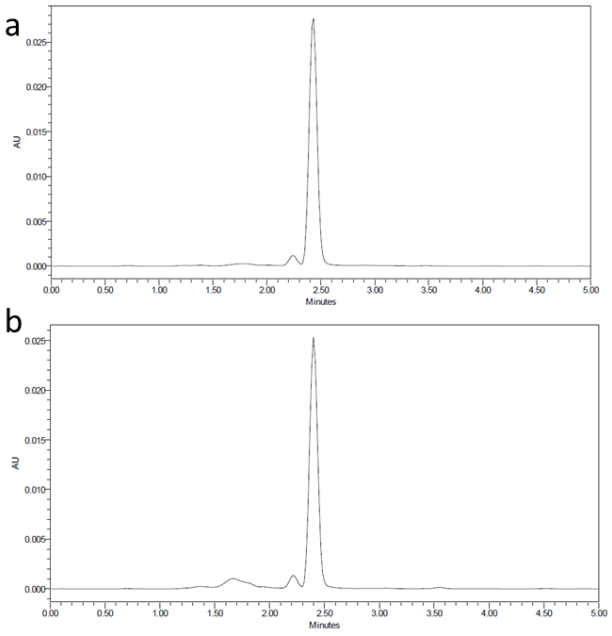

Figure 5.8 *Representative HPLC chromatogram of a standard Dexa/PBS solution at concentration of 3.2×10^{-4} mg/ml, b-PBS media recovered from in vitro release of PTMC/PLA 2 at Day 2.*

The PBS media recovered from *in vitro* tests at different time intervals was injected into the HPLC. The Dexa peak was still detected at 2.4 min elution time, indicating Dexa's properties are preserved (see Figure 5.8b). The Dexa concentration was then extrapolated using the calibration curve. Dexa release profile from electrospun fibres and PTMC/PLA fibre composites during five weeks are recorded in terms of cumulative release and actual Dexa concentration (Figure 5.9). All samples showed a quick release in the first four days *in vitro* and then the release rate decreases. A stable and sustained release profile is observed afterwards. The cumulative release profile suggested only small portions of Dexa are released during the test period, which can be explained by the slow degradation of both PLA and PTMC under the experimental conditions. PLA 2 exhibits the fastest release rate during the whole test period (initially 1.1×10^{-6} M then decreasing to 2.0×10^{-9} M after five weeks). By incorporating Dexa into PTMC, the elution kinetics is effectively reduced 6-10 fold in the first four days. Therefore a more stable Dexa release rate is achieved by incorporating PLA 2 into PTMC, whose release rate ranges from 1.4×10^{-7} M to 6.0×10^{-10} M. PLA 1 has the slowest initial release rate but shows a stable release profile, ranging from 4.1×10^{-9} M to 2.0×10^{-10} M. After integrating the PLA fibres into PTMC, the composites exhibit a much faster release rate than the fibres over the first three days (2-20 times); after which it keeps decreasing and finally maintains a stable release after ten days. The rapid initial Dexa release from the composites is ascribed to the incomplete coverage of PTMC on the fibre surface (see Figure 5.4). For *in vitro* cell assays (four weeks period), PTMC/PLA fiber composites (with both low and high Dexa loading PLA fibres and drug-free PLA 0 fibres) were used. From the release kinetics data, we can estimate by extrapolation the concentration of Dexa present in the culture media (for the *in vitro* experiment) at 9.4×10^{-7} M to 6.5×10^{-9} M for PTMC/PLA 2 and 6.4×10^{-7} M to 6.7×10^{-10} M for PTMC/PLA 1, based on 1.5 mg composites disc incubated in 200 µl culture media.

After 5 weeks of incubation in PBS, the PTMC/PLA fibre composites were characterized using SEM (see Figure 5.10). It is shown that composite structures were well preserved, similar to the ones illustrated in Figure 5.4, without major alterations (for both surface and cross-section). We can observe that the PLA fibres are still fully embedded within the PTMC matrix, indicating that the hybrid PTMC/PLA fibre structures remain stable during the 5 weeks of experiment.

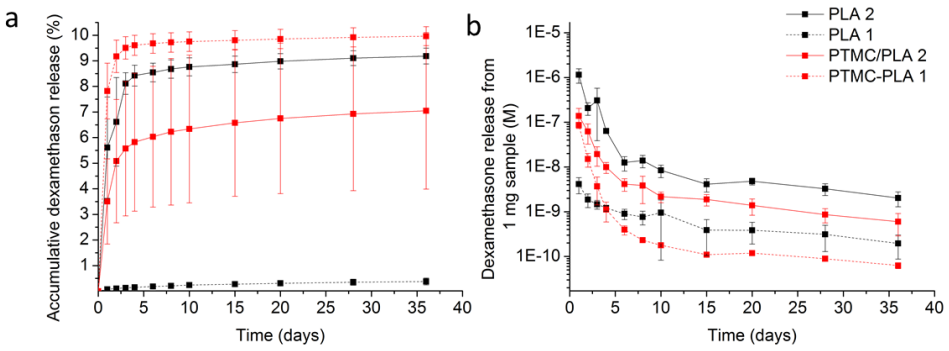

Figure 5.9 *a-Cumulative Dexa released from electrospun PLA fibres and PTMC/PLA fibre composites during in in vitro tests for 5 weeks; b-Dexa concentration released from electrospun PLA fibres and PTMC/PLA fibre composites (per 1.0 mg sample in 1.0 ml PBS at 37 ˚C, values presented as non-cumulated).*

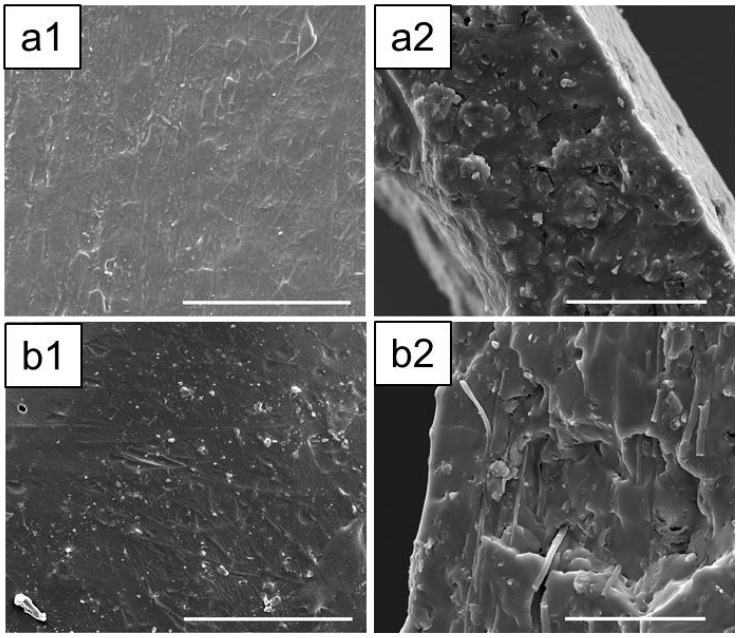

Figure 5.10 *SEM images of PTMC/PLA fibre composites after 35-days in vitro release tests: PTMC/PLA 1 (a1) surface, (a2) cross-section and PTMC/PLA 2 (b1) surface, (b2) cross-section (scale bar 20 µm).*

5.3.4 In vitro cell experiments

The aim of this work is to validate the new hybrid PTMC/PLA fibre composite structures as delivery systems able to maintain drug potency and biological activity. For this

purpose Dexa was selected as drug model as it exhibits a strong "concentration-dependent" biological activity on stem cells. For instance, depending on the charge of Dexa in the medium, it can favour *in vitro* hBMSCs proliferation and/or osteogenic differentiation. Both *et al.,* showed that a media supplemented with 10^{-8} M of Dexa, promoted both the proliferation and differentiation of hBMSCs [259]. However, reverse effects on hBMSCs potential to differentiate toward osteoblast lineage (with a shift toward adipogenic differentiation) and reduced ability to proliferate have been reported at higher dosage (i.e. 10^{-7} M [260, 261]). This biological versatility makes Dexa an excellent candidate to validate how we can control the release of Dexa in the current PTMC/PLA hybrid system.

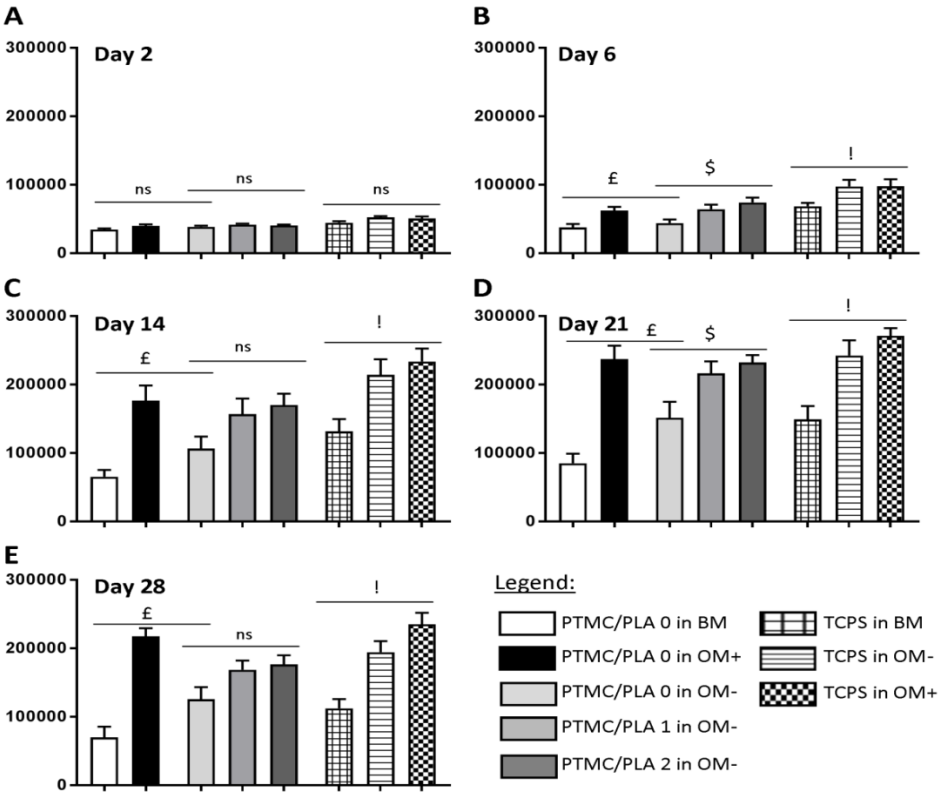

Figure 5.11 *CellTiter Blue quantification (values corresponding to fluorescent intensities) of hBMSCs proliferating on the different substrates in various medium (BM, OM- and OM+) at (a) Day 2, (b) Day 6, (c) Day 14, (d) Day 21 and (e) Day 28. £, ! and $ report significance on the variable nature of the media (£: on PTMC/PLA 0 and ! on control TCPS) and on Dexamethasone charges ($: PTMC/PLA 0, 1 and 2 in OM-).*

After two days post-seeding (Figure 5.11 a) no difference could be detected on hBMSCs density between the different groups (with or without Dexa, either in the media or

loaded in films). Indeed, when cells are seeded at a low density (here 6,000 cells/well), there is usually a 3 to 5 days lag phase before resuming a rapid growth phase [262]. This corroborates our results as the effect of Dexa could be first seen at Day 6 (Figure 5.11 b), with significant improvement of cell proliferation for all groups containing Dexa. Effective release of Dexa from PTMC/PLA 1 and PLA 2 was proven by the accelerated cell growth observed for those two groups (compared to Dexa-free PTMC/PLA 0, in media depleted of any Dexa (OM-)). Similar conclusions can be drawn for later time intervals (Day 14, 21 and 28, Figure 5.11 c,d, and e respectively), with superior hBMSCs proliferation on OM+ condition (observed for both PTMC/PLA 0 and control TCPS) and on PTMC/PLA loaded with Dexa (1 and 2) compared to PTMC/PLA 0 (even if not systematically significant). At Day 21, fluorescent values for the groups cultivated in OM+ ((PTMC/PLA 0) and TCPS) were similar to the PTMC/PLA 1 and 2, demonstrating the beneficial effect of Dexa released from the composite films (no significance between PTMC/PLA 0 and TCPS in OM+ compared to PTMC/PLA 1 and PTMC/PLA 2). As the cells reached a high degree of confluency following 21 days of cultivation, the fluorescent values measured at Day 28 were not increased compared to previous time intervals, but followed a similar feature (Figure 5.11 e). For all time intervals, cell proliferation was always the lowest in BM condition < OM- and < OM+, revealing that not only Dexa (present only in OM+), but also ascorbic acid is another stimulator of hBMSCs proliferation [263].

The sustained release of biologically active Dexa from PTMC/PLA hybrids is able to stimulate hBMSCs proliferation, but without following a concentration-dependent scenario, as values for PTMC/PLA 1 were similar to PTMC/PLA 2 for all the time intervals. Indeed, as shown by the release kinetics presented in Figure 5.9, the composites with Dexa loadings of 0.7 and 2.4 wt% released the drug at a concentration below the cytotoxic threshold of 10^{-7} M [260, 261].

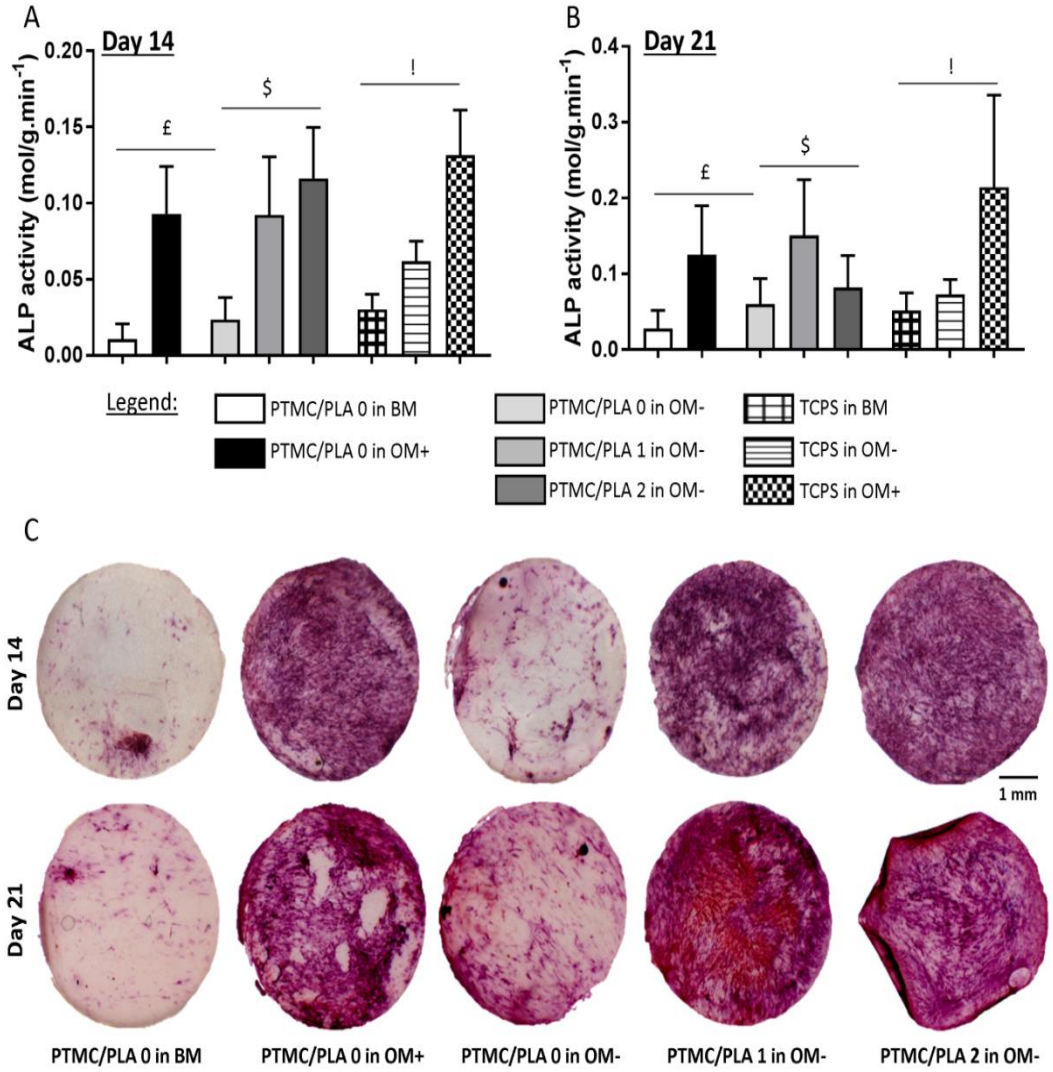

Figure 5.12 *Dexa released from PTMC/PLA composites recreates in vitro conditions similar to osteogenic media on hBMSCs ALP activity. ALP activity measured at (a) Day 14 and (b) Day 21 (with £,! and $ reporting significance on the variables: nature of the media (£ on PTMC/PLA 0 and ! on control TCPS) and on Dexamethasone loadings ($ PTMC/PLA 0, 1 and 2 in OM-). (c) ALP staining on hBMSCs monolayer cultivated on the different substrates (only shown for 1 donor, but similar staining was obtained for both donor).*

It is well known that supplementing media with the synthetic glucocorticoid Dexa induces hBMSCs to differentiate towards osteogenic lineage. One early marker commonly investigated to validate such evolution relies on the determination of alkalin phosphatase (ALP) [264, 265]. For both time intervals (Day 14 and Day 21, Figure 5.12 a

and b, respectively), the ALP activity was negligible on BM condition (on both PTMC/PLA 0 and TCPS) and on OM- (without Dexa). The ALP activity correlates with the ALP staining as shown in Figure 5.12 c (only shown for donor 1), with robust ALP staining on OM+ condition, but also for cells growing on PTMC/PLA 1 and 2 substrates. The continuous release of Dexa from the hybrid films allows to trigger stem cells differentiation, in a similar order of magnitude than under OM+, where media was constantly refreshed with 10 nM of Dexa, as no significant differences were observed between PTMC/PLA and TCPS in OM + and PTMC/PLA 1 and 2.

ALP is chronologically an early osteogenic marker, hence it is not surprising to see a decline in activity between Day 14 and Day 21 for some groups (e.g. PTMC/PLA 2), revealing that the peak of ALP activity is already passed between those two time intervals. In fact, as PTMC/PLA 2 releases more Dexa than PTMC/PLA 1 (Figure 5.9), we expect that the ALP peak actually appeared earlier in PTMC/PLA 2 then Day 21, with the corresponding ALP already being at a similar value than Dexa-free PTMC/PLA 0. This is a natural phenomenon as during cell maturation ALP naturally decreases and then cells start to deposit minerals (calcium and phosphorus), which is a later marker of osteogenic differentiation [266].

In vitro mineralization was monitored in our study using Alizarin Red Staining (ARS) and quantification.

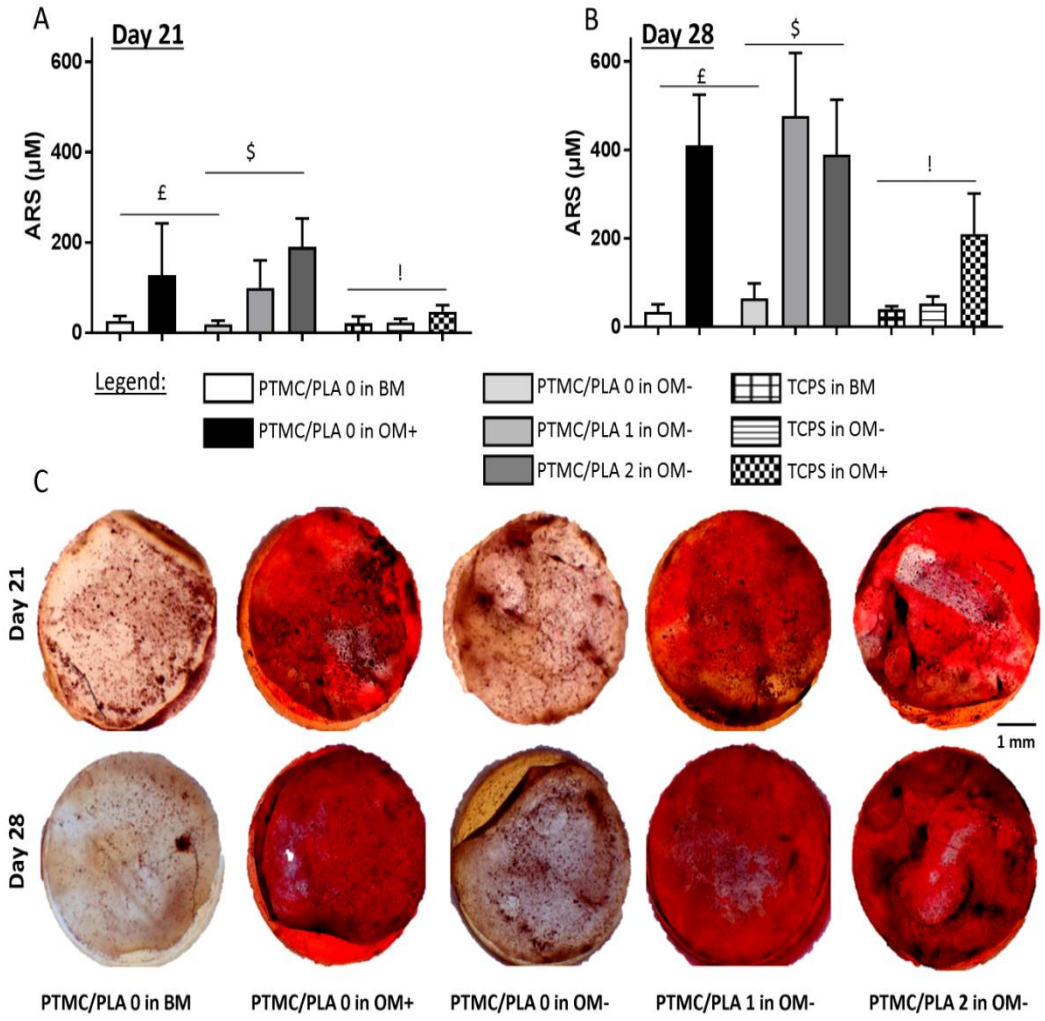

Figure 5.13 *Dexa loaded PTMC/PLA composite film successfully triggers hBMSCs differentiation towards mineralizing osteoblast-cell lineage. Calcium deposition from hBMSCs was measured at (a) Day 21 and (b) Day 28 (with £, ! and $ report significance on the variables: nature of the media (£ on PTMC/PLA 0 and ! on control TCPS) and on Dexamethasone charges ($ PTMC/PLA 0, 1 and 2 in OM-). (c) Alizarin Red Staining of* Ca^{2+} *secreted by hBMSCs cultivated on the divers substrates (only shown for 1 donor, but similar staining was obtained for both donor.*

Further signs of osteogenic differentiation of hBMSCs induced by the release of Dexa are shown by the staining and quantification of calcium deposition (Figure 5.13). At both Day 21 and Day 28, the Dexa-depleted medium, present in the BM and drug-free Dexa PTMC/PLA 0 in OM- conditions, did not permit cells to mineralize (Figure 5.13 b and c). In contrast, the presence of Dexa either exogenously supplemented (in OM+) or

diffusing from PTMC/PLA 1 and 2, allows the stem cells to fully undergo osteogenic differentiation with robust time-dependent biomineralization (as shown by the Alizarin Red Staining images, Figure 5.13 c). No significance was observed between Ca^{2+} formed in fully supplemented OM media (positive control OM+) and in the PTMC/PLA 1 and 2 for both time intervals. In this study, Dexa was selected as model system for osteogenic differentiation. For the positive controls (i.e. osteogenic condition), this exogenous factor was directly introduced into the culture medium of hBMSCs (OM+). It was concluded from the osteogenic study that the composite films loaded with Dexa successfully triggered hBMSCs to differentiate towards mature osteoblast lineage, as both early (ALP activity, Figure 5.12) and late (Ca^{2+} deposition, Figure 5.13) markers were up-regulated in similar intensity than for the positive OM+ condition.

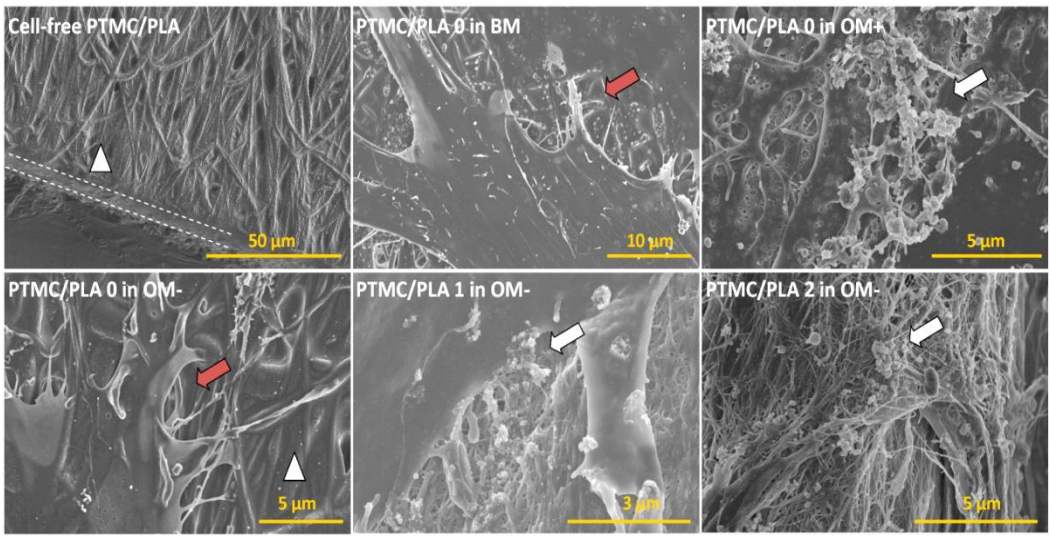

Figure 5.14 *Biomineralization is visible on cell monolayers cultivated on Dexa-loaded films like in OM+ condition. Illustration of PTMC/PLA composite film surface (dash lines denoted the cross-section and white triangles the PLA fibres). The red and white arrows denoted cell membranes and clusters of minerals, respectively. SEM images were taken at Day 28 of the in vitro culture experiment.*

SEM observations (Figure 5.14), corroborated the ARS results. Numerous particle clusters are observed from samples containing Dexa in OM- condition or samples with no Dexa but cultivated in OM+ condition. The particle clusters are speculated to be CaP minerals, which can be further validated with energy-dispersive X-ray spectroscopy (EDS). In contrast, no particle clusters deposited by the hBMSCs on the control groups

could be detected (structures cultivated in absence of Dexa, i.e. PTMC/PLA 0 in BM and in OM-). SEM images confirmed the potential of Dexa-loaded PTMC/PLA fibre composite films to stimulate stem cells differentiation and to promote the deposition of minerals, fundamental for any bone tissue engineering application.

In this study, biocompatible and degradable polymeric composites based on electrospun PLA fibres and photo-crosslinked PTMC were successfully fabricated. The PLA fibres were incorporated into PTMC macromer using compression moulding followed by UV-curing. The composites exhibited significant improvements in mechanical performance compared to pure PTMC. Young's modulus was increased by one-order of magnitude while tensile strength increased 3-fold. Fibres showed good interaction and bonding with the PTMC matrix as no fibre pull-out was observed for cold-fractured composites, while composites were stable even after 5 weeks of incubation in media. Dexamethasone was introduced into the composites through the use of Dexa-loaded electrospun PLA fibres, which were subsequently integrated into PTMC matrix. By doing so, a UV-triggered cross-reaction between Dexa and methacrylate-ended PTMC could be avoided; hence preserving the biological activity of Dexa. Moreover, by combining electrospun PLA fibres with PTMC matrix a stable and sustained Dexa release profile was obtained, which allowed for improved hBMSC proliferation and osteogenic differentiation.

To summarize, the concept of polymer/polymer composite structures offers a high degree of versatility as various therapeutics, especially those known to react with photo-crosslinkers, can be loaded. The current study shows great promise for drug-loaded scaffolds made by UV-based additive manufacturing techniques like stereolithography.

5.4 Conclusions

In this chapter, a PTMC matrix reinforced with PLA nanofibres loaded with dexamethasone was fabricated. The loading of dexamethasone within electrospun PLA fibres followed by the incorporating of these fibres in a PTMC photo-crosslinkable matrix allows for multiple improvements, including (i) enhancement of mechanical performances, (ii) preservation of biological activity of therapeutics and (iii) controlled release kinetics of the drug. This was validated by *in vitro* cell experiments, revealing

that the use of dexamethasone-loaded PTMC/PLA fibre composites had a direct impact on hBMSCs proliferation and osteogenic differentiation. As a proof of concept, the bioactive PLA fibres were loaded in PTMC to produce 2D composite films. The strategy offers great promise in the field of bioactive tissue engineering scaffolds, as it opens venues to drug-loaded constructs manufactured using additive manufacturing processes relying on photo-fabrication, such as stereolithography.

Chapter 6 - Functionalization of electrospun PLA fibres using amphiphilic block copolymers for use in carboxy-methyl-cellulose hydrogel composites

6.1 Introduction

Cellulose is the most abundant renewable resource on the planet and cellulose-based hydrogels are considered to have great potential in the fields of tissue engineering, drug delivery, food, agriculture, etc. [267] Cellulose hydrogels can be prepared by physical crosslinking through ionic, hydrogen bonding or other molecular interactions [268-270]. They are also produced via chemical crosslinking or radiation [271, 272]. The 3D network of carboxy-methyl-cellulose (CMC) hydrogels contains large amounts of water, which provide an attractive environment for cell growth. However, most hydrogel materials (especially single-phase gels) have poor mechanical properties whereas many biological gel tissues, such as cartilages, are usually strong and shock-absorbing [273]. Hence their scope for use in biomedical applications is limited. As a result, considerable efforts have been made to improve the mechanical performance of hydrogels. For instance, it was found by repeated freeze-thawing of hydrogels, that polymer molecules tend to aggregate under the expelling of water crystals, forming a crystallite; a two-phase gel structure contributing to an increased hydrogel strength [274, 275]. Alternatively, a double network gel can be produced which combines two independent gel networks to improve the gel strength and toughness [276, 277]. Instead of physical or covalent crosslinks as present in other gels, hydrogels made from supramolecules with topological interlocking exhibited good ductility as well as water adsorption [278].

The use of reinforcing fillers is a common way to improve the mechanical properties of hydrogels without chemical modification or specific synthesis. Nanoscale fillers such as cellulose nanowhiskers [279], carbon nanotubes [280] and silica nanoparticles [281] have received extreme interests due to their large surface area and functional

properties (drug carriers, sensors, actuators, etc.). Nevertheless, their reinforcing effects were often rather limited, while the use of high filler loadings could even lead to a reduction in mechanical performance due to filler aggregation and a disturbance of the hydrogel network.

Electrospinning is an easy and rapid technique for the production of high aspect-ratio polymer nanofibres. These fibres have great potential as reinforcements for hydrogels, opening up possibilities to tailor or design the mechanical properties of hydrogels. Their fibrous structure, high porosity and large surface area of electrospun fibres make them suitable as reinforcing fibres; while their high aspect ratio allows for effective stress transfer. Moreover, fibre reinforced hydrogels highly resemble biological tissues which often consist of micro- or nano-fibrous structures. Randomly oriented electrospun fibres as well as highly organized 3D printed electrospun fibre scaffolds have been used as reinforcements for hydrogels for use in tissue engineering [28, 282]. In addition to the use of continuous electrospun fibre mats, short electrospun fibres can also be used for hydrogel reinforcement while maintaining good flowability, processability and injectability [101, 283]. Poly(lactic acid) (PLA) is well-established nontoxic and biocompatible polymer material used for electrospinning. However, the hydrophobicity of PLA fibres does not allow easy integration into hydrogels or fibre wetting. Plasma treatment of PLA fibres has been used to facilitate improved fibre-hydrogel integration [284], however at the same time this technique also caused defects in fibres.

In this study, electrospun PLA fibre reinforced CMC hydrogel composites were prepared. CMC hydrogels were prepared in the presence of a crosslinker and photoinitiator. To improve fibre-matrix compatibility, electrospun fibres based on hybrids of PLA and amphiphilic block copolymer (BCP) poly(D,L-lactide)-block-poly[2-(dimethylamino)ethyl methacrylate] (PLA-b-PDMAEMA) were produced. The presence of PDMAEMA on the fibre surface provided hydrophilic surface properties. By varying the PDMAEMA chain length, the hydrophilicity of PLA could be controlled. Moreover, PDMAEMA was quaternized and co-electrospun with PLA fibres. The quaternized PDMAEMA further enhanced the interaction between fibre and hydrogel via ionic interaction. The physicochemical properties of electrospun fibres and CMC composite hydrogels were assessed. Finally, continuous electrospun fibre mats were chopped into short electrospun fibres and incorporated into CMC hydrogels. The rheological

properties of these composite hydrogels were evaluated. It is proposed that these short fibres are potentially suitable for the reinforcement of injectable composite hydrogel systems.

6.2 Experimental

6.2.1 Materials

All chemicals were obtained from Sigma-Aldrich unless specified. D,L-lactide was recrystallized in toluene; 4-(dimethylamino) pyridine (DMAP) (≥99%) was recrystallized in petroleum:ether-toluene 4:1 mixture; triethylamine (≥99.9%) was distilled over calcium hydride; 2-(dimethylamino) ethyl methacrylate (DMAEMA) (98%) was passed through aluminium oxide to remove inhibitor. Phosphate buffer saline (PBS) was prepared by dissolving one PBS tablet in 200 ml deionised water. Benzyl alcohol (anhydrous, 99.8%), dichloromethane (DCM) (anhydrous, ≥99.8%), α-bromoisobutyryl bromide (BB, 98%), N,N,N',N'',N''-pentamethyldiethylenetriamine (PMDETA) (99%), 5-bromo-1-pentene (95%), copper (I) bromide (98%), aluminium oxide (≥98%), poly(ethylene glycol) dithiol (PEG-dithiol, average M_n = 1,000 g/mol), 2-hydroxy-4'-(2-hydroxyethoxy)-2-methylpropiophenone (Irgacure 2959, 98%), allyl bromide (99%), toluene (anhydrous, ≥99.8%), petroleum ether (bp 40-60 ˚C, ≥90%), hexane (≥95%), tetrahydrofuran (THF) (anhydrous, ≥ 99.9%), methanol (≥99.9%), sulphuric acid (99.999%), hydrogen peroxide solution (30 wt% in water) were used as received. Silicon wafer was purchased from PI-KEM Ltd. CMC power (Aqualon® Sodium CMC, DS≈0.7) and PLA 2002D (M_w = 200,000 g/mol) were obtained from Hercules and Natureworks, respectively.

6.2.2 Synthesis of PLA-b-PDMAEMA and quaternization

PLA-b-PDMAEMA was synthesized by a combination of ring-opening polymerization (ROP) and atom transfer radical polymerization (ATRP). First, bromide-ended PLA (PLA-Br) was synthesized via ROP of lactide followed by end group functionalization. 3.0 g of D,L-lactide (2.1×10^{-2} mol) and 37.1 mg DMAP (3.0×10^{-4} mol) were placed in a round bottom flask equipped with a magnetic stirrer. The flask was flame dried under vacuum and purged by argon (Ar) prior to adding any reactants. The reactor was then sealed with a rubber septum and three cycles of vacuum-argon purge were conducted. 43.0 µl benzyl alcohol (4.2×10^{-4} mol) was injected into the reactor under Ar protection. The

reaction was carried out in an oil bath at 135 ˚C for 4 hrs. At the end of the reaction, 10.0 ml anhydrous DCM and 290.0 µl triethylamine (2.1×10^{-3} mol) were directly injected to dissolve the products. The reactor was transferred to a cold water bath followed by slowly adding 276.0 µl α-bromoisobutyryl bromide (2.1×10^{-3} mol) under Ar atmosphere. The functionalization was continued overnight. PLA-Br was achieved by precipitating in cold methanol twice and dried in a vacuum desiccator.

PLA-b-PDMAEMA was synthesized via ATRP. In flask A, 0.5g of PLA-Br (≈1.2×10^{-4} mol) and DMAEMA monomer were dissolved in 2.0 ml anhydrous THF, which was purged with Ar for 30 min. Meanwhile in flask B, 51 µl PMDETA (2.4×10^{-4} mol) and 17 mg copper (I) bromide (1.2×10^{-4} mol) were dissolved in 10.0 ml anhydrous THF and purged with Ar for 30 min. Afterwards, contents in flask B were transferred to flask A. The polymerization was continued in oil bath at 50 ˚C for 24 hrs. The reaction was stopped by exposing to air and the contents were diluted with 100 ml DCM and passed through alumina column to remove copper. The product solution was concentrated to 10 ml using a rota-vaporator (Buchi, Rotavapor RII) and precipitated in cold hexane twice. The product was dried in a vacuum desiccator for 48 hrs and stored in a nitrogen box. BCP with low, medium and high PDMAEMA content was synthesized, named as PDMAEMA (L), PDMAEMA (M) and PDMAEMA (H), respectively.

For quaternizing PDMAEMA, PDMAEMA (H) was dissolved in anhydrous DMF at 1.0 g/ml concentration. Then 2.5 eq. (mol) of 5-bromo-1-pentene was added and the reaction was carried out at 70 ˚C for 24 hrs. The product (named as PDMAEMA-Q) was recovered by precipitating in excessive cold diethyl ether and dried in a vacuum desiccator.

6.2.3 Spin-coating and electrospinning of PLA-b-PDMAEMA

The impact of PDMAEMA on PLA's hydrophilicity was first studied on spin-coated films. Homo PLA (PLA 2002D), PLA-b-PDMAEMA and homo PLA/PLA-b-PDMAEMA hybrids were prepared, respectively. To start, PLA-b-PDMAEMA was dissolved in chloroform/DMF mixed solvent at a concentration of 0.1 mg/ml. The mass ratio of chloroform to DMF was set at 3:1, which was also used for all other spin-coating experiments as well as for electrospinning. The solution was stirred until homogeneous. Meanwhile, silicon wafer was cut into 1.0×1.0 cm^2 substrates and functionalized to hydrophilic by treating them in sulphuric acid/hydrogen peroxide solution 3:1 (volume

ratio) at 100 ˚C for 1 hr. Substrates were then washed thoroughly with deionised water and purged with nitrogen. During spin coating, a few droplets of solution were transferred onto the substrate. The spin coating was performed by first spinning at 400 rpm for 10 sec and then 2000 rpm for 40 sec (G3P-8, Specialty Coating System). The spin coated substrates were left in a fume hood overnight to allow solvent evaporation and stored in a nitrogen box for further characterization. PLA (with and without PLA-b-PDMAEMA) spin-coated films were prepared on the same substrates following the same spin-coating routine. Due to a higher viscosity, they were dissolved until a diluted concentration (0.05 mg/ml). 15 wt% of PLA-b-PDMAEMA was added with respect to homo PLA.

Electrospinning was carried out using an in-house built experimental setup. Homo PLA and PLA-b-PDMAEMA (15 wt% with respect to homo PLA) were dissolved in chloroform:DMF 3:1 (mass ratio) at a total polymer concentration of 9 wt%. PLA-b-PDMAEMA on its own is not suitable for electrospinning due to its low molecular weight. The polymer solution was supplied to the spinning tip by a syringe pump (Kent Genie) at a feeding rate of 1.0 ml/h. This spinning tip was connected to a power unit (Glassman EQ) which generated 20-24 kV. Electrospun fibres were collected on aluminium foil and left in a fume hood to evaporate residual solvents. For comparison, PLA without BCP was electrospun using the same conditions as described above. In the end, five different fibres were prepared: homo PLA fibre, PLA/PDMAEMA (L) fibre, PLA/PDMAEMA (M) fibre, PLA/PDMAEMA (H) fibre and PLA/PDMAEMA-Q fibre.

6.2.4 Preparation of fibre reinforced CMC hydrogel composites

The CMC hydrogel was prepared by UV crosslinking of CMC and PEG-dithiol (crosslinker) aqueous solution with photoinitiator Irgacure 2959. First, the commercial CMC powder was modified by allyl bromide using an established method, which resulted in 13% molar ratio of alkene groups in CMC. In detail, 1.0 g CMC powder was dissolved in 50 ml water and stirred until fully dissolved. Another 50 ml DMF was added and this solution was mixed until homogeneous. Approximately 0.1 ml allyl bromide was added into CMC solution and the reaction was continued at 70 ˚C overnight. The functionalized CMC was obtained by precipitating in acetone twice and dried in vacuum desiccator. To make the precursor solution of hydrogel, functionalized CMC was dissolved in water at a concentration of 20 mg/ml; PEG-dithiol and Irgacure 2959 were dissolved in PBS and methanol respectively, at a concentration of 225 mg/ml (PEG-

dithiol) and 45 mg/ml (Irgacure 2959). A mixed solution of 1.0 ml CMC, 10.6 µl PEG-dithiol and 12 µl Irgacure were prepared (precursor solution).

To incorporate electrospun fibres, the as-spun fibre mat was cut into 20×30 mm^2 rectangular specimen (thickness 0.08-0.10 µm) and placed on a flat substrate. CMC precursor solution was cast to impregnate the fibre mats. To facilitate impregnation of the hydrophobic fibres, the mats were degassed in a vacuum desiccator for 15 min until the precursor solution infiltrated the fibre mats. A glass slide was placed and pressed on top to remove excessive solution. The whole system was UV crosslinked at 80 mW/cm^2 for 120 sec (Omnicure 1500). After UV crosslinking, composite hydrogels were incubated in PBS.

6.2.5 Molecular characterization of synthesized polymer

All synthesized polymers were characterized by ^{1}H-NMR and GPC. For ^{1}H-NMR spectra, samples were dissolved in deuterated chloroform ($CDCl_3$) at a concentration of 10 mg/ml and tested by a Bruker AVIII 400 spectrometer. Due to poor solubility of PDMAEMA-Q in $CDCl_3$, it was dissolved in deuterated dimethyl sulfoxide (DMSO) instead. For GPC, samples were dissolved in THF at 1.0 mg/ml and tests were performed using an Agilent Technologies 1260 Infinity equipped with a UV detector at 308 nm wavelength. THF (with 2.0 vol% triethylamine) was used as the eluent at a flow rate of 1.0 ml/min. Polystyrene (1,000-100,000 g/mol) was used as standard for calibration.

6.2.6 Physiochemical properties of BCP-functionalized PLA

Atomic force microscopy (AFM, NT-MDT, NTEGRA) was used to acquire topography and phase images of BCP-functionalized PLA spin-coated films in tapping mode. AFM was performed using a Bruker RTESP-300 probe (resonant frequency 300 kHz, spring constant 40 N/m) at set-point of 50-70% of free oscillation amplitude and an image scan rate of 1.0 Hz. The hydrophilicity of the spin-coated films and electrospun fibre mats was evaluated by contact angle measurements using drop shape analysis (DSA, Kruss DSA100). 5.0 µl liquid was carefully placed onto film samples and the contact angle was measured. To observe the morphology of electrospun fibres and hydrogels, samples were sputter coated with a thin gold layer and characterized using scanning electron microscopy (SEM, FEI Inspect F) at a distance of 10 mm and voltage of 10 kV. To investigate hydrogel-fibre interaction, composites were cold-fractured in liquid

nitrogen and lyophilized and then characterized by SEM. Thermal properties of electrospun fibres were measured by differential scanning calorimetry (DSC, Perkin-Elmer DSC 4000) and dynamic mechanical analysis (DMA, TA Instrument Q800). For DSC tests, samples were first equilibrated at 25 ˚C and then ramped to 180 ˚C at 10 ˚C/min. Glass transition temperature (T_g) was determined by the mid-point of the glass transition. The crystallinity of PLA was calculated by,

$$X_c = \frac{\Delta H_m}{\Delta H_{ref}} \times 100\% \quad (6.1)$$

where X_c is the crystallinity, ΔH_m is the experimental heat of fusion at melting point determined by DSC, ΔH_{ref} is the theoretical heat of fusion of fully crystalline PLA (93 J/g) [206]. Tensile tests were performed on electrospun fibre mats and hydrogel composites using dynamic mechanical analysis (DMA, TA Instrument Q800) in controlled force mode. Fibre mats and composite hydrogel films were cut into 20×5 mm rectangular strips before being mounted into the clamps. A preload of 0.05 N was applied and specimens were stretched at a rate of 0.1 N/min until failure at room temperature (RT). Three tests were performed for each sample. The Young's modulus was derived from the slope of the stress-strain curve at low strain (2%).

6.2.7 Fabrication of short fibres and rheological behaviour of short fibre CMC hydrogel composites

To create short fibres, electrospun fibre mats were cut into small pieces (10×10 mm) and added to 50 ml deionised water while a homogenizer (Heidolph Silent Crusher M) was employed to homogenize the fibre-water mixture at 14,000 rpm for 20 min. A fibre suspension was obtained after homogenization and chopped fibres were recovered by filteration. The recovered cut fibres were dried using a freeze dryer (Labconco FreeZone 2.5) and their morphology was characterized using SEM (operated in the same protocol as described previously). Three different types of short fibres were prepared from homo PLA fibre, PLA/PDMAEMA (H) fibre and PLA/PDMAEMA-Q fibre, respectively.

To prepare short fibre reinforced hydrogels, 0.5 wt% short fibres were added into the CMC precursor solution and stirred overnight (named as CMC-PLA fibre, CMC-PDMAEMA (H) fibre and CMC-PDMAEMA-Q fibre, respectively). Rheological tests on the fibre reinforced hydrogels were carried out using a rheometer (TA Instrument DHR-3), with stainless steel parallel plate geometry (20 mm). During the tests (at RT), around

0.2 ml fibre-loaded precursor solution was transferred between the plates and a 0.5 mm plate gap was applied. First, a time sweep was performed for 180 sec, with a displacement of 10^{-4} rad, frequency of 1.0 Hz and UV exposure at 80 mW/cm^2 (starting at 30 sec for 120 sec). Then a frequency sweep was performed from 0.1 Hz to 100 Hz at a displacement of 10^{-4} rad to assess hydrogel stability at different frequencies. Finally, a strain sweep was performed from 1 to 1000% at 1.0 Hz frequency to evaluate hydrogel stability at different deformations.

6.3 Results and Discussion

6.3.1 PLA-b-PDMAEMA synthesis

PLA was synthesized via ROP catalysed by an organic catalyst DMAP [285]. By using an organic catalyst, conventional metallic catalysts could be avoided [286, 287], which are potentially harmful in biomedical applications. PDMAEMA blocks were added to the PLA block via ATRP. A schematic of the synthesis process is shown in Figure 6.1. Representative ^{1}H-NMR spectra of products are presented in Figure 6.2. Peaks corresponding to different protons or solvents are identified and the molecular weight (M_n) is calculated by end group analysis. For PLA blocks, the M_n was calculated by comparing the peak integration of proton **a** (7.34 ppm) and **c** (5.16 ppm); for PDMAEMA blocks, the M_n was calculated by comparing the peak integration of proton **a** (7.34 ppm) and proton **h** (4.05 ppm). The ^{1}H-NMR spectra of BCP before and after quaternization are shown in Figure 6.2 b**.** The occurrence of peak **n** (5.88 ppm) and **n'** (5.07 ppm), with the complete shifting of peak **h** (from 3.99 to 4.43 ppm), **i** (from 2.50 to 3.59 ppm), **j** (from 2.20 to 3.29 ppm) indicate the successful quaternization of the PDMAEMA blocks. The reaction yield is calculated by comparing reactant mass and product mass. The yield for ROP, ATRP and quaternization are near 50.5%, 51.7% and 90.0% respectively. In addition, GPC was used to measure M_n and M_w/M_n. A detailed molecular characterization is listed in Table 6.1.

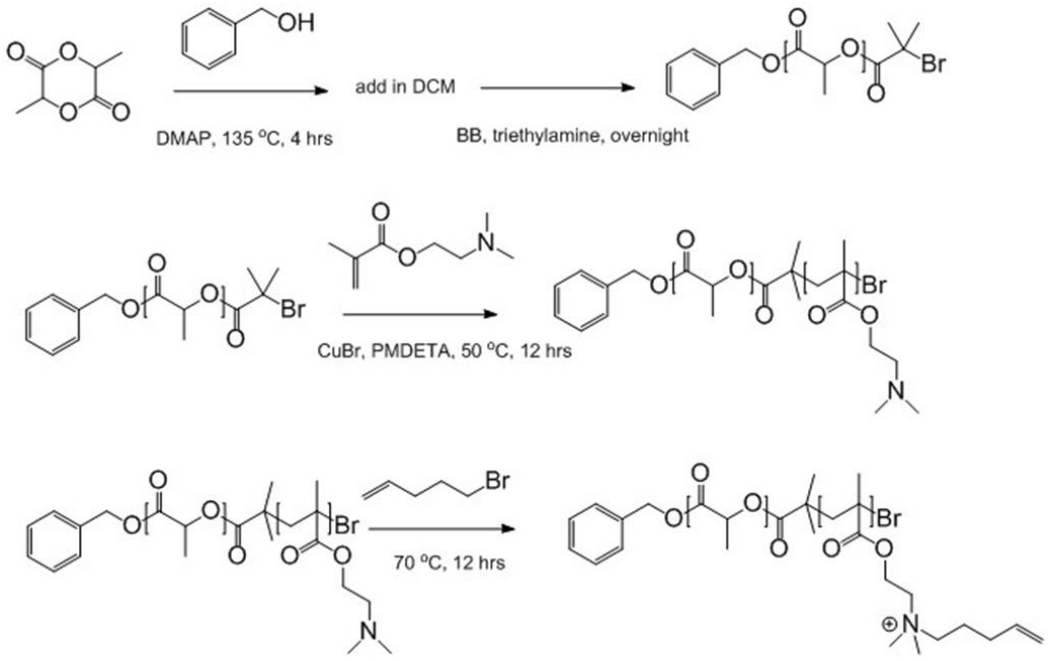

Figure 6.1 *Schematic showing synthesis and quaternization of PLA-b-PDMAEMA.*

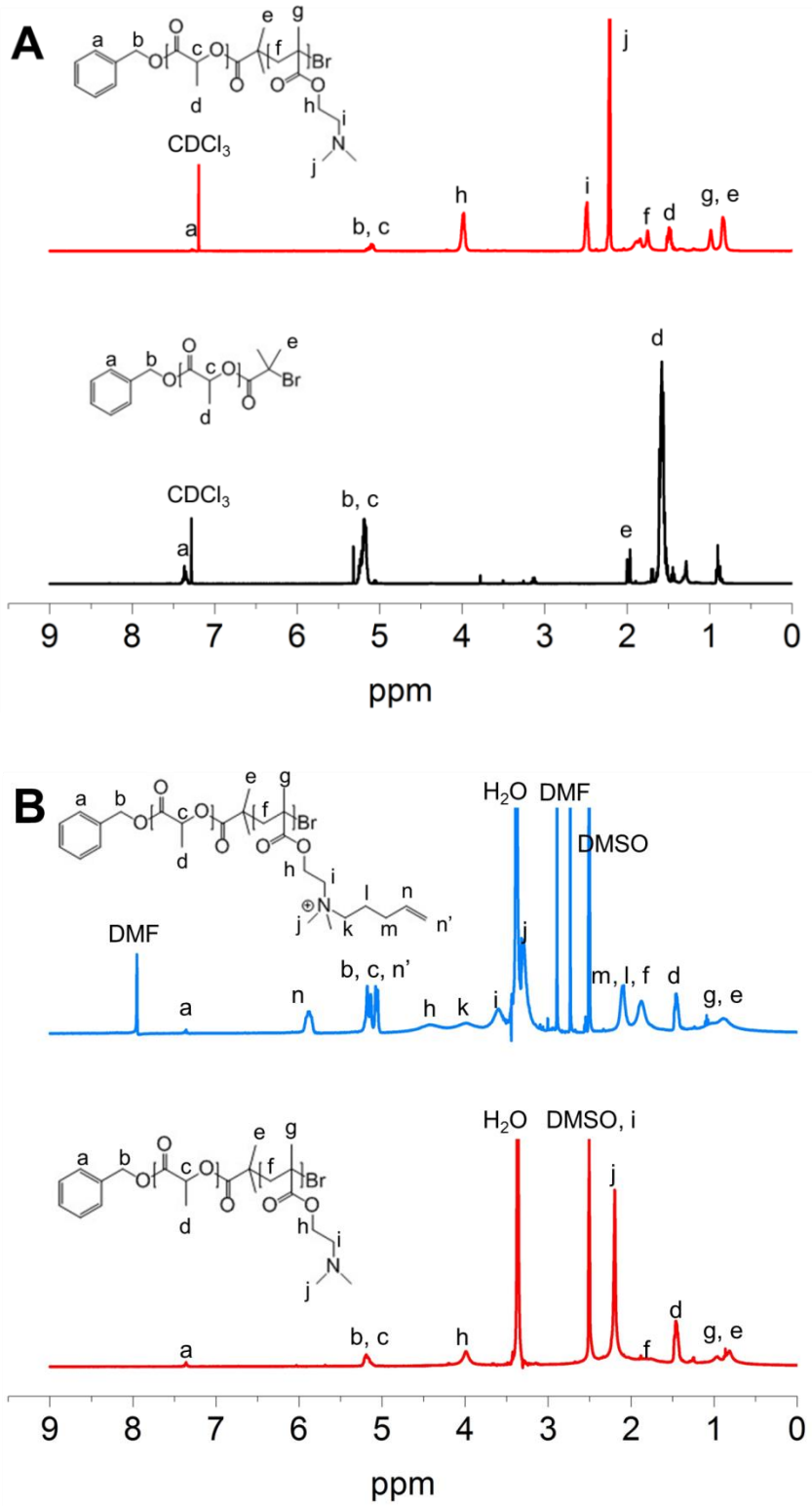

Figure 6.2 *(a) Representative [1]H-NMR of PLA-Br and PLA-b-PDMAEMA in deuterated chloroform (CDCl3); (b) [1]H-NMR of PDMAEMA (H) and PDMAEMA-Q in deuterated DMSO.*

Table 6.1 *Molecular characterization of PLA and BCP.*

Sample	$M_{n,PLA}$ [a]	$M_{n,PDMAEMA}$ [a]	M_n [b]	M_w/M_n [b]
PLA	3.2	N/A	7.5	1.7
PDMAEMA (L)	3.9	1.1	3.3	1.9
PDMAEMA (M)	3.1	6.5	5.5	1.5
PDMAEMA (H)	3.8	20	18	1.4

[a] Molecular weight calculated from ^{1}H-NMR end group analysis (kg/mol). [b] Obtained from GPC test (PS standard, kg/mol).

6.3.2 The influence of PDMAEMA content on PLA hydrophilicity

Due to the thermodynamic incompatibility between different blocks in block copolymers, the same blocks tend to maximize their interactions while minimizing the interactions between the different blocks, resulting in self-assembled domains. We expect phase separation to affect the distribution of the hydrophilic PDMAEMA phase, eventually determining the PLA surface hydrophilicity. It is therefore important to investigate the phase separation behaviour between PLA and PDMAEMA. Phase separation of PLA-b-PDMAMEA was investigated in spin-coated films (thickness ~1.0 µm) using AFM. In Figure 6.3 a1-b1, randomly distributed phases are observed in PDMAEMA (L) and PDMAEMA (M). With increasing PDMAEMA content, a homogeneous surface was obtained (Figure 6.3 c1, d1). To enhance the mobility of molecules and to drive phase separation, films were annealed in THF atmosphere (50 ˚C, 12 hrs). Phase images after THF-annealing are shown in Figure 6.3 a2-d2. No clear phase separation was seen for PDMAEMA (L), PDMAEMA (M) and PDMAEMA (H) (a2-c2). This is due to partial miscibility and insufficient incompatibility between PLA and PDMAEMA blocks, especially at low molecular weight [288]. However, clear phase separation was observed in PDMAEMA-Q, which can be explained by the poor compatibility between PLA and quaternized PDMAEMA.

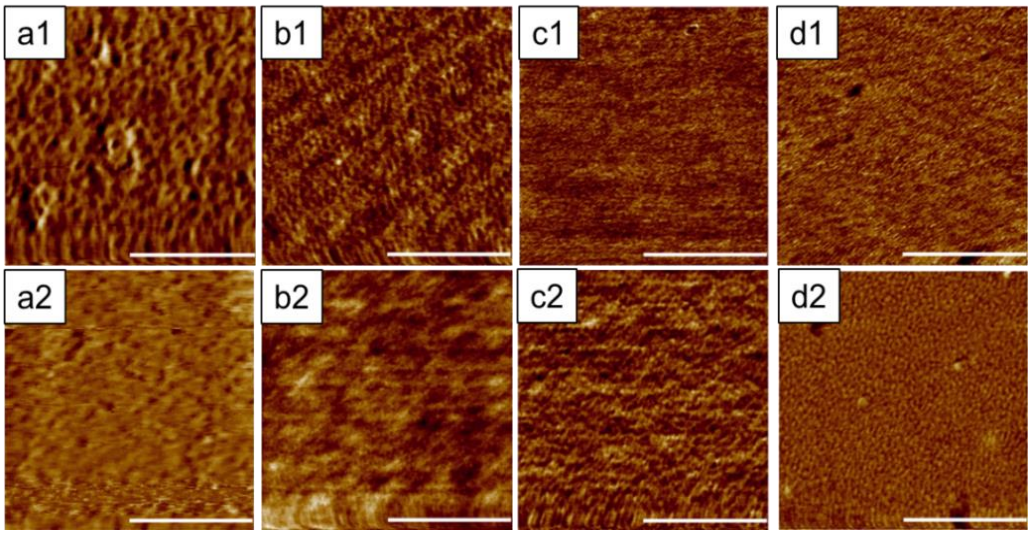

Figure 6.3 *AFM phase images of PLA-b-PDMAEMA spin-coated films with different PDMAEMA chain lengths before (a1-d1) and after (a2-d2) solvent annealing: (a) PDMAEMA (L), (b) PDMAEMA (M), (c) PDMAEMA (H), (d) PDMAEMA-Q (scale bar 500 nm).*

After spin-coating with homo PLA, the hybrid surface properties were investigated using AFM and DSA. Spin-coating produced rough and porous surfaces due to rapid solvent evaporation and homo PLA crystallization, while no self-assembly was observed (images not shown). The hybrid films were again solvent annealed to allow molecular migration and reduce roughness. After annealing, films became smoother with crystalline PLA domains observed in both topographic and phase images (Figure 6.4). However, PLA/PDMAEMA phase separation did still not occur due to the formation of PLA stereocomplexes which disrupt BCP self-assembly [288]. Therefore, the surface of PDMAEMA-functionalized PLA films is considered to have no phase separation.

The influence of PDMAEMA on PLA surface hydrophilicity was investigated by water contact angle measurements under both neutral and acidic conditions (Table 6.2). With increased PDMAEMA content, the water contact angle under neutral conditions decreased from 82.9° to 65.6°, implying an increase in PLA's hydrophilicity. Under acidic conditions, the water contact angle was further decreased, from 80.6° for homopolymer to 43.3° for PLA with PDMAEMA (H). The quaternized PDMAEMA only modified the hydrophilicity of PLA slightly compared with PDMAEMA. As PDMAEMA is

pH-responsive, the pH-dependent water contact angle results suggested the presence of PDMAEMA blocks on the hybrids' surface.

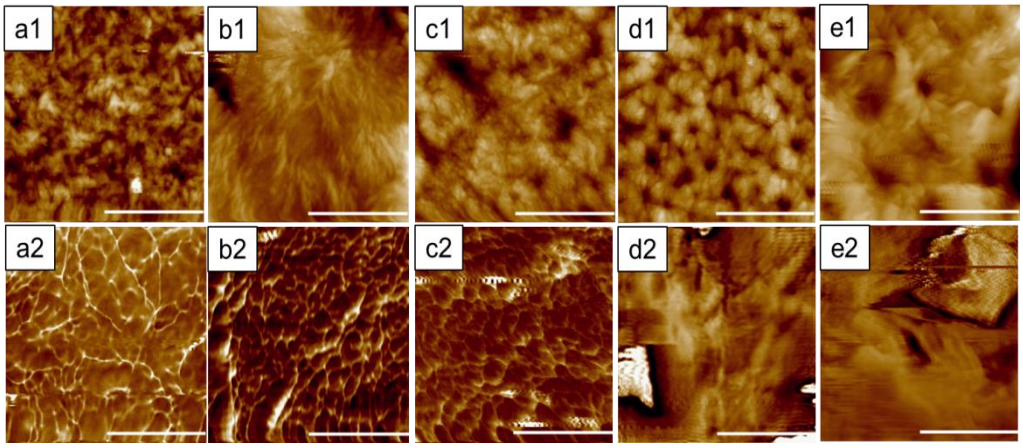

Figure 6.4 *AFM topography (a1-e1) and phase images (a2-e2) of PLA-b-PDMAEMA/homo PLA hybrid spin-coated films after solvent annealing: (a) homo PLA, (b) homo PLA/PDMAEMA (L), (c) homo PLA/PDMAEMA (M), (d) homo PLA/PDMAEMA (H), (e) homo PLA/PDMAEMA-Q (scale bar 500 nm).*

Table 6.2 *Contact angle data of spin-coated PLA/BCP hybrid films under neutral and acidic conditions.*

Composition	Contact angle (pH neutral)	Contact angle (pH 4.0)
PLA	82.9±5.7	80.6±5.7
PLA/PDMAEMA (L)	74.2±3.0	67.4±2.4
PLA/PDMAEMA (M)	66.3±2.1	59.3±1.6
PLA/PDMAEMA (H)	65.6±2.3	43.4±3.1
PLA/PDMAEMA-Q	78.0±0.5	74.4±3.1

6.3.3 Physiochemical properties of PLA-b-PDMAEMA functionalized PLA fibres and fibre reinforced CMC hydrogel composites

Homo PLA and hybrids with PLA-b-PDMAEMA were electrospun into fibres and their morphologies are characterized using SEM. Average fibre diameters were determined using Image J software and listed in Table 6.3. SEM images of fibres together with their

diameter distribution are presented in Figure 6.5**.** Both homo and functionalized PLA were electrospun into continuous fibres without beading. The addition of PLA-b-PDMAEMA results in a decrease in fibre diameter from 1.2 µm to 0.4-0.6 µm. The low molecular weight BCP lowered the viscosity of the spinning solution, which allowed for easier deformation and stretching of the solution jet during electrospinning. The incorporation of PLA-b-PDMAEMA also narrows the fibre diameter distribution. Fibre diameters become more uniform compared to homo PLA fibres. Thermal properties of the electrospun fibres are characterized by DSC. Their thermograms and data are presented in Figure 6.5 and *Table 6.3*. All samples have a melting peak (T_m) around 154 °C and a glass transition temperature (T_g) at 60-62 °C. Cold crystallization is seen in all fibre samples; its peak becomes narrower and the cold-crystallization temperature (T_{cc}) is shifted towards lower temperature. The crystallinity of PLA is increased by the addition of PDMAEMA. The highest crystallinity is found when using PDMAEMA-Q, indicating that PDMAEMA-Q facilitated PLA crystallization during electrospinning.

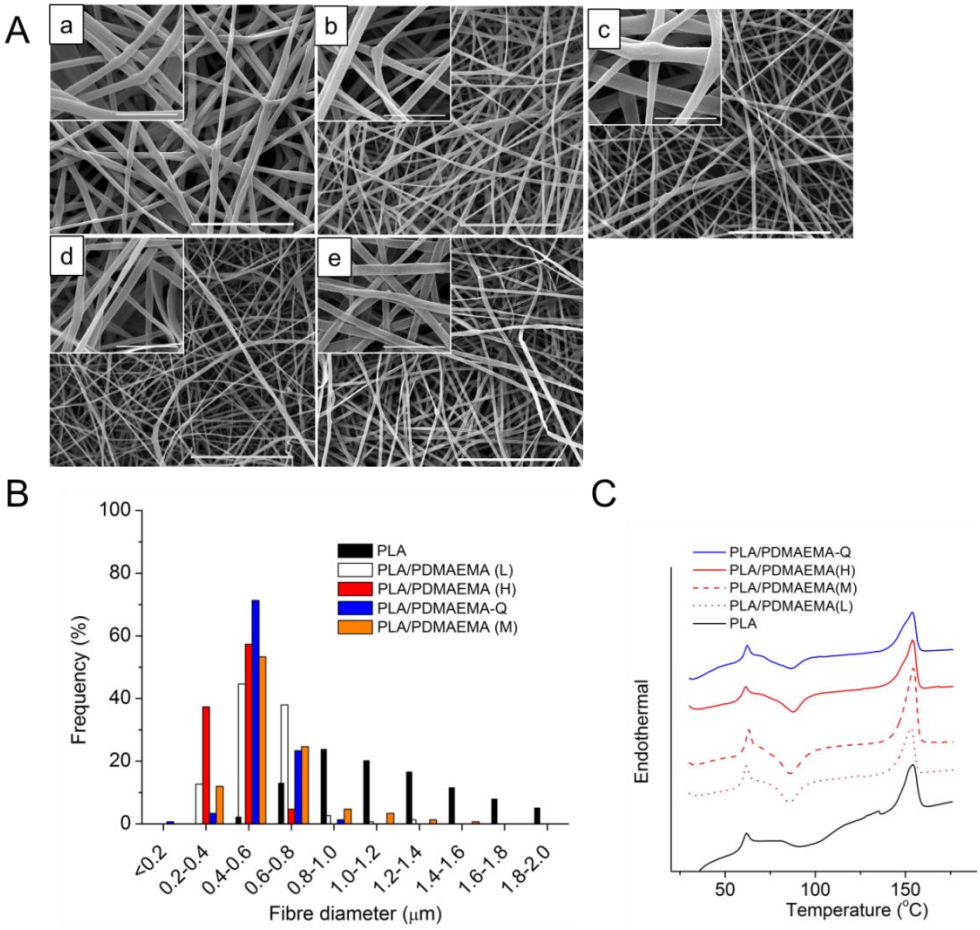

Figure 6.5 *(A) SEM images of electrospun PLA/PLA-b-PDMAEMA hybrid fibres: (a) homo PLA, (b) PLA/PLA-b-PDMAEMA (L), (c) PLA/PLA-b-PDMAEMA (M), (d) PLA/PLA-b-PDMAEMA (H), (e) PLA/PLA-b-PDMAEMA-Q (scale bar 20 μm). The inset shows SEM images taken at higher magnification (scale bar 3 μm); (B) Electrospun fibre diameter distribution; (C) DSC thermogram of electrospun fibres.*

Table 6.3 *Average diameter of electrospun fibres and their thermal properties.*

Composition	Fibre diameter (μm)	T_g (˚C)	T_m (˚C)	T_{cc} (˚C)	Crystallinity (%)
PLA	1.23±0.47	60.0	154.0	95.4	3.4
PLA/PDMAEMA (L)	0.58±0.17	60.6	153.0	85.9	8.8
PLA/PDMAEMA (M)	0.58±0.21	61.9	154.3	85.9	8.7
PLA/PDMAEMA (H)	0.42±0.10	60.0	154.0	87.9	10.4
PLA/PDMAEMA-Q	0.55±0.10	61.1	153.7	86.2	14.4

Water contact angles were measured on electrospun fibre mats. Homo PLA fibres exhibited a higher hydrophobicity than PLA films due to the air entrapped within the porous fibrous structure, with a water contact angle measured at 131±6˚. Addition of PDMAEMA (L) increased the contact angle to 152°±6˚ due to increased porosity (increased air entrapment) as a result of decreasing fibre diameter from 1.20 µm to 0.58 µm [289]. Water contact angle was not measured for fibres containing PDMAEMA (M), PDMAEMA (H) and PDMAEMA-Q as water droplets infiltrated quickly into the fibre mat. This quick wetting of electrospun fibre mats suggested greatly improved PLA fibre hydrophilicity after functionalization, which also allows for an easy integration and wetting of the fibres by the hydrogel.

After incorporating the fibres into the CMC hydrogel, the fibre-hydrogel interaction was characterized by SEM. By comparing the mass of fibres and mass of composite hydrogels, the weight fraction of the fibres in the hydrogel composites are calculated at 3.7±0.1 wt%. A hydrogel-rich layer was seen at the composites' surface. The cryo-fracture surfaces of lyophilized hydrogel composites are shown in Figure 6.6. Lyophilized CMC exhibits a porous structure (Figure 6.6 a) while all hydrogel composites exhibit a fibrous structures (Figure 6.6 b-f). However, it can be seen that as the PDMAEMA content increases, fibre pull-out and fibre protrusions become shorter, indicating improved fibre-matrix adhesion. CMC is adhering well to the fibres (Figure 6.6 d-f) due to increased fibre hydrophilicity and fibre-hydrogel interaction. Conversely, hydrophobic fibres (homo PLA and PLA fibres with low PDMAEMA contents) show detachment from the CMC matrix; while for hydrophilic or quaternized fibres, a stronger interaction between fibres and CMC is observed, leading to improved stress transfer and reinforcing efficiency of the PLA fibres in the hydrogel composite.

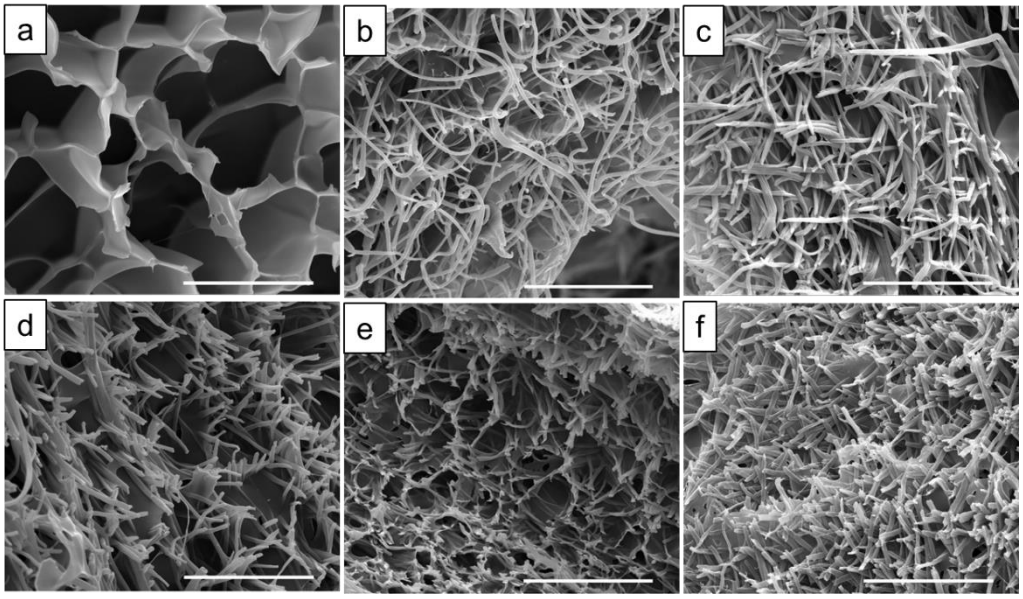

Figure 6.6 *SEM images of CMC hydrogels and electrospun fibre composite: (a) CMC, (b) CMC/PLA fibre, (c) CMC/PDMAEMA (L) fibre, (d) CMC/PDMAEMA (M) fibre, (e) CMC/PDMAEMA (H) fibre, (f) CMC/PDMAEMA-Q fibre. (scale bar 20 µm).*

The mechanical properties of CMC hydrogel composites were measured by tensile tests. In comparison, tensile tests were also performed on electrospun fibres mats. The stress-strain curves are presented in ***Figure 6.7*** and detailed test results are listed in Table 6.4. All fibre mats have much a lower modulus and strength than bulk PLA (3.5 GPa and 53 MPa, respectively, as provided by supplier). The weak mechanical performance of the fibre mats is caused by the high porosity, poor fibre alignment and poor fibre-fibre interactions resulting in sliding of fibres during tensile stretching. The observed decrease in Young's modulus and tensile strength of the fibre mats with increasing PDMAEMA content is caused by increased fibre sliding. For homo PLA fibres, some level of fibre-fibre fusion is observed, leading to a fibrous network (see Figure 6.5). Functionalization using PDMAEMA produces 'drier' fibres that show less fibre fusion, leading to a loosely packed fibrous structure. Strain-hardening is observed on fibres functionalised by PDMAEMA (M) and PDMAEMA (H). The mechanical properties of the CMC composite hydrogels are highly dependent on the mechanical properties of the electrospun fibres when fully integrated in the composites. Stronger fibre mats should produce stronger composite hydrogels. In contrast, CMC with PDMAEMA-Q fibres exhibit a higher Young's modulus and tensile strength than other composite

hydrogels despite the fact that these fibre mats have the lowest mechanical properties. The high Young's modulus and strength of these composites is the result of the excellent fibre-matrix adhesion and effective stress-transfer between PDMAEMA-Q fibres and CMC hydrogel. Here, CMC acts as a bridge between fibres, effectively limiting fibre sliding when the composites are stretched. As a result of the improved reinforcement efficiency of PDMAEAM-Q fibres the mechanical properties of the whole composite system are improved.

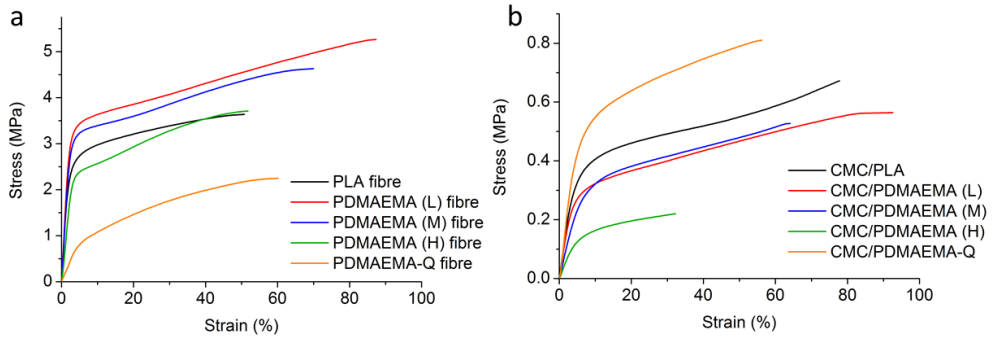

Figure 6.7 Representative stress-strain curves of: a-electrospun fibre mat and b-CMC/electrospun fibre composite hydrogel

Table 6.4 *Tensile properties of electrospun fibre mats and CMC-fibre composite hydrogels.*

Composition	Young's modulus (MPa) [a]	Failure strain (%)	Tensile strength (MPa)
PLA fibre	119±32	79±26	4.53±1.06
PDMAEMA (L) fibre	136±14	91±4	5.31±0.65
PDMAEMA (M) fibre	133±8	70±6	4.65±0.32
PDMAEMA (H) fibre	85±14	52±3	3.77±0.27
PDMAEMA-Q fibre	21±11	61±3	2.17±0.30
CMC/PLA	9.4±1.2	78±4	0.68±0.08
CMC/PDMAEMA (L)	8.0±0.2	94±8	0.57±0.04
CMC/PDMAEMA (M)	6.4±0.8	54±25	0.47±0.07
CMC/PDMAEMA (H)	3.9±0.7	28±5	0.24±0.04
CMC/PDMAEMA-Q	9.4±3.4	57±11	0.77±0.08

[a] Young's modulus is calculated from the slope of stress-strain curve at low strain (0-2.0%)

6.3.4 Rheological behaviour of short fibre CMC hydrogel composites

The morphology of fibres after homogenization and their hydrogel composites was characterized by SEM (Figure 6.8). The discontinuous fibre ends are indicated by yellow arrows in a1-c1. Fibre diameter hardly changed compared to as-spun fibres. Massive entanglement of PLA fibres was observed due to their poor hydrophilicity, while fibre aggregation occurred during homogenization. After functionalization, dispersion of fibres in water was greatly improved during homogenization. The chopped fibres were then integrated into the CMC hydrogels. PLA fibre bundles were found in lyophilized hydrogels, indicating poor fibre distribution. In contrast, PDMAEMA (H) and PDMAEMA-Q fibres were more homogeneously distributed, leading to a more controllable and stable composite hydrogel system.

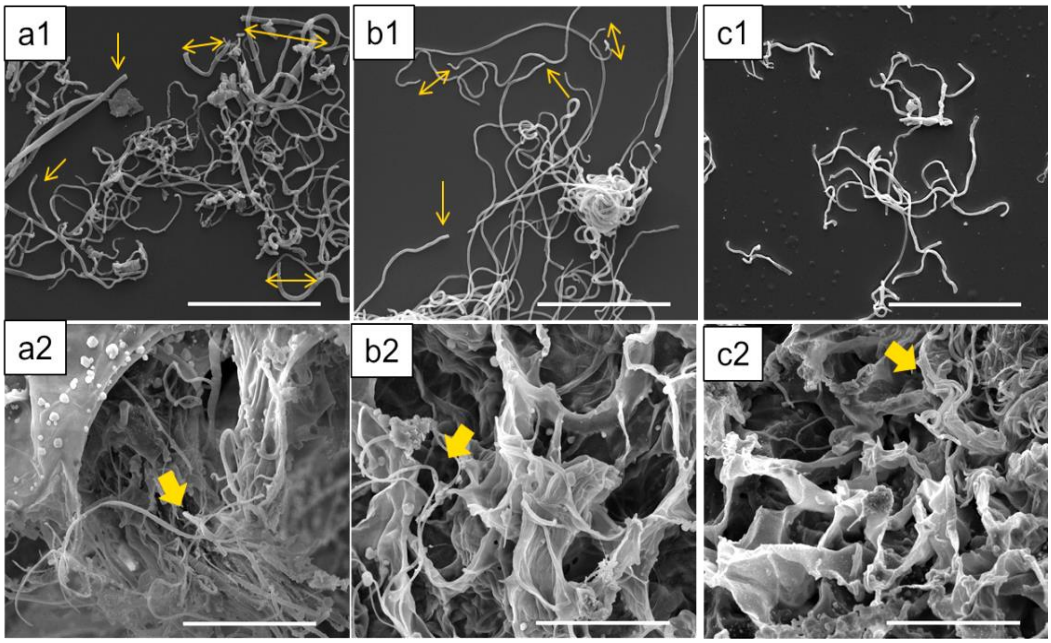

Figure 6.8 *SEM of chopped fibres and fibre reinforced CMC hydrogel composites: (a1,a2) PLA fibre and hydrogel composites; (b1,b2) PDMAEMA (H) fibre and hydrogel composites; (c1,c2) PDMAEMA-Q fibre and hydrogel composites (scale bar 20 µm, yellow arrows indicate the short fibres).*

Rheological tests of CMC precursor solution (without fibres) showed viscous fluid behaviour before UV exposure (loss modulus G'' > storage modulus G'). Upon UV exposure, quick gelation occurs (cross-over of G' and G'' after only 2.5 sec UV exposure) and G' reaches around 275 Pa after complete UV exposure. With the addition of 0.5 wt% fibres, the CMC solution becomes more viscous and behaves like a gel even prior to UV curing (G' > G''). PLA fibres showed no reinforcing effect in CMC hydrogel, which can be explained by the weak interaction between the PLA fibres and the CMC hydrogel as well as poor fibre distribution. The addition of PLA/PDMAEMA (H) fibres improved G' from 275 Pa to 390 Pa, indicating that functionalized PLA fibres provide better reinforcement of the CMC hydrogel. PLA/PDMAEMA-Q fibres showed the greatest increase in G' (960 Pa), implying further enhanced fibre-hydrogel interaction. Compared with previously reported short fibre reinforced hydrogels [101, 284], the composite hydrogels in our current work demonstrated significant fibre reinforcement of the hydrogel at low fibre loading. The frequency sweep presented a plateau in the range of 0.1 to 10 Hz, indicating that the hydrogels are stable under these oscillatory conditions. At higher frequencies (10 to 100 Hz), G' starts to decrease, which is due to a loss of inertia. The failure strain of the hydrogels was decreased with the addition of short electrospun fibres, possibly due to the low failure strain of the PLA fibres and the presence of fibre aggregates. Rheology tests indicated that the PLA/PDMAEMA-Q fibres exhibited the best reinforcement effect, which can be explained by ionic interactions between fibres and CMC hydrogel.

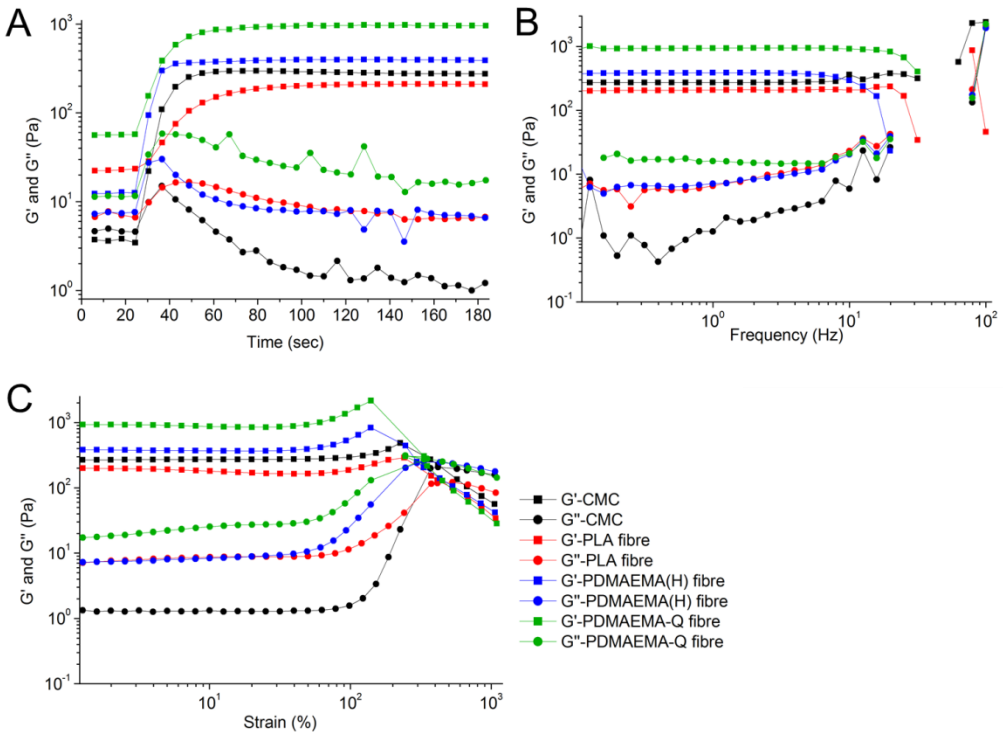

Figure 6.9 *Rheological tests of CMC and short fibre CMC hydrogel composite: (a) time sweep for 180 sec with UV exposure from 30 to 150 sec, at 10^{-4} rad displacement and 1 Hz frequency; (b) frequency sweep from 0.1 to 100 Hz at 10^{-4} rad displacement; (c) strain sweep from 1 to 1000% at 1 Hz frequency.*

Photographs demonstrating the injectability of the composite hydrogel systems are presented in Figure 6.10. For comparison, CMC precursor solutions with and without fibres were both dispensed using a syringe (needle diameter 0.5 mm) into PDMS mould. After UV curing, the free-standing fibre reinforced composite hydrogels were removed from the moulds while hydrogels without fibres were difficult to remove from the mould or to handle.

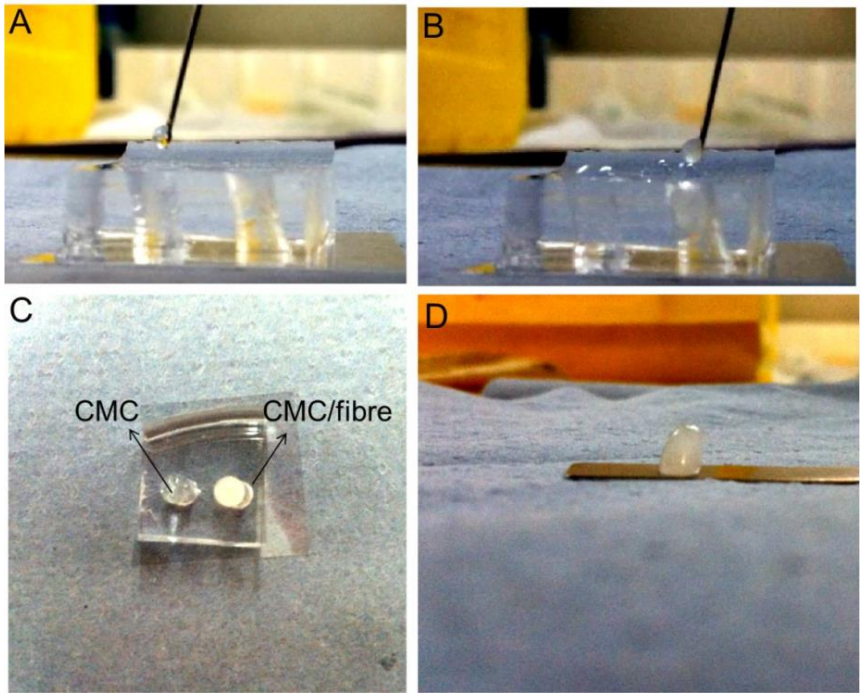

Figure 6.10 *Photographs demonstrating the injectable composite hydrogel system: (a) dispensing CMC precursor solution, (b) dispensing CMC/0.5 wt% short PDMAEMA-Q fibre precursor solution, (c) two solutions injected in PDMS mould; (d) free-standing fibre reinforced CMC hydrogel composite after UV curing.*

6.4 Conclusions

In this chapter, functionalized electrospun PLA fibres were fabricated by electrospinning of hybrids of homo PLA and amphiphilic block copolymer PLA-b-PDMAEMA. Block copolymers with different PDMAEMA block chain lengths were synthesized by a combination of ROP and ATRP. The introduction of PLA-b-PDMAEMA successfully increased the hydrophilicity of homo PLA due to the presence of PDMAEMA blocks on the fibre surface. By varying the PDMAEMA chain length, the hydrophilicity of the electrospun PLA fibres was modulated. Functionalized PLA fibres were easier to incorporate into CMC hydrogels and showed improved fibre-matrix bonding with increased PDMAEMA content or PDMAEMA quaternization. Compared with previous reports, the hydrophilicity of the PLA fibres was better controlled and more easily modulated without damaging the fibre structure and integrity. Functionalized PLA fibres were easily incorporated in the CMC hydrogel without any further treatment. Finally, chopped electrospun PLA fibres were produced and integrated into CMC hydrogel. The addition of a very small amount of functionalized

PLA fibres (0.5 wt%) resulted already in a three-fold increase in storage modulus of the CM hydrogel. Their easy integration, strong interfacial interaction and high reinforcing efficiency make PLA-b-PDMAEMA-functionalized PLA fibres a promising candidate for the reinforcement and design of novel injectable CMC based hydrogel composite systems.

Chapter 7 - Summary and future work

7.1 Summary

In this thesis, engineered electrospun PLA fibres were employed for the development of polymer-polymer composite biomaterials with novel functionalities and properties. Electrospun PLA nanofibres have already been extensively studied in various biomedical applications such as tissue engineering and drug release systems because of their commercial availability, ease of fabrication and unique microstructures (e.g., high surface area, high porosity, etc.). However, the use of electrospun fibres in composites is usually hindered by technical issues such as relatively poor fibre mechanical properties (compared with traditional reinforcing fibres), poor fibre alignment and the absence of large scale production methods [1, 38]. While the need for high strength and high stiffness electrospun fibres may be questioned for many biomedical applications, some other technical limitations still include the presence of extensive fibre entanglements in electrospun fibre mats which limits their use in composites processed using injection moulding, extrusion or 3D printing. Up to now, nearly all composites based on 2D electrospun fibre mats can only be shaped into relatively simple geometries, severely limiting flexibility in product design, fabrication and applications.

PTMC is an elastomeric material commonly used in additive manufacturing [12, 205, 244]. Its surface-erosion degradation mode and non-acidic degradation product make PTMC very attractive for various biomedical applications. However, PTMC usually has a weak mechanical performance, restricting it from certain applications that require good dimensional stability. Therefore, we proposed the incorporation of short PLA fibres into PTMC because short fibres not only provide mechanical reinforcement but also allow for liquid formulations and processes such as injection moulding or additive manufacturing. In Chapter 3, we first developed techniques of cutting electrospun fibres. Short fibres were obtained by either ultrasonication or mechanical stirring in mixed organic solvents. Ultrasonication produced short fibres but was found to damage the fibres' morphology. Mechanical stirring was able to disentangle and fragment PLA

fibres when performed in a PLA-swelling solvent. Fibres of 220 µm average length were obtained by mechanical stirring. Both continuous and short PLA fibre reinforced PTMC composites were prepared and studied. As expected, continuous electrospun fibre mats provided the best mechanical reinforcement with the Young's modulus increasing by more than two orders of magnitudes. Short fibres also showed good reinforcing potential, with 5 wt% chopped fibres increasing the Young's modulus and tensile strength by 300% without compromising composite ductility. PLA fibre and PTMC matrix showed good levels of interfacial interaction, implying good reinforcing efficiency. Moreover, the use of short fibres allowed for a wide range of potential composite manufacturing processes, not attainable with conventional electrospun fibre mats as reinforcement.

In Chapter 4, we developed shape memory polymer composites (SMPCs) using fully degradable and biocompatible materials. Electrospun PLA fibres (both continuous and discontinuous) were incorporated into a crosslinked PTMC network. The short fibres were prepared using the method developed in Chapter 3. In the SMPCs the PLA fibres acted as the transition phase during the shape memory programming. By first deforming the composites above T_g (of PLA) and then maintaining this deformation until below T_g (of PLA), the deformation was fixed. When re-heating the composites above T_g, the retraction force generated by the PTMC entropic energy was able to recover the composites' initial shape. Good shape memory properties were achieved by incorporating either continuous fibres or 50 wt% chopped fibres, with shape fixing ratios of more than 85% and shape recovery ratios around 95%. Compared to previous reports [4, 233, 236-239], these shape memory polymer composites were prepared from two well-studied materials; neither complicated nor specific polymer synthesis was involved. Moreover, the composites' shape memory properties were conveniently modulated by fibre aspect ratio, fibre loading and PTMC molecular weight. The shape memory transition temperature was also modulated by modifying the T_g of the PLA fibre through electrospinning of PLA with plasticizer. The conveniently controlled shape memory properties and flexible design of component geometries offers greatly enhanced flexibility for these smart composites in biomedical applications.

In Chapter 5, we proposed the use of electrospun PLA fibres as drug delivery systems for bioactive compounds (dexamethasone) when incorporating these compound-loaded fibres into UV-crosslinkable PTMC. UV-crosslinkable PTMC is commonly used in

stereolithography for producing three-dimensional (3D) architectures of high precision. However, PTMC scaffolds made by stereolithography have hardly been used as drug delivery systems because drugs (especially unstable drugs) are easily denatured by the UV crosslink reaction during the stereolithography process. By loading the drugs in electrospun PLA fibres first and then incorporating these bioactive fibres into PTMC, the drug's bioactivity was successfully preserved. Stable and sustained dexamethasone release was observed. At the same time, the mechanical performance of PTMC was improved. The bioactivity and sustained release of dexamethasone were further validated by culturing hBMSCs on PTMC/PLA fibre composites. The dexamethasone-loaded composites were found to enhance cell proliferation and osteogenic differentiation during the cell culture period. The concept of PTMC/PLA fibre composites offered a high degree of versatility for loading various therapeutics into UV-crosslinkable PTMC based systems without denaturation, providing a potential opportunity of building drug-loaded scaffolds using stereolithography.

In Chapter 6, we proposed the use of electrospun PLA fibres for the reinforcement of CMC hydrogels. PLA fibres were not only engineered into short fibres, but also functionalized to allow for an easier integration and distribution. Amphiphilic block copolymer PLA-b-PDMAEMA was employed to modify the hydrophilicity of the PLA fibres. By increasing the molecular chain length of PDMAEMA, the hydrophilicity of the PLA was successfully improved. Functionalized PLA fibres were more easily integrated into CMC hydrogels and showed improved interfacial adhesion between PLA fibres and CMC matrix with increasing PDMAEMA content. Further improved PLA fibre-CMC matrix adhesion was achieved by quaternizing PDMAEMA, which induced ionic interactions between fibre and matrix. Chopped PLA fibres were prepared by homogenizing electrospun PLA fibres in water. Hydrogels incorporating 0.5 wt% short PDMAEMA-Q fibres showed a more than three-fold increase in storage modulus. The use of short functionalized fibres in hydrogels not only enhanced the mechanical performance of these hydrogels but also showed great promise for the design of injectable composite hydrogel systems.

7.2 Future Work

In this thesis, engineered electrospun PLA fibres were successfully fabricated and integrated into PTMC and CMC hydrogel matrix, respectively for the design of novel composite biomaterials. PTMC/PLA fibre composites exhibited good mechanical performances and shape memory behaviour; they were also employed as drug delivery system, showing sustained and stable drug release profiles. Functionalized PLA fibres improved fibre-hydrogel interaction while the use of chopped fibres allows for the design of injectable hydrogel systems. In addition to current results, some further work is worth considering.

When investigating the mechanical properties of short fibre reinforced PTMC composites, the relationship between the short fibre loading and composite mechanical properties was studied. In Chapter 2, two different short PLA fibre loadings were employed (5 and 30 wt%). It is suggested to study additional fibre loadings like 10 wt% and 20 wt% in PTMC. In addition to different fibre loadings, it is interesting to investigate effect of fibre length on the composites' mechanical performance. Short fibres of different length should be fabricated and the relationship between composite modulus, strength and toughness and fibre length could be evaluated. By doing this, it is also possible to validate the critical fibre length L_c. In Chapter 2, the L_c of PLA fibre in PTMC matrix was calculated using $L_c = \sigma_f \cdot D/2\tau$, where τ (interfacial shear strength) was estimated from the tensile strength and σ_f (fibre strength) was taken as the strength of bulk PLA. The L_c equation was based on the assumption of perfect adhesion between PLA fibre and PTMC matrix. According to a previous report [217], critical fibre length (L_c) can be calculated by investigating the composites' modulus as a function of fibre length. By plotting a graph similar to Figure 7.1, the minimum fibre length required for either modulus, tensile strength or impact strength can be obtained. Through this it would be possible to create composites tailored to specific properties with a minimum fibre length. This would lead to beneficial effects such as improved processability and reduced entanglements and agglomerates. Moreover, the rheological behaviour of PTMC/PLA fibre systems needs to be studied to find appropriate conditions such as fibre loading, fibre length, resin viscosity, etc. for composite processing using liquid moulding techniques or stereolithography.

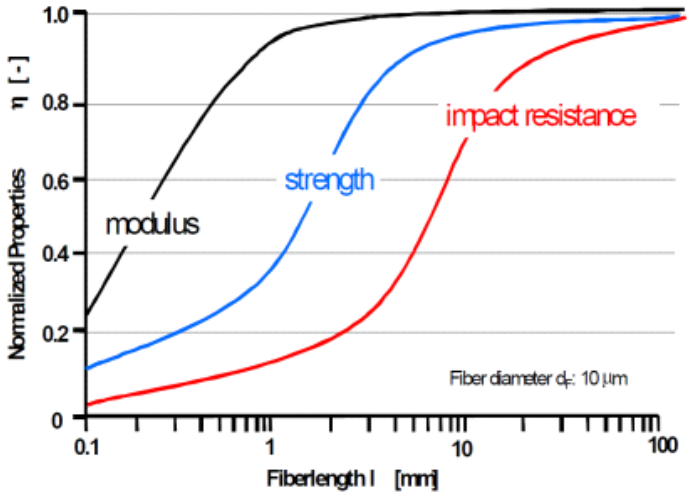

Figure 7.1 *Normalized mechanical properties of short fibre composites (polypropylene/glass) as a function of fibre length (figure source: Plasticomp).*

The shape memory polymer composites developed in Chapter 4 showed promising potential for the design of smart biomedical devices. Therefore, the biocompatibility and degradation properties of composites are to be tested. The flexible design and processing allows for the fabrication of composites of complex geometries. Future work should be directed towards the development of shape memory scaffolds of high precision using additive manufacturing. As an example, Figure 7.2 shows photographs of PTMC scaffolds incorporating hydroxyapatite (HA) made by stereolithography [244]. One essential factor for PTMC additive manufacturing is the viscosity of the PTMC resin system. In our experiments, the integration of PLA short fibres increased the viscosity of PTMC resin, especially at high fibre loading in order to achieve good shape memory behaviour. On the other hand, high PLA fibre loadings also cause fibre aggregation, which can lead to blockage of processing equipment or the creation of structural defects in products. Therefore it is crucial to further investigate the impact of fibre length on PTMC/PLA fibre composite properties. Short fibres ($L > L_c$) that maintain the composites' mechanical properties are considered to be a potential solution to alleviate fibre aggregation. A visualization of fibre distribution and orientation in PTMC/PLA fibre composites is also an important aspect to understand the shape memory mechanisms and how to improve it. Another important aspect is to modulate the shape memory transition temperature. In Chapter 4, PEG was used as a plasticizer

to modulate the T_g of PLA fibres in order to control the composites' shape memory transition temperature. However, due to solvent extraction, some of the PEG integrated in the PLA fibres was partially lost. Therefore, the use of a plasticizer that is not solvent-extracted or another method to lower the T_g (such replacing PLA with PLGA) could be an interesting alternative solution.

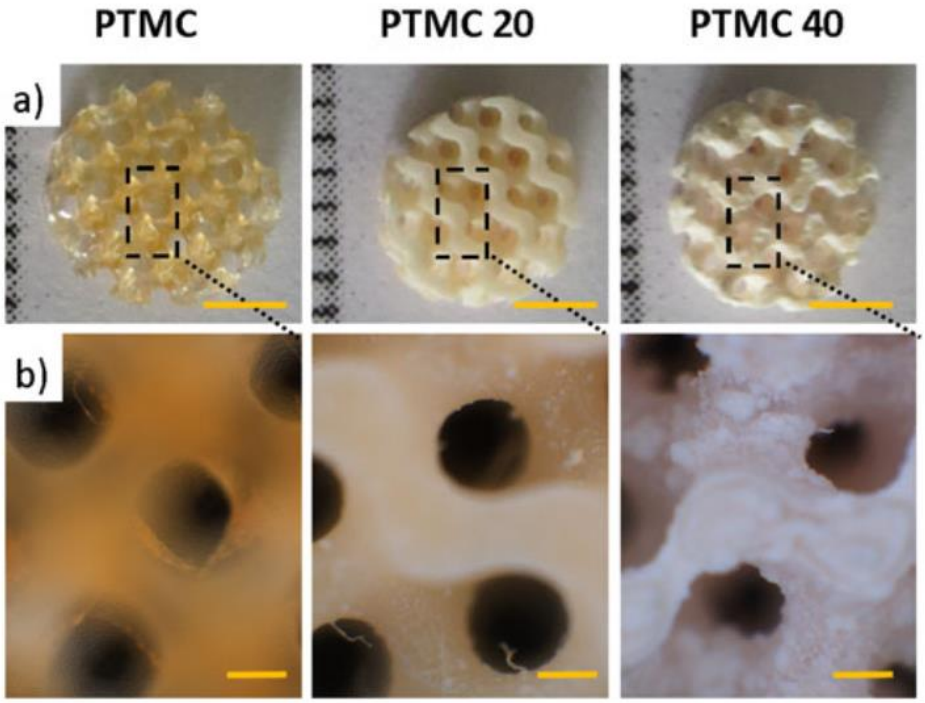

Figure 7.2 *Macroporous PTMC-HA scaffolds produced by stereolithography (adapted from [244]).*

The dexamethasone loaded PTMC/PLA fibre composite system offered stable and sustained drug release as well as a novel route of loading unstable drugs into UV-crosslinkable materials. However, here the composite preparation methodology needs to be optimized as fibre protrusions were seen on composite surfaces. These fibre protrusions will affect the drug release kinetics. Since PTMC degrades barely or extremely slow in non-enzymatic conditions, the degradation of PTMC after the incorporation of fibres should be investigated. A detailed degradation study of PTMC/PLA fibre composites should help to better understand the dexamethasone release mechanism. In Chapter 3 and 4, short PLA fibres have already demonstrated their advantages in flexible composite processing and design. It is therefore worth to develop drug-loaded short PLA fibres. These bioactive short PLA fibres can be

processed with different matrix materials into customized implantable drug delivery devices, as a way of incorporating drugs without denaturation.

Composites made up of hydrogel and electrospun fibres present many common features of natural tissue, which is composed of extra cellular matrix (ECM) and fibrous networks. The incorporation of fibres significantly improved the stiffness of the hydrogels, opening up possibilities for hydrogels in load-bearing applications. In addition to rheological tests, compression tests are also important to determine the mechanical properties of composite hydrogels. Most importantly, before any biomedical usage the cytotoxicity of the composite hydrogel has to be evaluated by analysing cell viability. Secondly, since cells can only feel the in-situ forces within hydrogel composites, it is considered important to have a homogeneous fibre dispersion in the hydrogel system. In the current work, different fibre densities are observed in the composites, which will influence cell behaviour at different levels. In addition, the composite hydrogels developed in Chapter 6 not only showed an improved shear modulus, but also stress relaxation (Figure 7.3). According to previous studies, stem cell spreading, proliferation and differentiation can be regulated by stress relaxation [290]. Therefore, it is interesting to carry out *in vitro* tests on composite hydrogels. Potential applications may include injectable scaffolds or cell carriers for tissue engineering.

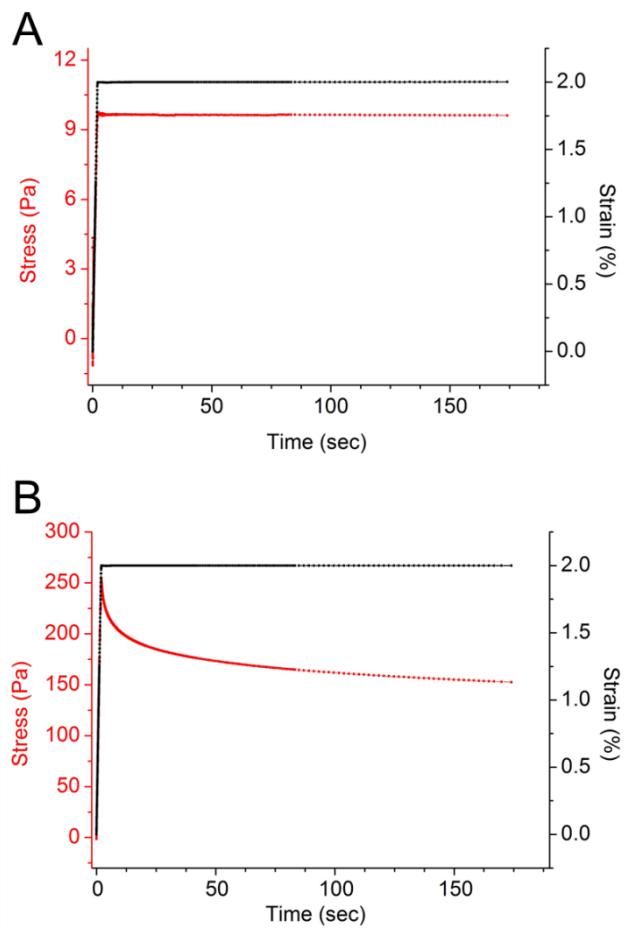

Figure 7.3 *Stress relaxation of (a) CMC hydrogel and (b) CMC/3.0 wt% PLA fibre composite hydrogel: measurements were performed between two parallel geometries (20 mm) at a distance of 0.5 mm. A strain of 2.0% was applied and stress relaxation was observed for 180 sec.*

References

1. Huang Z-M, Zhang YZ, Kotaki M, and Ramakrishna S. Composites Science and Technology 2003;63(15):2223-2253.
2. Shaohui L, Jiwei Z, Jinwen W, Shuangxi X, and Wenqin Z. ACS Appl Mater Interfaces 2014;6(3):1533-1540.
3. Bergshoef MM and Vansco GJ. Advanced Materials 1999;11(16):1362-1365.
4. Lawton MI, Tillman KR, Mohammed HS, Kuang W, Shipp DA, and Mather PT. ACS Macro Letters 2016;5(2):203-207.
5. Stone DA, Wanasekara ND, Jones DH, Wheeler NR, Wilusz E, Zukas W, Wnek GE, and Korley LTJ. ACS Macro Letters 2012;1(1):80-83.
6. Han N, Johnson J, Lannutti JJ, and Winter JO. J Control Release 2012;158(1):165-170.
7. Fukushima K. Biomater Sci 2015;4(1):9-24.
8. Huang ZM, He CL, Yang A, Zhang Y, Han XJ, Yin J, and Wu Q. J Biomed Mater Res A 2006;77(1):169-179.
9. Zhang Z, Kuijer R, Bulstra SK, Grijpma DW, and Feijen J. Biomaterials 2006;27(9):1741-1748.
10. Matsumura S, Harai S, and Toshima K. Macromolecular Rapid Communications 2001;22(3):215-218.
11. Bat E, van Kooten TG, Feijen J, and Grijpma DW. Acta Biomater 2011;7(5):1939-1948.
12. van Bochove B, Hannink G, Buma P, and Grijpma DW. Macromol Biosci 2016;16(12):1853-1863.
13. Jamshidian M, Tehrany EA, Imran M, Jacquot M, and Desobry S. Comprehensive Reviews in Food Science and Food Safety 2010;9(5):552-571.
14. Zaera F. Chem Soc Rev 2013;42(7):2746-2762.
15. Taylor R, Coulombe S, Otanicar T, Phelan P, Gunawan A, Lv W, Rosengarten G, Prasher R, and Tyagi H. Journal of Applied Physics 2013;113(1):011301.
16. Sun T, Zhang YS, Pang B, Hyun DC, Yang M, and Xia Y. Angew Chem Int Ed Engl 2014;53(46):12320-12364.
17. Ma TY, Ran J, Dai S, Jaroniec M, and Qiao SZ. Angew Chem Int Ed Engl 2015;54(15):4646-4650.
18. Berthelot J, Acimovic SS, Juan ML, Kreuzer MP, Renger J, and Quidant R. Nat Nanotechnol 2014;9(4):295-299.
19. Gujrati V, Kim S, Kim S-H, Min JJ, Choy HE, Kim SC, and Jon S. ACS Nano 2014;8(2):1525-1537.
20. Grzelczak M, Vermant J, Furst EM, and Liz-Marzan LM. ACS Nano 2010;4(7):3591-3605.
21. Ariga K, Yamauchi Y, Rydzek G, Ji Q, Yonamine Y, Wu KCW, and Hill JP. Chemistry Letters 2014;43(1):36-68.
22. Tian J, Liu Q, Asiri AM, and Sun X. J Am Chem Soc 2014;136(21):7587-7590.
23. Yang P, Ding Y, Lin Z, Chen Z, Li Y, Qiang P, Ebrahimi M, Mai W, Wong CP, and Wang ZL. Nano Lett 2014;14(2):731-736.
24. Keshtkar M, Nofar M, Park CB, and Carreau PJ. Polymer 2014;55(16):4077-4090.
25. Zhang H, Liu Y, Kuwata M, Bilotti E, and Peijs T. Composites Part A: Applied Science and Manufacturing 2015;70:102-110.

26. GhavamiNejad A, Rajan Unnithan A, Ramachandra Kurup Sasikala A, Samarikhalaj M, Thomas RG, Jeong YY, Nasseri S, Murugesan P, Wu D, Hee Park C, and Kim CS. ACS Appl Mater Interfaces 2015;7(22):12176-12183.
27. Luo Y, Shen H, Fang Y, Cao Y, Huang J, Zhang M, Dai J, Shi X, and Zhang Z. ACS Appl Mater Interfaces 2015;7(11):6331-6339.
28. Visser J, Melchels FP, Jeon JE, van Bussel EM, Kimpton LS, Byrne HM, Dhert WJ, Dalton PD, Hutmacher DW, and Malda J. Nat Commun 2015;6:6933.
29. Yao J, Pantano MF, Pugno NM, Bastiaansen CWM, and Peijs T. Polymer 2015;76:105-112.
30. Liu S-L, Long Y-Z, Zhang Z-H, Zhang H-D, Sun B, Zhang J-C, and Han W-P. Journal of Nanomaterials 2013;2013:1-9.
31. Mi HY, Salick MR, Jing X, Crone WC, Peng XF, and Turng LS. J Biomed Mater Res A 2015;103(2):593-603.
32. Arras MML, Grasl C, Bergmeister H, and Schima H. Science and Technology of Advanced Materials 2016;13(3):035008.
33. Youm J, Kim J, Kim C, Kim J, Kim Y, and Yang K. Journal of Applied Polymer Science 2016;133(37):43945(43941-43949).
34. De Vrieze S, Van Camp T, Nelvig A, Hagström B, Westbroek P, and De Clerck K. Journal of Materials Science 2008;44(5):1357-1362.
35. Li D and Xia Y. Advanced Materials 2004;16(14):1151-1170.
36. Agarwal S, Wendorff JH, and Greiner A. Adv Mater 2009;21(32-33):3343-3351.
37. Peijs T. Reference Module in Materials Science and Materials Engineering 2017.
38. Yao J, Bastiaansen C, and Peijs T. Fibers 2014;2(2):158-186.
39. Zhang CL and Yu SH. Chem Soc Rev 2014;43(13):4423-4448.
40. Bognitzki M, Czado W, Frese T, Schaper A, Hellwig M, Steinhart M, Greiner A, and J.H.Wendorff. Advanced Materials 2001;13(1):70-72.
41. Megelski S, Stephens JS, Chase DB, and Rabolt JF. Macromolecules 2002;35(22):8456-8466.
42. Liu Z, Zhao J-h, Liu P, and He J-h. Applied Surface Science 2016;364:516-521.
43. Lin J, Ding B, Yang J, Yu J, and Sun G. Nanoscale 2012;4(1):176-182.
44. Liu W, Huang C, and Jin X. Nanoscale Res Lett 2015;10(1):949.
45. Putti M, Simonet M, Solberg R, and Peters GWM. Polymer 2015;63:189-195.
46. Sun Z, Zussman E, Yarin AL, Wendorff JH, and Greiner A. Advanced Materials 2003;15(22):1929-1932.
47. Forward KM, Flores A, and Rutledge GC. Chemical Engineering Science 2013;104:250-259.
48. Zhao Y, Cao X, and Jiang L. Journal of American Chemical Society 2007;129(4):764-765.
49. McCann JT, Marquez M, and Xia Y. Journal of American Chemical Society 2006;128(5):1436-1437.
50. Chen J-T, Chen W-L, and Fan P-W. ACS Macro Letters 2012;1(1):41-46.
51. Naraghi M, Chasiotis I, Kahn H, Wen Y, and Dzenis Y. Applied Physics Letters 2007;91(15):151901.
52. Tang S, Li Y, Liu WK, and Huang XX. Macromolecules 2014;47(18):6503-6514.
53. Chen JT, Kao YH, Kuo TY, Liu CT, Chiu YJ, Chu CW, Chi MH, and Tsai CC. Macromol Rapid Commun 2016;37(3):239-245.
54. Müller GFJ, Stürzel M, and Mülhaupt R. Advanced Functional Materials 2014;24(19):2860-2864.
55. Haider A, Ozgit-Akgun C, Kayaci F, Okyay AK, Uyar T, and Biyikli N. Apl Materials 2014;2(9):096109.

56. Saetia K, Schnorr JM, Mannarino MM, Kim SY, Rutledge GC, Swager TM, and Hammond PT. Advanced Functional Materials 2014;24(4):492-502.
57. Jing X, Mi HY, Wang XC, Peng XF, and Turng LS. ACS Appl Mater Interfaces 2015;7(12):6955-6965.
58. Che H, Huo M, Peng L, Fang T, Liu N, Feng L, Wei Y, and Yuan J. Angew Chem Int Ed Engl 2015;54(31):8934-8938.
59. Devarayan K, Kim HY, and Kim BS. Carbohydr Polym 2015;117:408-413.
60. Zandén C, Voinova M, Gold J, Mörsdorf D, Bernhardt I, and Liu J. European Polymer Journal 2012;48(3):472-482.
61. Xue CH, Li YR, Zhang P, Ma JZ, and Jia ST. ACS Appl Mater Interfaces 2014;6(13):10153-10161.
62. Hughes-Brittain NF, Qiu L, Picot OT, Wang W, Peijs T, and Bastiaansen CW. Polymer 2017;In Press.
63. Chen H, Di J, Wang N, Dong H, Wu J, Zhao Y, Yu J, and Jiang L. Small 2011;7(13):1779-1783.
64. Wang X, Yuan Y, Huang X, and Yue T. Journal of Applied Polymer Science 2014;132(16):41811(41811-41819).
65. Gupta A, Eral HB, Hatton TA, and Doyle PS. Soft Matter 2016;12(11):2826-2841.
66. Wang M, Fang D, Wang N, Jiang S, Nie J, Yu Q, and Ma G. Polymer 2014;55(9):2188-2196.
67. Katsogiannis KAG, Vladisavljević GT, and Georgiadou S. European Polymer Journal 2015;69:284-295.
68. Nayani K, Katepalli H, Sharma CS, Sharma A, Patil S, and Venkataraghavan R. Industrial & Engineering Chemistry Research 2012;51(4):1761-1766.
69. Chen G, Guo J, Nie J, and Ma G. Polymer 2016;83:12-19.
70. Tang K, Yu Y, Mu X, van Aken PA, and Maier J. Electrochemistry Communications 2013;28:54-57.
71. Darling SB. Progress in Polymer Science 2007;32(10):1152-1204.
72. Bates FS and Fredrickson GH. Physics Today 1999;52(2):32.
73. Mai Y and Eisenberg A. Chem Soc Rev 2012;41(18):5969-5985.
74. Sing CE, Zwanikken JW, and Olvera de la Cruz M. Nat Mater 2014;13(7):694-698.
75. Kennemur JG, Yao L, Bates FS, and Hillmyer MA. Macromolecules 2014;47(4):1411-1418.
76. Radjabian M and Abetz V. Adv Mater 2015;27(2):352-355.
77. Sprouse D, Jiang Y, Laaser JE, Lodge TP, and Reineke TM. Biomacromolecules 2016;17(9):2849-2859.
78. Qiu H, Hudson ZM, Winnik MA, and Manners I. Science;347(6228):1329-1332.
79. Brosnan SM, Schlaad H, and Antonietti M. Angew Chem Int Ed Engl 2015;54(33):9715-9718.
80. Zhang WJ, Hong CY, and Pan CY. Macromol Rapid Commun 2015;36(15):1428-1436.
81. Lin W, Zheng C, Wan X, Liang D, and Zhou Q. Macromolecules 2010;43(12):5405-5410.
82. Cheng X, Jin Y, Fan B, Qi R, Li H, and Fan W. ACS Macro Letters 2016;5(2):238-243.
83. Kapllani A, Tran C, and Kalra V. Soft Matter 2013;9(46):11014.
84. Kalra V, Mendez S, Lee JH, Nguyen H, Marquez M, and Joo YL. Advanced Materials 2006;18(24):3299-3303.
85. Ma M, Krikorian V, Yu JH, Thomas EL, and Rutledge GC. Nano Lett 2006;6(12):2969-2972.

86. Zhao H, Gu W, Thielke MW, Sterner E, Tsai T, Russell TP, Coughlin EB, and Theato P. Macromolecules 2013;46(13):5195-5201.
87. Zhai F-Y, Huang W, Wu G, Jing X-K, Wang M-J, Chen S-C, Wang Y-Z, Chin I-J, and Liu Y. ACS Nano 2013;7(6):4892-4901.
88. Zhang X, Geven MA, Grijpma DW, Gautrot JE, and Peijs T. Materials Today Communications 2016;8:53-63.
89. Jiang S, Duan G, Schöbel J, Agarwal S, and Greiner A. Composites Science and Technology 2013;88:57-61.
90. Kriha O, Becker M, Lehmann M, Kriha D, Krieglstein J, Yosef M, Schlecht S, Wehrspohn RB, Wendorff JH, and Greiner A. Advanced Materials 2007;19(18):2483-2485.
91. Thieme M, Agarwal S, Wendorff JH, and Greiner A. Polymers for Advanced Technologies 2009:n/a-n/a.
92. Duan G, Jiang S, Jérôme V, Wendorff JH, Fathi A, Uhm J, Altstädt V, Herling M, Breu J, Freitag R, Agarwal S, and Greiner A. Advanced Functional Materials 2015;25(19):2850-2856.
93. Xu W, Feng Y, Ding Y, Jiang S, Fang H, and Hou H. Materials Letters 2015;161:431-434.
94. Ren Y, Wang S, Liu R, Dai J, Liu X, and Yu J. RSC Adv. 2016;6(36):30139-30147.
95. Langner M and Greiner A. Macromol Rapid Commun 2016;37(4):351-355.
96. Mulky E, Yazgan G, Maniura-Weber K, Luginbuehl R, Fortunato G, and Buhlmann-Popa AM. Mater Sci Eng C Mater Biol Appl 2014;45:277-286.
97. Sawawi M, Wang TY, Nisbet DR, and Simon GP. Polymer 2013;54(16):4237-4252.
98. Stoiljkovic A and Agarwal S. Macromolecular Materials and Engineering 2008;293(11):895-899.
99. Kim TG and Park TG. Macromolecular Rapid Communications 2008;29(14):1231-1236.
100. Fathona IW and Yabuki A. Fibers and Polymers 2016;17(8):1238-1244.
101. Regev O, Reddy CS, Nseir N, and Zussman E. Macromolecular Materials and Engineering 2013;298(3):283-291.
102. Fathona IW and Yabuki A. Current Applied Physics 2014;14(5):761-767.
103. Fathona IW and Yabuki A. Journal of Materials Processing Technology 2013;213(11):1894-1899.
104. Ge J, Fan G, Si Y, He J, Kim HY, Ding B, Al-Deyab SS, El-Newehy M, and Yu J. Nanoscale 2016;8(4):2195-2204.
105. Cao Z, Wang D, Lyu L, Gong Y, and Li Y. RSC Adv. 2016;6(13):10641-10649.
106. Wang W, Ciselli P, Kuznetsov E, Peijs T, and Barber AH. Philos Trans A Math Phys Eng Sci 2008;366(1870):1613-1626.
107. Wang Z, Qian Y, Li L, Pan L, Njunge LW, Dong L, and Yang L. J Biomater Appl 2016;30(6):686-698.
108. Yang C, Yu DG, Pan D, Liu XK, Wang X, Bligh SW, and Williams GR. Acta Biomater 2016;35:77-86.
109. Ma C, Li Y, Shi J, Song Y, and Liu L. Chemical Engineering Journal 2014;249:216-225.
110. Bahramzadeh A, Zahedi P, and Abdouss M. Journal of Applied Polymer Science 2016;133(5):42944 (42941-42949).
111. Cheng Q, Lee BL, Komvopoulos K, Yan Z, and Li S. Tissue Eng Part A 2013;19(9-10):1188-1198.
112. Ali MA, Mondal K, Singh C, Malhotra BD, and Sharma A. Nanoscale 2015;7(16):7234-7245.

113. Thielke MW, Bruckner EP, Wong DL, and Theato P. Polymer 2014;55(22):5596-5599.
114. Arslan O, Aytac Z, and Uyar T. ACS Appl Mater Interfaces 2016;8(30):19747-19754.
115. Kangwansupamonkon W, Tiewtrakoonwat W, Supaphol P, and Kiatkamjornwong S. Journal of Applied Polymer Science 2014;131(21):40981(40981-40989).
116. Viswanathan P, Themistou E, Ngamkham K, Reilly GC, Armes SP, and Battaglia G. Biomacromolecules 2015;16(1):66-75.
117. Liu S and Zhai J. J. Mater. Chem. A 2015;3(4):1511-1517.
118. Li L, Zhou G, Wang Y, Yang G, Ding S, and Zhou S. Biomaterials 2015;37:218-229.
119. Chou SF, Carson D, and Woodrow KA. J Control Release 2015;220(Pt B):584-591.
120. Lee JH, Park JH, El-Fiqi A, Kim JH, Yun YR, Jang JH, Han CM, Lee EJ, and Kim HW. Acta Biomater 2014;10(6):2750-2761.
121. Esfahani H, Prabhakaran MP, Salahi E, Tayebifard A, Keyanpour-Rad M, Rahimipour MR, and Ramakrishna S. J Colloid Interface Sci 2015;443:143-152.
122. Shafiq M, Jung Y, and Kim SH. J Biomed Mater Res A 2016;104(6):1352-1371.
123. Zuidema JM, Hyzinski-Garcia MC, Van Vlasselaer K, Zaccor NW, Plopper GE, Mongin AA, and Gilbert RJ. Biomaterials 2014;35(5):1439-1449.
124. Huang L, Arena JT, and McCutcheon JR. Journal of Membrane Science 2016;499:352-360.
125. He L, Tang S, Prabhakaran MP, Liao S, Tian L, Zhang Y, Xue W, and Ramakrishna S. Macromol Biosci 2013;13(11):1601-1609.
126. Kayaci F, Vempati S, Ozgit-Akgun C, Biyikli N, and Uyar T. Applied Catalysis B: Environmental 2014;156-157:173-183.
127. Xie J, Liu W, MacEwan MR, Bridgman PC, and Xia Y. ACS Nano 2014;8(2):1878-1885.
128. Vaquette C, Ivanovski S, Hamlet SM, and Hutmacher DW. Biomaterials 2013;34(22):5538-5551.
129. Huang L, Arena JT, Manickam SS, Jiang X, Willis BG, and McCutcheon JR. Journal of Membrane Science 2014;460:241-249.
130. Cho HJ, Perikamana SK, Lee JH, Lee J, Lee KM, Shin CS, and Shin H. ACS Appl Mater Interfaces 2014;6(14):11225-11235.
131. Celebioglu A, Demirci S, and Uyar T. Applied Surface Science 2014;305:581-588.
132. Harrison RH, Steele JA, Chapman R, Gormley AJ, Chow LW, Mahat MM, Podhorska L, Palgrave RG, Payne DJ, Hettiaratchy SP, Dunlop IE, and Stevens MM. Adv Funct Mater 2015;25(36):5748-5757.
133. Higaki Y, Kabayama H, Tao D, and Takahara A. Macromolecular Chemistry and Physics 2015;216(10):1103-1108.
134. Wang X, Fu Q, Wang X, Si Y, Yu J, Wang X, and Ding B. J. Mater. Chem. B 2015;3(36):7281-7290.
135. Lee MW, An S, Jo HS, Yoon SS, and Yarin AL. ACS Appl Mater Interfaces 2015;7(35):19546-19554.
136. Chalco-Sandoval W, Fabra M, Lopez-Rubio A, and Lagaron J. Journal of Applied Polymer Science 2016;133(36):43903(43901-43909).
137. Cheng L, Ma SY, Li XB, Luo J, Li WQ, Li FM, Mao YZ, Wang TT, and Li YF. Sensors and Actuators B: Chemical 2014;200:181-190.
138. Lu W, Sun J, and Jiang X. Journal of Materials Chemistry B 2014;2(17):2369.
139. Bao M, Lou X, Zhou Q, Dong W, Yuan H, and Zhang Y. ACS Appl Mater Interfaces 2014;6(4):2611-2621.

140. Jin Y, Wang N, Yuan B, Sun J, Li M, Zheng W, Zhang W, and Jiang X. Small 2013;9(14):2410-2414.
141. Salifu AA, Lekakou C, and Labeed F. J Biomed Mater Res A 2016.
142. Rayatpisheh S, Heath DE, Shakouri A, Rujitanaroj PO, Chew SY, and Chan-Park MB. Biomaterials 2014;35(9):2713-2719.
143. Baiguera S, Del Gaudio C, Lucatelli E, Kuevda E, Boieri M, Mazzanti B, Bianco A, and Macchiarini P. Biomaterials 2014;35(4):1205-1214.
144. Sadeghi D, Karbasi S, Razavi S, Mohammadi S, Shokrgozar MA, and Bonakdar S. Journal of Applied Polymer Science 2016;133(47):44171(44171-44179).
145. Ashworth JC, Best SM, and Cameron RE. Materials Technology 2014;29(5):281-295.
146. Duan N, Geng X, Ye L, Zhang A, Feng Z, Guo L, and Gu Y. Biomed Mater 2016;11(3):035007.
147. Zhou H and Lee J. Acta Biomater 2011;7(7):2769-2781.
148. Bao M, Wang X, Yuan H, Lou X, Zhao Q, and Zhang Y. J. Mater. Chem. B 2016;4(31):5308-5320.
149. Dhand C, Ong ST, Dwivedi N, Diaz SM, Venugopal JR, Navaneethan B, Fazil MH, Liu S, Seitz V, Wintermantel E, Beuerman RW, Ramakrishna S, Verma NK, and Lakshminarayanan R. Biomaterials 2016;104:323-338.
150. Chen W, Sun B, Zhu T, Gao Q, Morsi Y, El-Hamshary H, El-Newehy M, and Mo X. Materials Letters 2017.
151. Uhrich KE, Cannizzaro SM, Langer RS, and Shakesheff KM. Chemical Reviews 1999;99(11):3181-3198.
152. Langer R. Nature 1998;392(6679 Suppl) 5-10.
153. Zeng J, Xu X, Chen X, Liang Q, Bian X, Yang L, and Jing X. Journal of Controlled Release 2003;92(3):227-231.
154. Cheng L, Sun X, Zhao X, Wang L, Yu J, Pan G, Li B, Yang H, Zhang Y, and Cui W. Biomaterials 2016;83:169-181.
155. Spano F, Quarta A, Martelli C, Ottobrini L, Rossi RM, Gigli G, and Blasi L. Nanoscale 2016;8(17):9293-9303.
156. Wu S, Wu J, Yue J, To MKT, Pan H, Lu WW, and Zhao X. Materials Letters 2015;161:716-719.
157. Zheng F, Wang S, Wen S, Shen M, Zhu M, and Shi X. Biomaterials 2013;34(4):1402-1412.
158. Ma J, Meng J, Simonet M, Stingelin N, Peijs T, and Sukhorukov GB. J Mater Sci Mater Med 2015;26(7):205.
159. Luo D, Zhang X, Shahid S, Cattell MJ, Gould DJ, and Sukhorukov GB. Biomater Sci 2016;5(1):111-119.
160. Yoo HS, Kim TG, and Park TG. Advanced Drug Delivery Reviews 2009;61(12):1033-1042.
161. Kim HS and Yoo HS. J Control Release 2010;145(3):264-271.
162. Xie S, Tai S, Song H, Luo X, Zhang H, and Li X. J. Mater. Chem. B 2016;4(42):6820-6829.
163. Abrigo M, McArthur SL, and Kingshott P. Macromol Biosci 2014;14(6):772-792.
164. Lowe A, Bills J, Verma R, Lavery L, Davis K, and Balkus KJ, Jr. Acta Biomater 2015;13:121-130.
165. Spasova M, Manolova N, Paneva D, Mincheva R, Dubois P, Rashkov I, Maximova V, and Danchev D. Biomacromolecules 2010;11(1):151-159.
166. Kataria K, Gupta A, Rath G, Mathur RB, and Dhakate SR. Int J Pharm 2014;469(1):102-110.

167. Lai HJ, Kuan CH, Wu HC, Tsai JC, Chen TM, Hsieh DJ, and Wang TW. Acta Biomater 2014;10(10):4156-4166.
168. Li Y, Chen F, Nie J, and Yang D. Carbohydr Polym 2012;90(4):1445-1451.
169. Wei Q, Xu F, Xu X, Geng X, Ye L, Zhang A, and Feng Z. Frontiers of Materials Science 2016;10(2):113-121.
170. Jin G, Prabhakaran MP, and Ramakrishna S. Photochem Photobiol 2014;90(3):673-681.
171. Lendlein A and Kelch S. Angewandte Chemie International Edition 2002;41(12):2034-2057.
172. Xiao X, Qiu X, Kong D, Zhang W, Liu Y, and Leng J. Soft Matter 2016;12(11):2894-2900.
173. Rabani G, Luftmann H, and Kraft A. Polymer 2006;47(12):4251-4260.
174. Gautrot JE and Zhu XX. Macromolecules 2009;42(19):7324-7331.
175. Cha DI, Kim HY, Lee KH, Jung YC, Cho JW, and Chun BC. Journal of Applied Polymer Science 2005;96(2):460-465.
176. Budun S, İşgören E, Erdem R, and Yüksek M. Applied Surface Science 2016;380:294-300.
177. Shirole A, Sapkota J, Foster EJ, and Weder C. ACS Appl Mater Interfaces 2016;8(10):6701-6708.
178. Yao Y, Wei H, Wang J, Lu H, Leng J, and Hui D. Composites Part B: Engineering 2015;83:264-269.
179. Luo X and Mather PT. Advanced Functional Materials 2010;20(16):2649-2656.
180. Zhang X, Geven MA, Grijpma DW, Peijs T, and Gautrot JE. Polymer 2017;122:323-331.
181. Gong T, Li W, Chen H, Wang L, Shao S, and Zhou S. Acta Biomater 2012;8(3):1248-1259.
182. Zhang Q, Kratz K, and Lendlein A. Polymers for Advanced Technologies 2015;26(12):1468-1475.
183. Tan L, Gan L, Hu J, Zhu Y, and Han J. Composites Part A: Applied Science and Manufacturing 2015;76:115-123.
184. Carothers WH, Dorough GL, and van Natta FJ. Journal of American Chemical Society 1932;54(2):761-772.
185. Li H, Chang J, Qin Y, Wu Y, Yuan M, and Zhang Y. Int J Mol Sci 2014;15(2):2608-2621.
186. Han J, Branford-White CJ, and Zhu L-M. Carbohydrate Polymers 2010;79(1):214-218.
187. Kim J and Lee J. Polymer Journal 2002;34(3):203-208.
188. Pêgo AP, Grijpma DW, and Feijen J. Polymer 2003;44(21):6495-6504.
189. Yang L-Q, He B, Meng S, Zhang J-Z, Li M, Guo J, Guan Y-M, Li J-X, and Gu Z-W. Polymer 2013;54(11):2668-2675.
190. Schuller-Ravoo S, Feijen J, and Grijpma DW. Acta Biomater 2012;8(10):3576-3585.
191. van Leeuwen AC, Bos RR, and Grijpma DW. J Biomed Mater Res B Appl Biomater 2012;100(6):1610-1620.
192. Lin S, Cai Q, Ji J, Sui G, Yu Y, Yang X, Ma Q, Wei Y, and Deng X. Composites Science and Technology 2008;68(15-16):3322-3329.
193. Greiner A and Wendorff JH. Angew Chem Int Ed Engl 2007;46(30):5670-5703.
194. Dong Y, Mosaval T, Haroosh HJ, Umer R, Takagi H, and Lau K-T. Journal of Polymer Science Part B: Polymer Physics 2014;52(9):618-623.
195. Stachewicz U, Modaresifar F, Bailey RJ, Peijs T, and Barber AH. ACS Appl Mater Interfaces 2012;4(5):2577-2582.

196. Yao J, Li G, Bastiaansen CWM, and Peijs T. Polymer 2015;76:46-51.
197. Zuo Y, Yang F, Wolke JG, Li Y, and Jansen JA. Acta Biomater 2010;6(4):1238-1247.
198. Fu S-Y, Mai Y-W, Lauke B, and Yue C-Y. Materials Science and Engineering: A 2002;323(1-2):326-335.
199. Karsli NG, Aytac A, and Deniz V. Journal of Reinforced Plastics and Composites 2012;31(15):1053-1060.
200. Sarasua JR, Arraiza ALp, Balerdi P, and Maiza I. Polymer Engineering & Science 2005;45(5):745-753.
201. Zhang X, Nakagawa R, Chan KHK, and Kotaki M. Macromolecules 2012;45(13):5494-5500.
202. Mai F, Tu W, Bilotti E, and Peijs T. Fibers 2015;3(4):523-538.
203. Odelius K, Hoglund A, Kumar S, Hakkarainen M, Ghosh AK, Bhatnagar N, and Albertsson AC. Biomacromolecules 2011;12(4):1250-1258.
204. Schuller-Ravoo S, Teixeira SM, Feijen J, Grijpma DW, and Poot AA. Macromol Biosci 2013;13(12):1711-1719.
205. Geven MA, Varjas V, Kamer L, Wang X, Peng J, Eglin D, and Grijpma DW. Polymers for Advanced Technologies 2015;26(12):1433-1438.
206. Mathew AP, Oksman K, and Sain M. Journal of Applied Polymer Science 2006;101(1):300-310.
207. Fathona IW and Yabuki A. Journal of Materials Science 2014;49(9):3519-3528.
208. Inam F, Reece MJ, and Peijs T. Journal of Composite Materials 2011;46(11):1313-1322.
209. Zhu X, Cui W, Li X, and Jin Y. Biomacromolecules 2008;9(7):1795-2008.
210. Inam F, Wong DWY, Kuwata M, and Peijs T. Journal of Nanomaterials 2010;2010:1-12.
211. Wu D, Wu L, Zhou W, Sun Y, and Zhang M. Journal of Polymer Science Part B: Polymer Physics 2010;48(4):479-489.
212. Cui W, Li X, Zhu X, Yu G, Zhou S, and Weng J. Biomacromolecules 2006;7(5):1623-1629.
213. Sato S, Gondo D, Wada T, Kanehashi S, and Nagai K. Journal of Applied Polymer Science 2012;129(3):1607-1617.
214. Martin O and Avérous L. Polymer 2001;42(14):6209-6219.
215. Fu S-Y and Lauke B. Composites Science and Technology 1996;56(10):1179-1190.
216. Thomason JL, Vlug MA, Schipper G, and Krikor HGLT. Composites Part A: Applied Science and Manufacturing 1996;27(11):1075-1084.
217. Peijs T, Garkhail S, Heijenrath R, van Den Oever M, and Bos H. Macromolecular Symposia 1998;127(1):193-203.
218. Yu Z, Brisson J, and Ait-Kadi A. Polymer Composites 1994;15(1):64-73.
219. Garkhail S, Heijenrath R, and Peijs T. Applied Composite Materials 2000;7(5):351-372.
220. Krenchel H. Fibre Reinforcement. Copenhagen, Denmark: Akademisk Forlag, 1964.
221. Naraghi M, Arshad SN, and Chasiotis I. Polymer 2011;52(7):1612-1618.
222. Carman GP and Reifsnider KL. Composites Science and Technology 1992;43(2):137-146.
223. Coleman JN, Khan U, Blau WJ, and Gun'ko YK. Carbon 2006;44(9):1624-1652.
224. Manchado MAL, Valentini L, Biagiotti J, and Kenny JM. Carbon 2005;43(7):1499-1505.
225. Xie T. Polymer 2011;52(22):4985-5000.

226. Lendlein A, Jiang H, O. J, and Langer R. Nature 2005;434(7035):879-882.
227. Huang WM, Yang B, An L, Li C, and Chan YS. Applied Physics Letters 2005;86(11):114105.
228. Leng JS, Lan X, Liu YJ, Du SY, Huang WM, Liu N, Phee SJ, and Yuan Q. Applied Physics Letters 2008;92(1):014104.
229. Song S, Feng J, and Wu P. Macromol Rapid Commun 2011.
230. Meng H and Li G. Polymer 2013;54(9):2199-2221.
231. Luo X and Mather PT. Soft Matter 2010;6(10):2146.
232. Koerner H, Price G, Pearce NA, Alexander M, and Vaia RA. Nat Mater 2004;3(2):115-120.
233. Luo X and Mather PT. Macromolecules 2009;42(19):7251-7253.
234. Zhang H, Wang H, Zhong W, and Du Q. Polymer 2009;50(6):1596-1601.
235. Robertson JM, Birjandi Nejad H, and Mather PT. ACS Macro Letters 2015;4(4):436-440.
236. Lendlein A and Langer R. Science 2002;296(5573):1673-1676.
237. Xue L, Dai S, and Li Z. Biomaterials 2010;31(32):8132-8140.
238. Koji N, Yuichi U, Tatsuro O, and Yuichi O. Biomacromolecules 2009;10(7):1789-1794.
239. Rochette JM and Ashby VS. Macromolecules 2013;46(6):2134-2140.
240. Ulery BD, Nair LS, and Laurencin CT. Journal of Polymer Science Part B: Polymer Physics 2011;49(12):832-864.
241. Kelly CA, Naylor A, Illum L, Shakesheff KM, and Howdle SM. Advanced Functional Materials 2012;22(8):1684-1691.
242. Hu Y, Hu YS, Topolkaraev V, Hiltner A, and Baer E. Polymer 2003;44(19):5681-5689.
243. Qin Y, Yang J, and Xue J. Journal of Materials Science 2014;50(3):1150-1158.
244. Guillaume O, Geven MA, Grijpma DW, Tang TT, Qin L, Lai YX, Yuan H, Richards RG, and Eglin D. Polymers for Advanced Technologies 2016.
245. Guerin W, Helou M, Carpentier J-F, Slawinski M, Brusson J-M, and Guillaume SM. Polym. Chem. 2013;4(4):1095-1106.
246. Bordag N, Klie S, Jurchott K, Vierheller J, Schiewe H, Albrecht V, Tonn JC, Schwartz C, Schichor C, and Selbig J. Sci Rep 2015;5:15954.
247. Pittenger MF, Mackay AM, Beck SC, Jaiswal RK, Douglas R, Mosca JD, Moorman MA, Simonetti DW, Craig S, and Marshak DR. Science 1999;284(5411):143-147.
248. Jaiswal N, Haynesworth SE, Caplan AI, and Bruder SP. Journal of Cellular Biochemistry 1997;64(2):295-312.
249. Costa PF, Puga AM, Diaz-Gomez L, Concheiro A, Busch DH, and Alvarez-Lorenzo C. Int J Pharm 2015;496(2):541-550.
250. Astolfi L, Guaran V, Marchetti N, Olivetto E, Simoni E, Cavazzini A, Jolly C, and Martini A. J Biomed Mater Res B Appl Biomater 2014;102(2):267-273.
251. Kim DH and Martin DC. Biomaterials 2006;27(15):3031-3037.
252. Webber MJ, Matson JB, Tamboli VK, and Stupp SI. Biomaterials 2012;33(28):6823-6832.
253. Jiang K, Weaver JD, Li Y, Chen X, Liang J, and Stabler CL. Biomaterials 2017;114:71-81.
254. Hu X, Liu S, Zhou G, Huang Y, Xie Z, and Jing X. J Control Release 2014;185:12-21.
255. Zeng J, Yang L, Liang Q, Zhang X, Guan H, Xu X, Chen X, and Jing X. J Control Release 2005;105(1-2):43-51.
256. Yu D-G, Chian W, Wang X, Li X-Y, Li Y, and Liao Y-Z. Journal of Membrane Science 2013;428:150-156.

257. Hu C, Liu S, Zhang Y, Li B, Yang H, Fan C, and Cui W. Acta Biomater 2013;9(7):7381-7388.
258. Yohe ST, Colson YL, and Grinstaff MW. J Am Chem Soc 2012;134(4):2016-2019.
259. Huang J, Yuan L, Wang X, Zhang TL, and Wang K. Life Sci 2007;81(10):832-840.
260. Walsh S, Jordan GR, Jefferiss C, Stewart K, and Beresford JN. Rheumatology (Oxford) 2001;40(1):74-83.
261. Wang GJ, Cui Q, and Balian G. Clin Orthop Relat Res 2000(370):295-310.
262. Both SK, van der Muijsenberg AJ, van Blitterswijk CA, de Boer J, and de Bruijn JD. Tissue Eng 2007;13(1):3-9.
263. Choi K-M, Seo Y-K, Yoon H-H, Song K-Y, Kwon S-Y, Lee H-S, and Park J-K. Journal of Bioscience and Bioengineering 2008;105(6):586-594.
264. Jaiswal N, Haynesworth SE, Caplan AI, and Bruder SP. J Cell Biochem 1997;64(2):295-312.
265. Mendes SC, Tibbe JM, Veenhof M, Both S, Oner FC, van Blitterswijk CA, and de Bruijn JD. J Mater Sci Mater Med 2004;15(10):1123-1128.
266. Birmingham E, Niebur GL, McHugh PE, Shaw G, Barry FP, and McNamara LM. Eur Cell Mater 2012;23:13-27.
267. Chang C and Zhang L. Carbohydrate Polymers 2011;84(1):40-53.
268. Li C, Rowland MJ, Shao Y, Cao T, Chen C, Jia H, Zhou X, Yang Z, Scherman OA, and Liu D. Adv Mater 2015;27(21):3298-3304.
269. Zhang H, Zhai D, and He Y. RSC Adv. 2014;4(84):44600-44609.
270. Liu H, Huang S, Li X, Zhang L, Tan Y, Wei C, and Lv J. Materials Letters 2013;90:142-144.
271. Chang C, Duan B, Cai J, and Zhang L. European Polymer Journal 2010;46(1):92-100.
272. Fei B, Wach RA, Mitomo H, Yoshii F, and Kume T. Journal of Applied Polymer Science 2000;78(2):278-283.
273. Calvert P. Advanced Materials 2009;21(7):743-756.
274. Stauffer SR and Peppast NA. Polymer 1992;33(18):3932-3936.
275. Holloway JL, Lowman AM, and Palmese GR. Soft Matter 2013;9(3):826-833.
276. Yin L, Fei L, Cui F, Tang C, and Yin C. Biomaterials 2007;28(6):1258-1266.
277. Sun JY, Zhao X, Illeperuma WR, Chaudhuri O, Oh KH, Mooney DJ, Vlassak JJ, and Suo Z. Nature 2012;489(7414):133-136.
278. Okumura Y and Ito K. Advanced Materials 2001;13(7):485-487.
279. McKee JR, Appel EA, Seitsonen J, Kontturi E, Scherman OA, and Ikkala O. Advanced Functional Materials 2014;24(18):2706-2713.
280. Shin SR, Jung SM, Zalabany M, Kim K, Zorlutuna P, Kim Sb, Nikkhah M, Khabiry M, Azize M, Kong J, Wan K-t, Palacios T, Dokmeci MR, Bae H, Tang XS, and Khademhosseini A. ACS Nano 2013;7(3):2369-2380.
281. Alvarez GS, Hélary C, Mebert AM, Wang X, Coradin T, and Desimone MF. Journal of Materials Chemistry B 2014;2(29):4660.
282. Hong Y, Huber A, Takanari K, Amoroso NJ, Hashizume R, Badylak SF, and Wagner WR. Biomaterials 2011;32(13):3387-3394.
283. Wang TY, Bruggeman KF, Kauhausen JA, Rodriguez AL, Nisbet DR, and Parish CL. Biomaterials 2016;74:89-98.
284. Poveda-Reyes S, Mellera-Oglialoro LR, Martínez-Haya R, Gamboa-Martínez TC, Gómez Ribelles JL, and Gallego Ferrer G. Macromolecular Materials and Engineering 2015;300(10):977-988.
285. Nederberg F, Connor E, Möller M, Glauser T, and Hedrick J. Angewandte Chemie International Edition 2001;40(14):2712-2715.
286. Seo M and Hillmyer MA. Science 2012;336(6087):1422-1425.

287. Zalusky AS, Olayo-Valles R, Wolf JH, and Hillmyer MA. Journal of American Chemical Society 2002;124(43):12761-12773.
288. Boissé S, Kryuchkov MA, Tien N-D, Bazuin CG, and Prud'homme RE. Macromolecules 2016;49(18):6973-6986.
289. Soliman S, Sant S, Nichol JW, Khabiry M, Traversa E, and Khademhosseini A. J Biomed Mater Res A 2011;96(3):566-574.
290. Chaudhuri O, Gu L, Klumpers D, Darnell M, Bencherif SA, Weaver JC, Huebsch N, Lee HP, Lippens E, Duda GN, and Mooney DJ. Nat Mater 2016;15(3):326-334.